DESIGN OF FeCo NANOALLOY MORPHOLOGY VIA CONTROL OF REACTION KINETICS

A Dissertation
Presented to
The Academic Faculty

by

Melissa Ann Zubris Williams

In Partial Fulfillment
of the Requirements for the Degree
Doctor of Philosophy in the
School of Materials Science and Engineering

Georgia Institute of Technology
December 2005

DESIGN OF FeCo NANOALLOY MORPHOLOGY VIA CONTROL OF REACTION KINETICS

Approved by:

Dr. Rina Tannenbaum, Advisor
School of Materials Science and Engineering
Georgia Institute of Technology

Dr. Rosario Gerhardt
School of Materials Science and Engineering
Georgia Institute of Technology

Dr. Hamid Garmestani
School of Materials Science and Engineering
Georgia Institute of Technology

Dr. Karl Jacob
School of Polymer, Textile, and Fiber Engineering
Georgia Institute of Technology

Dr. Nily Dan
Department of Chemical and Biological Engineering
Drexel University

Date Approved: October 26, 2005

For my family and friends

ACKNOWLEDGEMENTS

I would like to thank my advisor, Dr. Rina Tannenbaum, for guidance, support, and wisdom through my graduate work. I would also like to thank my thesis committee, Dr. Rosario Gerhardt, Dr. Hamid Garmestani, Dr. Karl Jacob, and Dr. Nily Dan for their assistance. I would also like to acknowledge my group members throughout my time at Georgia Tech; Astra Zeno, Erica Tadd, Kasi David, Wren Greene, Jeremy Walker, Larry Pranger, Dan Ciprari, Erin Camponeschi, and Cantwell Carson.

TABLE OF CONTENTS

LIST OF TABLES

LIST OF FIGURES

SUMMARY

Nanoalloys are an exciting new class of materials in the growing field of nanotechnology. Nanoalloys consist of the nanoscale co-aggregation of two or more metals with a potential to form compositionally-ordered phases or superstructures that have properties unlike those of the individual metal clusters or of bulk alloys of the constituent metals. This research seizes the opportunity that the nanoscale domain has to offer, and focuses on the synthesis of iron and cobalt nanoalloys via the simultaneous decomposition of iron cobalt organometallic precursors in a stabilizing environment, accompanied by the thorough characterization of the resulting nanoclusters.

Zero-valent FeCo nanoalloys may potentially have interesting uses as magnetic materials. Since these clusters have sizes less than the size of their magnetic domain, the clusters will exhibit single domain magnetism. This magnetism may be observed by the presence of chain structures of FeCo nanoclusters due to the alignment of their single magnetic domains.

In order to create a near-atomically homogeneous nanoalloy without preferential aggregation of its metal atom constituents, no clustering and phase separation should take place. In the bulk, alloys of iron and cobalt phase separate over most of the compositional range. Conversely, at the nanoscale, it may be possible to synthesize nanoalloy structures that are not normally favorable at given compositions, by the manipulation of reaction kinetics. In order to produce an atomically mixed nanoalloy, the transformation reactions of the organometallic precursors should display similar kinetic features, i.e. similar reaction rates. Therefore, the reaction kinetics of all the species in the reaction must be

similar to avoid competition between them. As a result, kinetic control of the individual transformation reaction rates of each species may be used to modulate the aggregation and phase separation of the different species, and consequently control cluster morphology. This work has provided the framework for the design of synthesis methods that enable the control of the structure of FeCo nanoalloys with careful attention to precursor decomposition kinetics and the correlation between reaction kinetics and nanoalloy morphology.

CHAPTER 1

INTRODUCTION

Nanotechnology is one of the fastest growing fields in materials research today. Nanostructures have unlimited possibilities for use in electronic applications, medicine, and catalysis reactions due to their size and interesting properties. A unique characteristic of operating at the nanoscale is the ability to create structures, compositions, and morphologies that are not traditionally available in the bulk.[1-4] Researchers have shown that phases and compositions that are not possible to obtain in the bulk can often be created at the nanoscale by the manipulation of reaction kinetics, and there is a need to construct new nanoscale phase diagrams and develop detailed methods for the design of controlled composition nanoclusters.[5-9]

In the bulk, the alloying of two metals is often used to create new materials with a combination of the benefits of their constituent metals. These combinations are limited, however, by the bulk phase diagram and thermodynamics. At the nanoscale there are different options for alloy compositions that might not be possible in the bulk. These "nanoalloys" combine the benefits of their metal constituents with unique properties due to their size. Changing the composition of these nanoalloys can drastically impact their properties (such as magnetic strength, conductivity, surface chemistry), so careful attention must be paid to synthesis methods and control of morphology.

Due to the potential benefit of nanoalloys, it is important to determine the optimum formation conditions for these unique materials. As researchers attempt to

synthesize nanoalloys in-situ, careful attention must be paid to the kinetics of the two metal systems. Researchers have created mixed-composition nanoalloys in limited cases, with their success restricted by the kinetics of the precursors. In order to form mixed-composition nanoalloys, the constituent metal clusters must form concurrently. However, the precursors used for the formation of metal clusters may have drastically different kinetic mechanisms. Control of the kinetics of the precursors directly controls the nucleation and growth of the resulting nanoalloys, and the control of the nucleation and growth of these species results in control of the nanoalloy morphologies. To effectively control the morphology of synthesized nanoclusters, the kinetics of cluster formation need to be clarified.

The overarching goal of this study was to develop a system to produce controlled morphology FeCo nanoalloys via control of reaction kinetics. Careful attention was paid to the kinetics of the iron and cobalt precursors used to synthesize these nanoalloys, and the manipulation of these kinetics and other reaction parameters allows the control of the resulting cluster morphologies.

In this study, organometallic metal carbonyl precursors are thermally decomposed in a stabilizing polymer/solvent system to synthesize FeCo nanoalloys. The kinetics of the decompositions of the metal carbonyl precursors were thoroughly studied. Throughout the decompositions, FT-IR analysis was performed in order to determine the decomposition rate. The iron carbonyl chosen for these studies was $Fe(CO)_5$ (chosen because of its previous kinetic investigation)[10,11], and it was co-decomposed with a variety of cobalt precursors in order to determine ideal reaction conditions for the formation of mixed-composition nanoalloys.

Nanoalloys were created with $Fe(CO)_5$ and $Co_2(CO)_8$, $Fe(CO)_5$ and $Co_4(CO)_{12}$, $Fe(CO)_5$ and $Co(CO)_2C_5H_5$. The decomposition kinetics of $Fe(CO)_5$ and $Co_2(CO)_8$ have been thoroughly investigated in these polymer/solvent systems, but the kinetics of their co-decomposition needed to be studied. From previous work it is known that the decomposition of $Co_2(CO)_8$ occurs much more quickly than the decomposition of $Fe(CO)_5$ and the reaction is a first order process as compared to the decomposition of $Fe(CO)_5$, which is a second-order process. Knowing this, it was necessary to construct reaction conditions that induced equal initial decomposition rates of the two species.

$Co_4(CO)_{12}$ was chosen as a possible cobalt carbonyl precursor because of its molecular size. Larger and more complex than $Co_2(CO)_8$, it is predicted than this species will decompose more slowly than $Co_2(CO)_8$. A slower decomposition rate might better match the decomposition rate of $Fe(CO)_5$, producing more thoroughly mixed nanoalloys.

$Co(CO)_2C_5H_5$ was chosen as another possible cobalt carbonyl precursor because of its structure. It is predicted that the presence of the C_5H_5 group attached to the cobalt will hinder the release of the CO groups from the cobalt atoms and slow the overall decomposition process. If this decomposition is relatively slow, it may be a better match for the $Fe(CO)_5$ initial decomposition rate than $Co_2(CO)_8$.

These cobalt precursors were decomposed in the polymer/solvent systems and their decomposition kinetics were evaluated. Using their individual rate constants, relationships between kinetics and concentrations of precursors that would induce equal initial decomposition rates were constructed. These relationships were used to create synthesis methods that will produce atomically mixed nanoalloys.

The prepared nanoalloys were characterized using transmission electron microscopy, electron diffraction, and thermogravimetric analysis to evaluate the effectiveness of the synthesis processes in producing mixed-composition nanoclusters.

CHAPTER 2

BACKGROUND

2.1 Overview

This chapter provides background information on transition metal nanoalloys. Section 2.2 will discuss possible uses of transition metal nanoparticles, and specific benefits of using transition metal nanoparticles. Section 2.3 will discuss a variety of methods used to synthesize metal nanoclusters. Section 2.4 will describe the characterization methods used in this work.

2.2 Advantages and potential applications for metal nanoparticles

2.2.1 Magnetic properties

Transition metal nanoparticles have interesting magnetic properties, more significant than the magnetic properties of their bulk materials. The magnetic properties of metal oxide nanoparticles are generally much weaker than those of their zero-valent metal counterparts. Even though they have this potential drawback, metal oxides are more commonly used instead of zero-valent metals because of the difficulties of storage of unprotected zero-valent species in air.[12] As will be discussed later, the synthesis method used to produce the FeCo nanoalloys in this study creates a polymer "cap" of material around the nanoparticle which limits its size and growth. This polymer cap may have the additional benefit of serving as an oxidation barrier, allowing the maintenance of the properties of these zero-valent clusters in solution or in films.[12]

Bulk transitional metals have ferromagnetic properties, but nanoclusters of the same materials have much stronger magnetic response per volume.[12] Nanoclusters exhibit single domain magnetism, where each cluster has a large magnetic moment in a single direction and a large amount of magnetic energy outside the cluster. Larger clusters of atoms may exhibit closed domain magnetism, where the cluster has multiple magnetic moments that oppose each other.

Energetic considerations are the basis for the domain structure. It is energetically unfavorable for magnetic moments in a sample to line up in a single direction. The overall magnetic energy is reduced if the material is broken up into domains.[13] Each domain that is created opposes the moment of another domain, and the domains cancel each other out and reduce the energy of the system. However, these domains also need energy for maintenance. Equilibrium will be reached in the system when the amount of energy used to construct one more domain equals the energy reduction caused by constructing that wall.[13] At this point, the energy of the system is minimized.

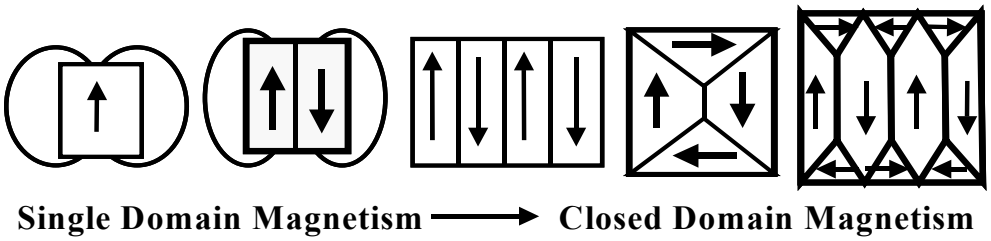

Figure 2.1: Magnetic moment alignment in the transition between single and closed domain structures[13]

Below a critical size, a particle only has enough energy to support one magnetic domain. If a cluster is small enough (10-60 nm in diameter), it will not have enough energy to support more than one domain boundary and will exhibit single domain magnetism.[14] This domain will contain a single large spin with moment 10^3-10^5 μB.[14] At low temperatures, all of the moments in a sample will point in an energetically favorable direction.[14] Above a certain "blocking temperature", thermal fluctuations can overcome the anisotropy barrier in the system.[14] At this point, the moments can rotate in many directions, reducing the magnetic strength.[14] The system is then superparamagnetic.[14]

Electrical and magnetic devices that may depend on these nanoparticles require high frequencies for use in applications such as high-speed switching, magnetic recording, and microwave applications.[15] Thus, there is a need for examination of the response characteristics of these materials over dynamic frequencies.[15]

2.2.2 Potential applications of metal nanoparticles

As will be discussed in detail later in this work, nanoalloys can be created in-situ in polymer stabilizing solutions. Therefore, these nanoparticles in polymer solutions can be cast into a variety of different polymer-composite structures. These polymer-metal nanocomposites have potential application in electronic, optical, magnetic, and medical applications. Transition metal nanoclusters may be used as a tool for magnetic nanodevice fabrication.[16] A tightly packed section of these nanoparticles could be used for high-density storage media.[16] A uniform assembly with a high degree of ordering is required for storage media, so the self-assembling aspect of these nanoclusters is important. Magnetic nanoparticles embedded in binding materials such as a polymer sheet may be useful for data storage and creating media like magnetic recording tape.[15]

Ferromagnetic and ferrite nanoparticles are particularly useful, due to their large coercivities.[15] Also, the nanoclusters may be attached to an AFM (atomic force microscope) to achieve improved sensitivity in magnetic force sensing.[16] They may also be used for magnetic field assisted drug delivery when coupled with biomolecules.[16]

Uses of metastable Co clusters formed by solution phase synthesis include catalysis and size-tunable optical and electronic devices.[12] These ferromagnetic nanoclusters may also be the basis for conventional magnetic storage media, such as hard drives.[12] The quality of the magnetic recording ability improves as the cluster size is reduced to a point; once they reach a very small diameter (under 10 nm) they become superparamagnetic.[12] At this point, the magnetization of the cluster fluctuates randomly at room temperature and they can no longer be used for magnetic storage.[12] Using ferromagnetic nanoclusters, one can reach magnetic recording densities between 100 Gb/in^2 and 1 Tb/in^2.[12] Transition metal nanoclusters are also used to produce magnetic tapes, ferrofluids, and magnetic refrigerants.[19]

Small metal or semiconductor particles may also be used to construct an array of quantum dots.[20] This array can be used as a series of tunnel resonance resistors where one resistor is a pair of metal nanoparticles.[20] However, high stability and low reactivity are required for use in electronic applications.[20] In this case, the required capping material can also serve as a stabilizer.

In addition to magnetic applications, Fe nanoparticles may be very useful in catalysis reactions that are important for environmental reasons.[21] Possible reaction scenarios include water-gas shifts, where CO and H_2O are combined at a 1:1 ratio and 60% of the CO is converted into CO_2 and H_2.[21] Also, CO oxidation may be

accomplished by the addition of O_2 gas, and converted to CO_2 and H_2.[21] Other reactions in which Fe may be an important catalyst include the reduction of NO by H_2 or CO gas, where the reactants may be converted to N_2O, H_2O, and CO_2.[21] Other catalysis reactions include the hydrogenation of ethylene, benzene, and stylene monomer into ethane, cyclohexane, and ethyl benzene.[21]

2.3 Synthesis of transition metal nanoalloys

2.3.1 General overview and discussion of importance of polymer solution

The synthesis of transition metal nanoclusters has been accomplished in many different systems. Most of the systems designed to form nanoparticles in-situ involve a metal precursor, a stabilizing polymer, and a solvent in which both are miscible.

When zero-valent metal atoms are generated via the thermal decomposition of organometallic precursors or metal salts, there is a thermodynamic tendency for the

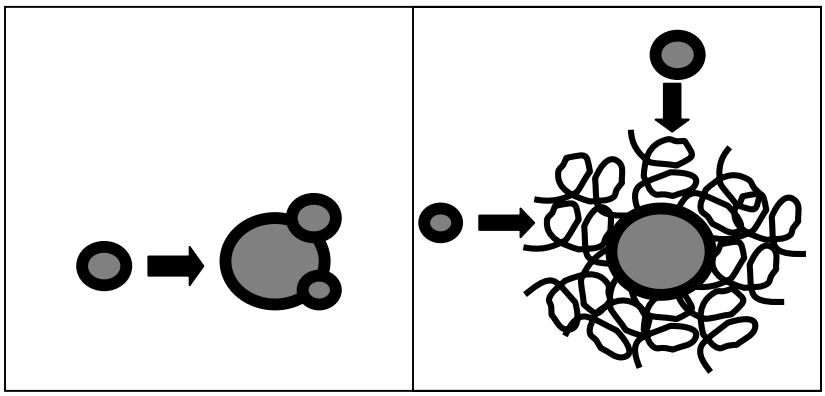

Figure 2.2: (a) Metal clusters without polymer capping are free to agglomerate, (b) metal clusters with polymer caps cannot agglomerate

atoms to agglomerate. This agglomeration is an attempt to reduce surface energy. When allowed to agglomerate freely, the atoms will combine and take on the properties of the bulk metal. However, the addition of a polymer or other organic stabilizer limits the agglomeration of metal to a small number of atoms per cluster via one of two mechanisms.

First, the stabilizer interacts irreversibly with the surface of the cluster. This physically blocks atoms from attaching to the surface of the cluster. Second, the presence of a stabilizer often increases the viscosity of the solution, slowing down the diffusion rate of atoms moving in the solvent, thereby reducing their ability to reach agglomerates. In addition, the presence of polymer provides nucleation sites, increasing the initial rate of formation of clusters, for example, with the decomposition of metal carbonyls. The polymer molecules provide the necessary solid-state support for the atoms released from the decomposition reaction.[10,11]

2.3.2 Methods for synthesis of metal nanoclusters

Common methods used to create or synthesize nanoclusters include metal evaporation, grinding of bulk metal, sputtering, solution phase metal salt reduction, and organometallic precursor decomposition.[12] The magnetic properties resulting from the synthesis of these nanoclusters depend on the size, crystal structure, and any defects in the material.[12]

A solution phase synthesis allows the possibility of organized assembly. In one such case, multilayer assemblies have been constructed with Fe and Pt clusters deposited on a functionalized substrate.[16] These assemblies show good regularity and few defects due to the self-assembly process, Figure 2.3.

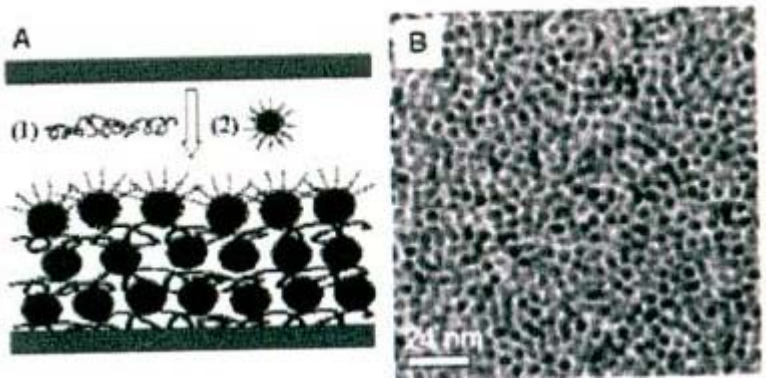

Figure 2.3: (a) Self-assembly of FePt nanoparticles by alternating absorption of particles and polymer on a substrate (b) TEM image of three layers of assembled FePt particles on PEI substrate[16]

Iron nanoparticles have been successfully synthesized in a cellulose acetate polymer.[17] The polymer provides stabilization for cluster formation and gives good control over cluster size.[17] Also, by adjusting metal precursor concentration and thermal heating conditions, final particle size and size dispersion may be controlled.[17] In this reaction, there is an electrostatic interaction between the acetate polymer and the iron ions, which promotes the capping process.[17] The loading of the cellulose films with iron nanoparticles can increase the T_g of the material by 25-30°C.[17]

Self-organizing cobalt nanoparticles have been synthesized in polymer using traditional carbonyl decomposition methods.[16] The magnetic response of these particles was determined by modeling the remanent and field induced magnetizations and combining the results with X-ray and TEM of the particles.[16] This enables the relation of magnetic properties to the particle size and structure.

Surfactant micelles have been used to control the size of iron nanoclusters, Figure 2.4.[18] The size of the clusters is controlled by nucleation and growth in the interior of the surfactant aggregates.[18] Inside these aggregates, the micelle size, reaction chemistry, and proximity to other micelles determines the final size.[18] The iron particles are synthesized by the reduction of salts in the hydrophilic center of the micelles, either $Fe(BF_4)_2$ or $FeCl_3$.[18] These reductions were performed under oxygen in order to produce zero-valent species.[18] The resulting clusters were determined to be fcc, though alpha bcc is traditionally expected at room temperature for iron.[18] These unexpected morphologies are apparent in many studies with work at the nanoscale.

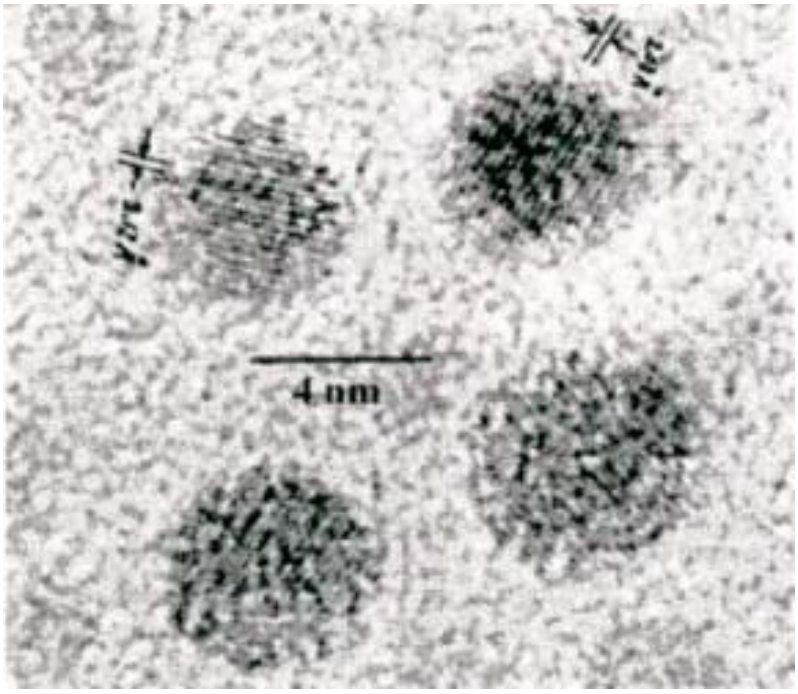

Figure 2.4: HRTEM of Fe clusters formed within micelles[18]

Monodisperse Co nanoclusters have been synthesized via the phase reduction of CoCl salts in the presence of stabilizers.[12] This synthesis method produces ε-Co, an

unexpected phase.[12] This result is possible because solution phase chemical synthesis is not thermodynamically controlled.[12] Using these methods, one can synthesize solids of metastable phases.

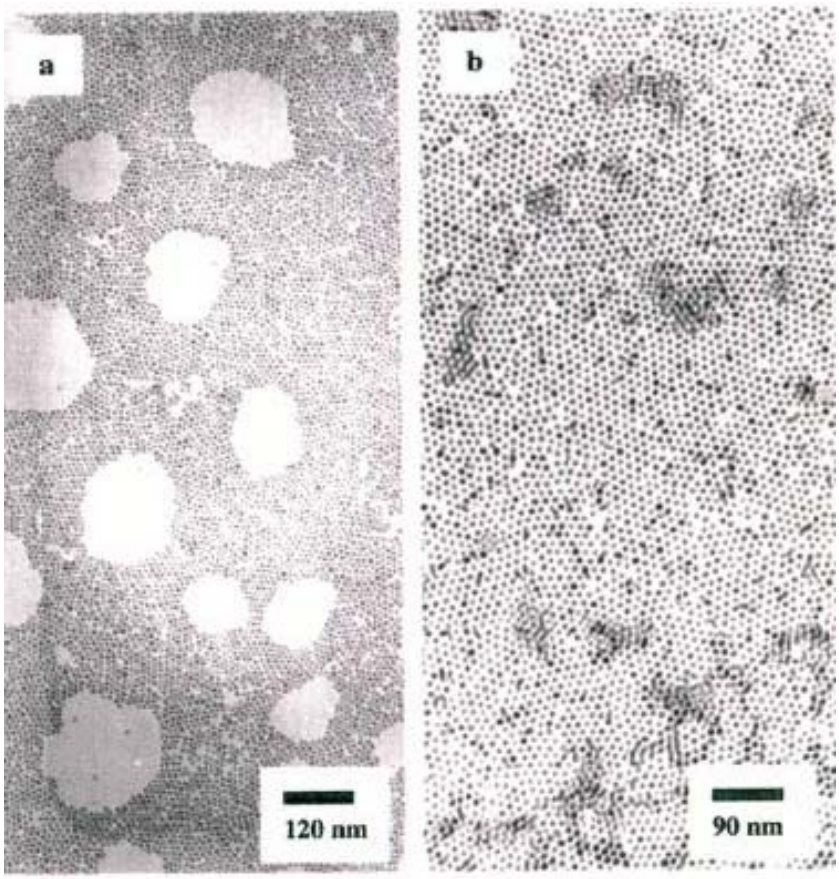

Figure 2.5: TEM micrographs of arrays of Co clusters[12] with diameters (a) 6 nm and (b) 9 nm

In another work, Fe and Co nanoclusters were synthesized by chemical vapor condensation (CVC).[19] Helium was bubbled through a solution of liquid precursor. A heat source was used for controlled decomposition of the precursor, $Fe(CO)_5$ or

$Co_2(CO)_8$.[19] As it is heated, the precursor pyrolyzes and metal nanoclusters condense on a chiller.[19] The clusters are scraped off the chiller and collected.[19]

Oxide layers form on the surface of these particles when they are exposed to air. The oxide layer thickness is dependent on the method of cooling; liquid N_2 cooling produces a thin amorphous oxide layer and room temperature cooling produces a thick crystalline layer.[19] The higher heat transfer rate provided by the liquid N_2 cooling enables the formation of a thinner protective oxide layer.[19]

The particles produced in this study form long chain structures due to their magnetic energy.[19] Lining up all the magnetic moments and forming these intricate strands minimizes the magnetic energy of the system. The particle sizes produced varied with precursor decomposition temperature.[19] As the decomposition temperature was increased, the particle size increased. However, the particles are only stable at a certain saturation vapor pressure. If the vapor pressure is too high, the particles will grow uncontrolled. If it is too low, the precursor will evaporate. Careful attention must be paid to the synthesis conditions for nanocluster formation.

Saturation magnetism of these particles was measured with respect to particle size.[19] The magnetic strength of the particles decreased as size decreased, due to the higher volume ratio of metal oxide versus metal for small particles.[19]

Ordered gold and silver nanoalloys with narrow cluster size distribution have been produced via salt reduction procedures.[20] The particles are stabilized with C_{10}-thiols to control size and protect the surface.[20] The gold and silver clusters are produced independently in toluene, and then mixed to form the nanoalloy. These systems exhibit self-assembly when the colloidal system is dropped onto a substrate and the solvent is

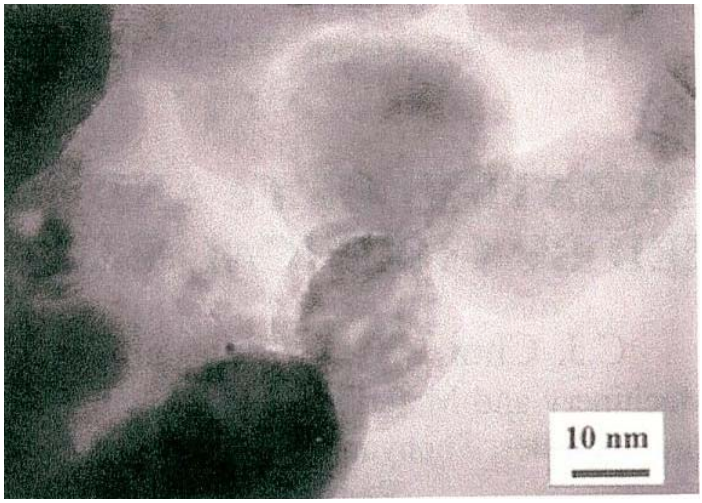

Figure 2.6: Fe nanoparticles synthesized via CVC[19]

evaporated.[25] A monomodal system of particles will develop an hcp structure, and bimodal systems will develop an ordered 2-D array.[25] The structure is determined by the size ratio of the particles.

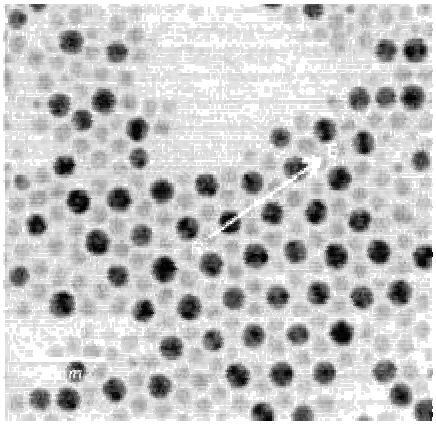

Figure 2.7: TEM image of an ordered Au/Ag colloidal nanoalloy[25]

The nanoalloy structures produced were examined with STEM and line scan EDX was used for chemical analysis of the particles.[25]

Gold and silver nanoclusters were produced via the reduction of $KAuCl_4$ and $KAg(CN)_2$.[21] The clusters were synthesized in a solution of dodecane thiol in order to limit cluster size.[21] UV-vis analysis was performed in order to follow the formation of the Au and Ag clusters in solution.[21] In this work, morphology was addressed. Different salt ratios were used in order to create different structures; the morphology was controlled by these ratios. Because of a difference in kinetics (reduction rate of the salts), a core-shell structure will be formed when equal amounts of the two salts are used and reacted simultaneously.[21] As the amount of shell species is increased, the average particle size in the sample should also increase. However, if, there is no increase in particle size, one can assume that the structure is not core-shell. This work shows some attention to kinetics, but not a thorough investigation. The authors accept the role of kinetics in the process, but do not go to great lengths to manipulate them.

Fullerene encapsulated ferromagnetic clusters have been produced via the decomposition of metallocenes $M(C_5H_5)_2$ of Ni or Co.[22] The clusters are coated with carbon to prevent oxidation.[22]

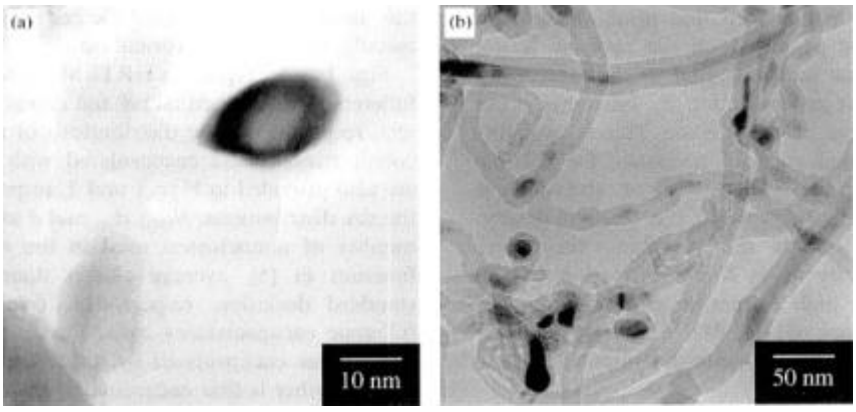

Figure 2.8: Co nanoclusters with (a) carbon onion structure and (b) carbon nanotube structure coatings[22]

For magnetic strength measurements, γ-Fe_2O_3 was used instead of zero-valent Fe in order to avoid sample oxidation during measurements and the resulting fluctuations in properties.[22] The products of the synthesis were analyzed using X-ray diffraction, HRTEM, and MPM (Magnetic Property Measurement System).[22] The Ni clusters were determined to be fcc in structure, and the Co were fcc with a trace of hcp structure.[22]

The magnetic analysis of the Co clusters shows the presence of hysteresis loops, indicating ferromagnetic behavior with high coercivities.[22] Very small clusters exhibit superparamagnetic behavior and are not suitable for applications that require maintained magnetic moment directions. However, nanoclusters of larger sizes have very good magnetic properties. Single domain magnetism, the strongest type of magnetism, is present in these clusters of size 10-50 nm.[22]

Fe and Co nanocluster wires have also been synthesized by decomposing metal carbonyl vapors with a resistive heater.[23] Carbonyl precursors, $Fe(CO)_5$ and $Co_2(CO)_8$ were used and this procedure was completed under vacuum to reduce oxidation.[23] The wires form between disc magnets along the lines of magnetic flux and align due to their magnetic moments.[23] The clusters are 8-10 nm in diameter and the wires are a few mm long.[23]

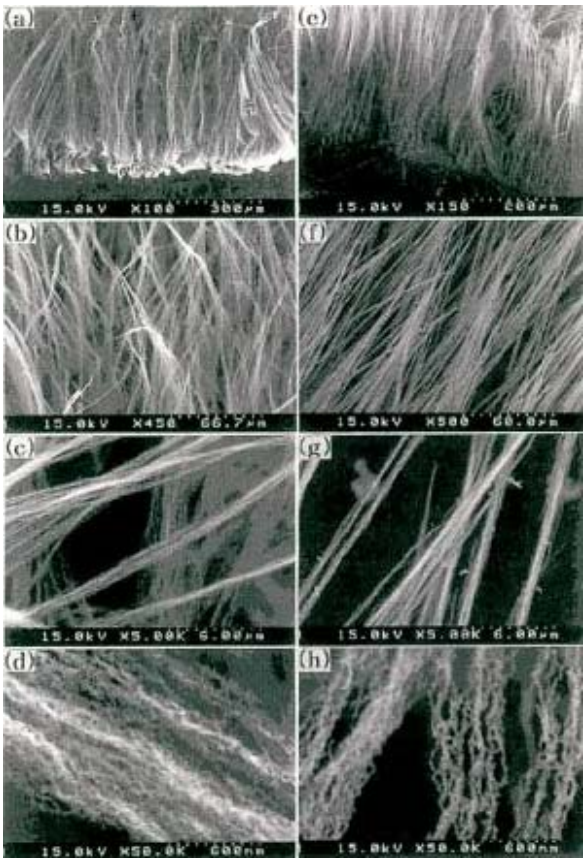

Figure 2.9: SEM micrographs of Fe nanocluster wires (a-d) and Co nanocluster wires (e-h)[23]

The structures were confirmed using HRTEM, X-ray diffraction, and SEM.[23] From this information, it was determined that the clusters consisted of individual elements, not mixed nanoalloys.[23] These samples exhibited hysteresis loops parallel and perpendicular to the wires, indicating the presence of good magnetic behavior.[23]

Solid solution and core-shell CoPt nanoclusters were produced via transmetalation reactions.[24] Each of these nanoclusters may be used as an independent magnetic bit for information storage.[24] These nanoalloys also have high magnetic anisotropy, enhanced magnetic susceptibility, and large coercivitity.[24] They also have good chemical stability upon corrosion.[24] For good magnetic performance, it is necessary

to have control of the growth mechanism. This includes controlling non-random nucleation and growth, large crystalline sizes, and broad size distributions.[24] Chemical approaches, rather than physical grinding provide better control of the size and growth of the particles.[24] To form solid solution particles, $Co_2(CO)_8$ and $Pt(hfac)_2$ were used in a redox transmetalation reaction.[24] To form a core-shell structure, $Pt(hfac)_2$ was reacted with pre-formed Co nanoparticles.[24]

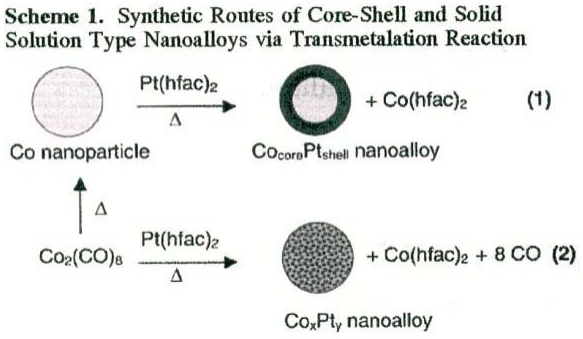

Figure 2.10: Synthesis schematic for CoPt nanoalloys[24]

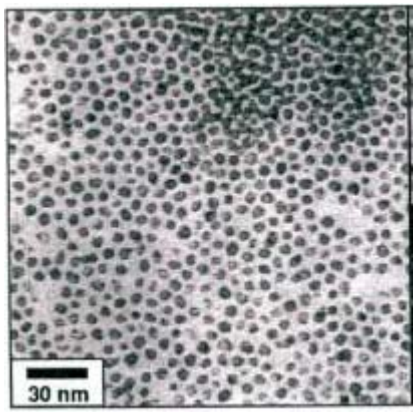

Figure 2.11: $CoPt_3$ nanoalloy synthesized by simultaneous cluster formation[24]

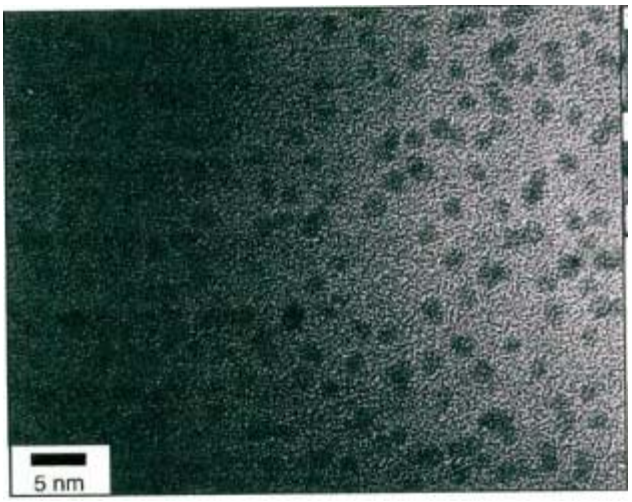

Figure 2.12: $Co_{core}Pt_{shell}$ nanoalloy[24]

TEM results indicate non-agglomerated, monodisperse nanoparticles with average diameter 1.8 nm.[24]

When gold nanoclusters with a narrow size distribution are created, the system is able to self assemble and develop ordering.[20] For example, a bimodal size distribution of particles may exhibit 3-D ordering.[25] Also, using the solution method of assembly, the system may show long range ordering.[25]

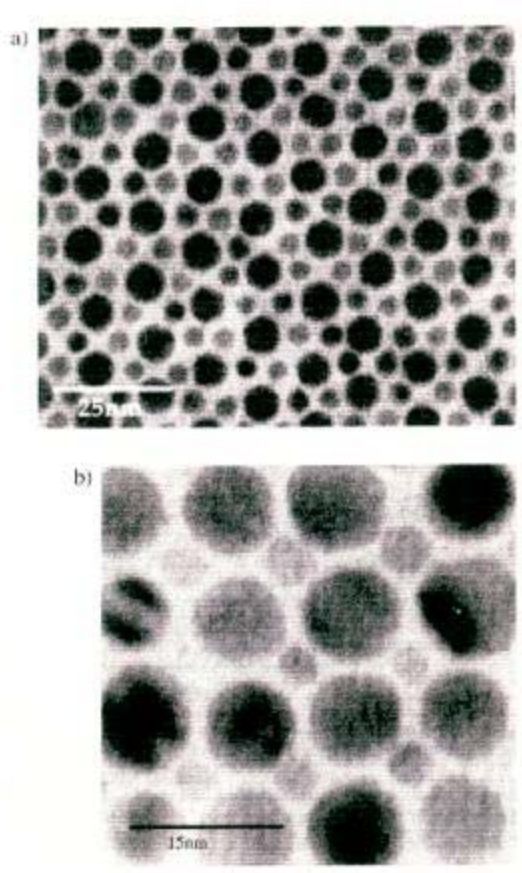

Figure 2.13: Bimodal Au particles form (a) ordered AB_2 and (b) ordered AB superlattice arrays[20]

Co nanoclusters have been produced via solution phase synthesis via the reduction of CoCl in solution containing colloidal stabilizers.[26] Metastable Co clusters can be produced via this method, capped with a 2 nm thick monolayer of oleic acid stabilizer.[26] These particles are dispersed in octane and allowed to settle into a nanocrystalline superlattice.[26] Lithography was used to form electrodes using the array of particles, which form an hcp structure.[26] Annealing of the structures also removes the

oxide coat that forms on the structure during handling.[26] The hcp structure is well ordered over the critical device size, making this system suitable for constructing a uniform device.[26] The lithography process makes it possible to create structures that have current carrying paths less than 7 nanocrystals in width.[26] Because of the oleic acid coating, the nanocrystals are electrically isolated from each other, eliminating the possibility for short circuits across particles.[26]

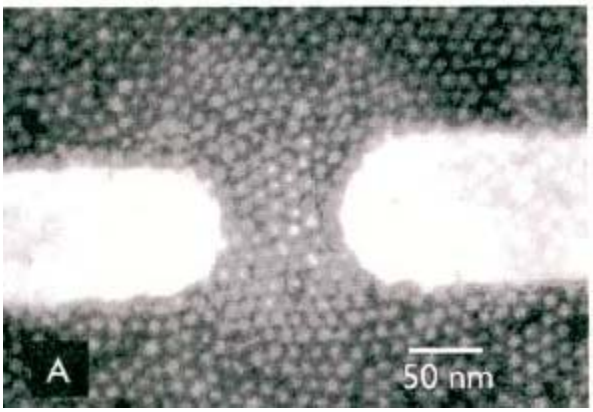

Figure 2.14: SEM image of self-assembled CO superlattice device[26]

Stable nanosized iron colloids have been produced via sonochemical decomposition of organometallic compounds.[27] The colloids have a narrow size distribution, an important aspect for magnetic storage possibilities.[27] The sonochemical method involves the formation, growth, and collapse of bubbles in liquid.[27] The bubble collapses create areas with very high transient temperatures and very large cooling rates.[27] These areas are ideal for the decomposition of the organometallic compounds. Without a stabilizer, the metal atoms formed by this thermal decomposition will agglomerate freely and form bulk material. In the presence of a stabilizer, nanosized iron

colloids may be produced.[27] In this system, polyvinylpyrrolidone (PVP) was used as a stabilizer while $Fe(CO)_5$ was decomposed in octanol under argon.[27] The iron particles produced via this synthesis method are fairly monodisperse, with average diameters 3-8 nm.[27]

Also, oleic acid has been used as a stabilizer.[27] The double bond in the oleic acid interacts with the cluster surface, and the clusters are a bit larger (8 nm diameter) but much more uniform in size. These particles show no hysteresis loops in magnetic analysis and are superparamagnetic. This property is important for the preparation of magnetic ferrofluids.[27]

A benefit of metal nanoparticles over bulk metals is the ability to greatly increase the surface area exposed and the ability to functionalize the surface.[28] In another work, monodisperse FePt nanoparticles were produced with controlled size and composition and have positioned themselves into superlattice assemblies.[28] These particles have been deposited on thin films.[28]

Stabilizers, oleic acid and oleyl amine, were used to limit particle size.[28] The metal clusters were formed by the reduction of $Pt(acac)_2$ and thermal decomposition of $Fe(CO)_5$.[28] Size and composition of these particles are controlled by adjusting reaction conditions. Composition is altered by changing the ratio of $Pt(acac)_2$ and $Fe(CO)_5$ precursors. The particle size is controlled by growing seed particles of a specific size in solution, then adding more precursor to cap the particles.[28]

Nanoalloys of Fe and Pt may be important due to their unique magnetic properties. They have a very large uniaxial magnetic anisotropy. [28] Because of this anisotropy, these particles may be suitable for magnetic recording. When the particles

are annealed, they may change phase and become even more useful. The coercivities of the particles may be tuned by adjusting annealing temperature of the particles, the annealing time, the final particle size, and the Fe:Pt ratio.[28] The distance between particles (maintained by the presence of the oleic acid or oleyl amine coating) may be adjusted by ligand exchange reactions, replacing the long chains with shorter ones. [28]

Nanoparticles for industrial usage need to be uniform in size, shape, composition, structure, and surface chemistry in order to be useful for industrial applications.[29] Nanoclusters of monodisperse sizes can be used to create close packed solids. These solids have unique properties, which combine the characteristics of the individual clusters with those of the interacting nanoclusters. [29]

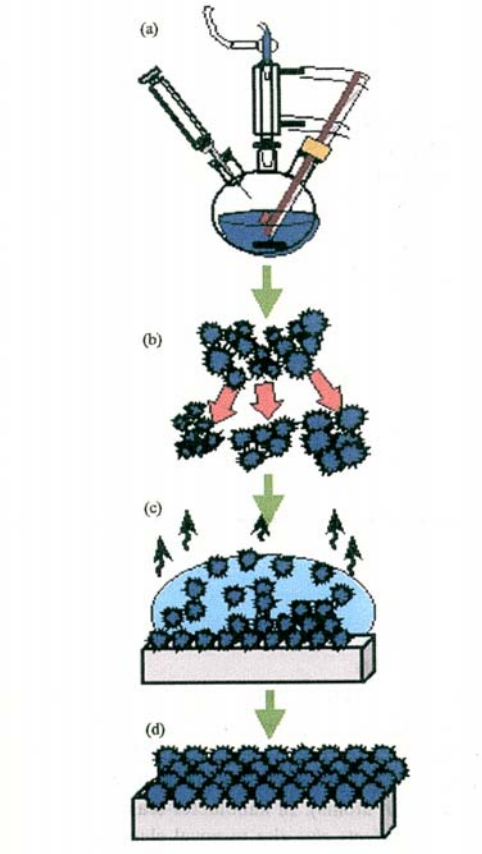

Figure 2.15: Diagram of self-assembly process (a) synthesis, (b) selection of monodisperse particles, (c) self-assembly of particles on surface, (d) 3-D superlattice[29]

2.4 Relevance of background and current project

A variety of methods have been discussed in this background to synthesize metal nanoparticles and nanoalloys. Many of these methods have drawbacks (such as by-products in solution or safety issues) or have not paid careful attention to important aspects of the kinetics of the formation process, which does not allow for the control of composition of the produced nanoclusters. In this study, nanoalloys have been synthesized in this work via the decomposition of organometallic carbonyl precursors. The kinetics of metal cluster formation via the decomposition of these precursors may be analyzed using Fourier transform infrared spectroscopy (FT-IR). As the precursor decomposes, characteristic carbonyl bands from the samples will disappear. This represents the formation of clusters and release of CO gas. In this study, the kinetics associated with the decomposition of the metal carbonyls, and consequently the formation of metal nanoalloys will be considered of utmost importance. The decomposition of metal carbonyls has been previously used to produce nanoalloys, but little emphasis has been placed on the kinetics of the systems so it is impossible to assume that the morphologies are controlled. Therefore, this study will determine the conditions needed to optimize control nanoparticle formation by investigating decomposition kinetics of individual precursors and mixed metal carbonyl systems. A variety of metal carbonyls have been chosen to determine the effect of composition on the kinetics of decomposition and the resulting formation of nanoparticles.

CHAPTER 3

EXPERIMENTAL PROCEDURES

3.1 Overview

This chapter discusses the materials, experimental procedures, and characterization techniques used in this work. Section 3.2 discusses the materials used for the synthesis of FeCo nanoalloys. Section 3.3 discusses the experimental procedure used to decompose metal carbonyls, and therefore, for metal nanoparticles. Section 3.4 discusses the formation of nanoalloys using $Fe(CO)_5$ and $Co_2(CO)_8$. Section 3.5 discusses the formation of FeCo nanoalloys from precursors other than $Fe(CO)_5$ and $Co_2(CO)_8$. Section 3.6 discusses techniques used to characterize the metal nanoalloys.

3.2 Materials

Polymethyl methacrylate (120,000 M_W) and poly(vinylidene fluoride) were obtained from Aldrich and polystyrene (100,000 M_W) was obtained from Avocado Chemicals. $Fe(CO)_5$, $Co_2(CO)_8$, $Co_4(CO)_{12}$, and $Co(CO)_2C_5H_5$ were obtained from Alfa Aesar.

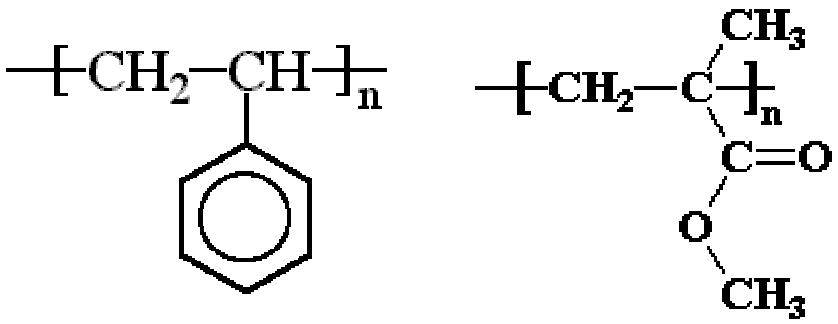

Figure 3.1: Structure of a) polystyrene and b) polymethyl methacrylate[32]

3.3 Kinetic analysis of the decomposition of metal carbonyls

3.3.1 General overview of metal carbonyl decomposition

As mentioned previously, in this study FeCo nanoalloys were formed from the decomposition of metal carbonyls in the presence of a polymer solution. Of utmost importance for the formation of controlled-composition FeCo nanoalloys, is a kinetic analysis of the decompositions of the materials. In order to obtain kinetic data, metal carbonyls were decomposed in a polymer solution. For the majority of decompositions, the polymer was dissolved in solvent to obtain a solution with polymer concentration just below c* (critical coil overlap). Critical coil overlap is the concentration where polymer chains begin to overlap, and is calculated as follows:

$$C^* = \frac{1}{K} \cdot M^{-a}$$

where K and a are system defined constants, and M is the molecular weight of the polymer. Two polymers, polystyrene and polymethylmethacrylate were used most commonly in this study. The properties of these materials can be found in Table 3.1.

Table 3.1: C* calculated for the polymer/solvent combinations used for carbonyl decompositions[33]

Polymer	**Solvent**	**Molecular Weight**	**k**	**a**	**c***
Polystyrene (PS)	Toluene	100,000	0.00754	0.783	1.86 wt%
Polymethylmethacrylate (PMMA)	Chlorobenzene	120,000	0.00724	0.76	1.87 wt%

The solution was heated at 70°C for 12 hours in order to dissolve the polymer. Once the polymer was dissolved, the solution was heated in a jacketed three-neck flask to 90°C via an ethylene glycol bath, and flushed with dry nitrogen. The three necks of the flask were attached to an Ahllin condenser for water cooling, a rubber stopper for sample access, and a nitrogen line to minimize iron oxidation, respectively.

A 0.5 mL aliquot of the polymer solution was removed with a syringe from the flask via the rubber stopper and introduced into a Spectra-Tech liquid demountable cell with a 0.2mm Teflon spacer and KBr windows. During sample removal, nitrogen was used to purge the flask and keep oxidation to a minimum. The cell was placed into a Nexus 870 FT-IR spectrometer, and after the infrared sample compartment was sealed and purged, an initial solution spectrum was taken. After data acquisition, the cell was cleaned and rinsed using a vacuum system and excess solvent.

Once the initial spectrum of the polymer solution was taken, the appropriate amounts of metal carbonyl were added to the three-neck flask to obtain a known concentration carbonyl solution. The solution was flushed with nitrogen while the carbonyl was added and the mixture was continuously heated at 90°C. An initial sample of the undecomposed metal carbonyl in solution was removed via the rubber stopper neck. A spectrum of the initial metal carbonyl solution was measured and subsequently, the cell was flushed and cleaned as previously described. Aliquots were removed every 10 or 15 minutes during the decomposition and their infrared spectra were recorded.

The spectra were analyzed using Nicolet Omnic 5.2 software. Once the characteristic carbonyl bands on the spectrum had completely disappeared, the reaction was stopped and the solution was stored in vials under nitrogen. The spectrum from the

polymer solution was subtracted from each decomposition spectrum in order to observe only the vanishing carbonyl bands present in the decomposing carbonyl species. Peak heights for the characteristic peaks were recorded with respect to time.

3.3.2 Analysis of kinetic data

Carbonyl concentrations in the polymer solution were calculated using the following relationship:

$$A = \varepsilon \cdot d \cdot c$$

where A is the absorbance (proportional to the peak height), ε is the extinction coefficient, d is the optical path (equal to the spacing between the cell windows) and c is the concentration. The extinction coefficient for the system was determined using a series of standards with known concentrations. The optical path for the system is a fixed parameter and knowing the absorbance and optical path, one can calculate extinction coefficient. Using the extinction coefficient, the carbonyl concentrations at given times throughout the decomposition process were calculated, thereby providing kinetic information.

To determine reaction order of the decompositions, plots of carbonyl concentration versus time were constructed. A linear plot of ln (c/c_o) versus time indicates a first order decomposition system, and a linear plot of $1/(c/c_o)$ versus time indicates a second order decomposition system.

Table 3.2: Characteristic IR carbonyl bands for precursors used in this study[34]

$Fe(CO)_5$	$Co_2(CO)_8$	$Co_4(CO)_{12}$	$Co(CO)_2C_5H_5$
2019 cm^{-1} and 1996 cm^{-1} asymmetric and symmetric CO stretches	1858 cm^{-1} bridging CO groups 2030, 2065 cm^{-1} terminal CO groups	1867 cm^{-1} bridging CO group 2058 cm^{-1} terminal CO group	2026 cm^{-1} and 1963 cm^{-1} asymmetric and symmetric CO stretches

3.4 Synthesis of nanoalloys via thermal decomposition of $Fe(CO)_5$ and $Co_2(CO)_8$

3.4.1 Kinetic impact on synthesis method

Since the decomposition rate and reaction order of $Fe(CO)_5$ have been extensively studied[29,30], its reaction kinetics were combined with those of $Co_2(CO)_8$ (also previously studied) in order to construct reaction parameters that induce equal precursor decomposition rates. The appropriate iron and cobalt carbonyl concentrations to co-decompose were chosen in order to relate concentration to decomposition rate constant, which will be further discussed in Chapter 4. Adding the appropriate amounts of these precursors to a solution of polystyrene and toluene and decomposing them simultaneously, the attempt was to create mixed-composition nanoalloys.

The kinetics of this mixed carbonyl decomposition was also studied as previously described in order to test the effectiveness of controlling decomposition rate with the carbonyl concentration ratio. Aliquots of the resulting solution were removed to create TEM samples. The solution was dried in a Petri dish and analyzed with TGA, which burned away the polymer. After TGA the powder was not protected from oxidation, but composition analysis will account for the presence of oxidized metal (in the shell) and zero-valent metal (in the core, protected by the shell metal).

3.4.2 Utilization of bulk phase diagrams to produce nanoalloys

Another method for manipulating the microstructure and composition of nanoalloys was a study of the bulk binary phase diagram of the Fe-Co system. At 90°C (the synthesis temperature with the organometallic decomposition technique) there are three types of possible FeCo crystal structures depending on composition. Two decomposition scenarios were constructed to create nanoalloys with compositions in either the hcp or α+β regions in the phase diagram at the synthesis temperature. The chosen compositions were 2wt% Fe/ 98wt% Co (hcp region) and 10wt% Fe/ 90wt% Co (α+β region). The controlled release of metal ions was performed by determining the correct ratios of metal carbonyl needed in the solution upon decomposition. For one system, the ratio of Fe to Co ions released during decomposition was 2/98 while in a second system, a 10/90 ratio was chosen. These experiments were performed in a c* solution of polystyrene and toluene. The kinetics of these systems were studied as previously explained. Aliquots of the resulting solution were removed to create TEM samples. The solution was dried in a Petri dish and analyzed with TGA, which burned away the polymer.

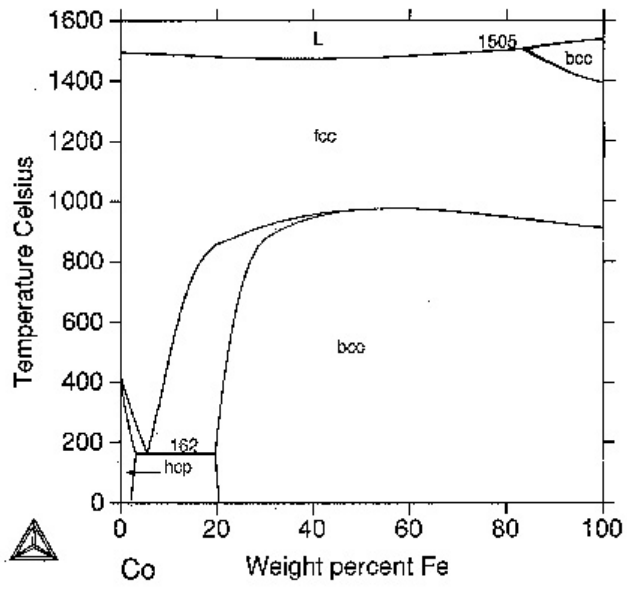

Figure 3.2: Bulk phase diagram of the binary FeCo system[35]

3.4.3 Determination of the effect of polymer composition

The previous syntheses were performed in a solution of polystyrene and toluene. Previous work has shown a change in resulting nanocluster structure when the stabilizing polymer is varied.[38] Therefore, to determine the effect of polymer composition on the formation of nanoalloys, several decompositions were performed in PMMA and chlorobenzene (c* concentration) solutions in order to study the kinetic and structural differences when the solvent system is changed. First, $5 \cdot 10^{-3}$ M $Fe(CO)_5$ was decomposed alone in a PMMA/chlorobenzene solution in order to examine its reaction kinetics in this solvent system. The kinetics of $Co_2(CO)_8$ in this solvent system was previously established.[36] Once the kinetics of the individual metal carbonyls were established, a second decomposition of equal amounts ($5 \cdot 10^{-3}$M of each) of $Fe(CO)_5$ and $Co_2(CO)_8$ was performed in order to examine the mutual influence, if any, on each others decompositions.

A third decomposition was performed using specifically chosen concentrations of the metal carbonyls in order to induce equal initial decomposition rates, which will be discussed further in Chapter 4.

3.4.4 Optimization of decomposition conditions

Using the kinetics of the precursor decompositions, a ratio of concentrations and rate constants was constructed in order to determine appropriate concentrations of metal carbonyls to combine to induce equal initial decomposition rates. Inputting in the experimentally determined individual rate constants and choosing the concentration of $Co_2(CO)_8$ to be $5 \cdot 10^{-3}$ M, the appropriate concentration of $Fe(CO)_5$ to add was calculated as $6.22 \cdot 10^{-2}$ M. These amounts of metal carbonyl were co-decomposed as previously described and the decomposition kinetics were closely monitored and analyzed. Aliquots of the resulting solution were removed to create TEM samples. The solution was dried in a Petri dish and analyzed with TGA, which burned away the polymer.

3.4.5 Synthesis of mixed-metal nanoalloys

A different approach was taken to synthesize mixed-metal nanoalloys with a unique morphology. Previous work involved the synthesis of Fe_2O_3 particles by the decomposition of $Fe(CO)_5$ (.3217 M) in a solution of poly vinylidene fluoride (PVF_2, Alfa Aesar) in N,N dimethylformamide (DMF, Fisher)[37,40]. This procedure was modified to include $Fe(CO)_5$ and $Co_2(CO)_8$ in order to create mixed composition nanoalloys. 1g of PVF_2 pellets were added to 9.48 ml DMF and mixed for 6 days. $Fe(CO)_5$ and $Co_2(CO)_8$ were added to the solution (each at .16 M) and magnetically stirred. The solution was mixed for six days at room temperature. Since the decomposition of the carbonyl species occurred without added simultaneous heat and drying, this method was considered to be a

"cold method". The resulting nanoclusters were assumed to be mixed-metal oxides, as during the procedure the solution was not protected from air. FT-IR analysis was impossible for this method due to the high concentrations of polymer and metal carbonyls in the solution. After decomposition, aliquots were removed for TEM analysis.

3.5 Utilization of other cobalt carbonyls to form nanoalloys

3.5.1 Kinetic analysis and nanoalloys from $Fe(CO)_5$ and $Co_4(CO)_{12}$

Because of the drastically different decomposition rates of $Fe(CO)_5$ and $Co_2(CO)_8$ and the desire to create mixed nanoalloys, there was a need to find more kinetically similar precursors. One such possibility is the replacement of $Co_2(CO)_8$ with $Co_4(CO)_{12}$.

$Co_4(CO)_{12}$ is an intermediate in the decomposition of $Co_2(CO)_8$ into Co and CO gas, and it follows that the decomposition of $Co_4(CO)_{12}$ is the rate-determining step in this process.[36] A $5 \cdot 10^{-3}$ M solution of $Co_4(CO)_{12}$ in polystyrene and toluene was decomposed at 90°C in order to determine its decomposition rate constant and reaction order. Found to be a first order process, its rate constant and reaction order were used to construct a relationship between kinetics and solution concentrations. Choosing the concentration of $Co_4(CO)_{12}$ to be $2.5 \cdot 10^{-3}$ M, the appropriate concentration of $Fe(CO)_5$ as $6.94 \cdot 10^{-3}$ M was determined. This ratio of concentrations should produce conditions that will induce equal decomposition rates and thus mixed composition nanoalloys. In order to determine the mutual effects of the decompositions of $Co_4(CO)_{12}$ and $Fe(CO)_5$ on each other, equal amounts ($2.5 \cdot 10^{-3}$ M of each) were simultaneously decomposed. A third decomposition with reverse molar ratios of the "equal rates" method was performed in order to examine the mutual influence of these decompositions over a broader range of

compositions ($2.5 \cdot 10^{-3}$ M $Co_4(CO)_{12}$, $7 \cdot 10^{-3}$ M $Fe(CO)_5$). The kinetics of all of the trials were combined and manipulated in order to determine the ideal molar concentration ratios for producing well-mixed composition nanoclusters. Aliquots of the resulting solutions from these decompositions were removed to create TEM samples. The solutions were dried in a Petri dish and analyzed with TGA, which burned away the polymer.

3.5.2 Kinetic analysis and nanoalloys from $Fe(CO)_5$ and $Co(CO)_2C_5H_5$

A third cobalt precursor was studied, $Co(CO)_2C_5H_5$. This species is not commonly utilized in laboratory conditions and its decomposition kinetics has not been well characterized. However, the presence of the cyclopentyl ligand presents the possibility of slowing down the release of the CO ligands, thus better matching the decomposition rate of the $Fe(CO)_5$ species.

Initially, a solution of $Co(CO)_2C_5H_5$ ($5 \cdot 10^{-3}$ M) was decomposed in a polystyrene/toluene solution. Its decomposition kinetics was studied and determined to be a second order process with a relatively slow reaction rate (as described in subsequent chapters). Because its reaction order matched that of the $Fe(CO)_5$ species and the decomposition rates were fairly similar, the construction of a relationship connecting kinetics and concentrations was unnecessary. Equal amounts of these precursors co-decomposed should have the same reaction order and similar reaction rates, creating mixed composition clusters. The next decomposition, an attempt to create mixed composition nanoalloys, involved equal amounts ($2.5 \cdot 10^{-3}$ M of each) of $Fe(CO)_5$ and $Co(CO)_2C_5H_5$. A third decomposition, with $1.75 \cdot 10^{-3}$ M $Co(CO)_2C_5H_5$ and $1.72 \cdot 10^{-3}$ M $Fe(CO)_5$ was performed in order to further examine the mutual effects of these species

decompositions. Kinetics of all of these reactions were studied using FT-IR. Aliquots of the resulting solutions were removed to create TEM samples. The solution was dried in a Petri dish and analyzed with TGA, which burned away the polymer.

3.6 Characterization methods

3.6.1 TEM

Transmission electron microscopy was used in order to determine the morphology and composition of metal nanoclusters. TEM produces a two-dimensional projection image of a three-dimensional structure. Samples are thin specimens that may be magnified between 100-100,00 times.[30] Using TEM, one may determine the structure of a crystalline sample using selected area apertures with electron diffraction. A disadvantage of this technique is that the samples must be very thin. If the samples are not adequately thin, the number of inelastic collisions will increase dramatically, causing a loss of resolution.[30] Resolution may also be limited by diffraction aberrations, chromatic aberrations due to unstable beam or lens current, astigmatism, or spherical aberrations due to lens imperfections.[30] Thin samples for this study were produced via a liquid method, dipping a film-coated grid into a solution of the nanoalloys.

Characterization of nanoparticles and nanoalloys were performed using TEM. Nanoparticles were deposited on copper TEM grids (Ted Pella) by dropping a dilute concentration of polymer-nanoparticle solution onto the TEM grid. The solvent was then allowed to air dry.

TEM was performed using a Hitachi 100C. TEM micrographs were obtained using Kodak electron microscopy film and developing the film in a darkroom. TEM

images were used to determine the size and shape of nanoclusters formed under the given conditions. Particle sizes (in the case of spherical particles, diameters) were measured on the negatives and converted to actual sizes using the magnification of the microscope. These particle sizes were compiled and statistically analyzed to determine average particle size and deviation in size. Electron diffraction spectra were also obtained for several of the samples. Electron diffraction was used to determine the crystal structure of the nanoclusters to allow for comparison against the structure of bulk systems.

3.6.2 TGA

TGA was used to decompose polymer matrix in the polymer-nanoparticle systems. TGA was performed using a Thermal Analysis (TA) Model XY TGA. Some samples were also tested using a Netzsch STA409 PC Luxx TGA/DSC. Samples were heated a rate of 10 ^{o}C/min to 600. The two polymers decompose between 300-400 ^{o}C by a chain scission mechanism, and therefore lose ~ 95 % of their weight.

TGA was used for two different purposes in this study. First, analysis of the rate of decomposition gives insight into the surface chemistry of the clusters and how the polymer is bound to the metal nanoclusters surfaces, and in turn this gives insight into nanocluster structure. Second, TGA was used to remove the polymer from the metal nanoparticles for characterization techniques that required bare clusters. This powder was not protected from oxidation, but compositional analysis examines the presence of metal oxides (in the shell of the clusters) and zero-valent metals (in the cores of the clusters, protected from oxidation by the shell metal).

3.6.3 Infrared Spectroscopy

Fourier transform infrared spectroscopy is a method of identifying chemical species present in a sample. Each molecule has a specific ground state energy that is a product of vibrational, electron, rotational, and electromagnetic energies.[31] These energies can be increased or decreased by the absorption of electromagnetic radiation at discrete frequencies.[31] Only specific radiation that strikes a polymer system is in the infrared region of the spectrum.[31] At certain absorbed frequencies, this radiation is converted into asymmetric molecular motions between dissimilar atoms. The atoms must be dissimilar in order to observe an absorption- the molecule must have an intrinsic dipole. For example, this radiation can manifest itself as a C-H stretch, a C-H twist, or a C-H wagging.[31] FT-IR measures the absorption of each of these motions and using computer software, plots the absorbance versus frequency, or wavenumber.[31] By analyzing these molecular motions, the chemical makeup of an unknown sample may be determined. For this research, a known sample will be used as a standard and other samples will be analyzed with respect to this sample to track the progress of the decomposition reaction.

3.6 Relevance of background and current project

A variety of methods have been discussed in this thesis to synthesize metal nanoparticles and nanoalloys. Many of these methods have drawbacks (such as by-products in solution or safety issues) or have not paid careful attention to important aspects of the kinetics of the formation process, which does not allow for the control of composition of the produced nanoclusters. In this study, nanoalloys have been synthesized in this work via the decomposition of organometallic carbonyl precursors. The kinetics of

metal cluster formation via the decomposition of these precursors may be analyzed using Fourier transform infrared spectroscopy (FT-IR). As the precursor decomposes, characteristic carbonyl bands from the samples will disappear. This represents the formation of clusters and release of CO gas. In this study, the kinetics associated with the decomposition of the metal carbonyls, and consequently the formation of metal nanoalloys will be considered of utmost importance. The decomposition of metal carbonyls has been previously used to produce nanoalloys, but little emphasis has been placed on the kinetics of the systems so it is impossible to assume that the morphologies are controlled. Therefore, this study will determine the conditions needed to optimize control nanoparticle formation by investigating decomposition kinetics of individual precursors and mixed metal carbonyl systems. A variety of metal carbonyls have been chosen to determine the effect of composition on the formation of the kinetics of decomposition and the resulting nanoalloys.

CHAPTER 4

$Fe(CO)_5$ and $Co_2(CO)_8$ Based Systems

4.1 Chapter Overview

This chapter discusses several synthesis methods that were developed for the production of FeCo nanoalloys using $Fe(CO)_5$ and $Co_2(CO)_8$. Section 4.2 will discuss the impact and control of kinetics in order to promote equal decomposition rates of the two metal carbonyl species. 4.3 involves creating nanoalloys based on the bulk binary phase diagram. 4.4 describes the effect of polymer stabilizer on the formation of nanoalloys. 4.5 discusses the formation of FeCo oxides with a novel shape in PVF_2 and DMF.

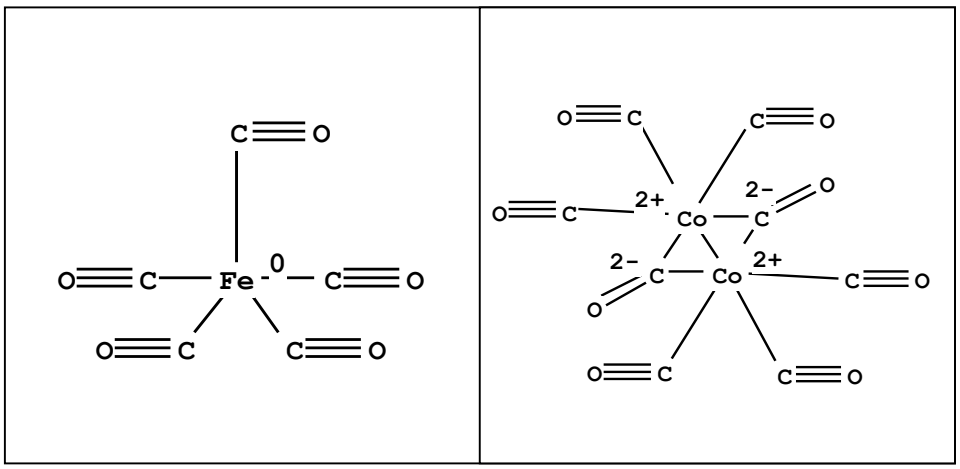

Figure 4.1: $Fe(CO)_5$ and $Co_2(CO)_8$, the metal carbonyls used in this portion of the study

4.2 Control of kinetics to form mixed-composition nanoalloys

In order to synthesize mixed-composition nanoalloys, the kinetics of both the iron and the cobalt precursors need to be considered. If one species decomposes much more quickly than the other, there is the possibility of creating nanoclusters composed of single

metals or nanoclusters with a "capped" structure, with the quicker-decomposing species forming a core and the slower-decomposing species forming a shell later on that core. The decomposition kinetics of $Fe(CO)_5$ and $Co_2(CO)_8$ have been extensively studied previously,[10,36,39] and this information was compiled in order to construct reaction conditions that would produce mixed-composition nanoalloys. For these conditions, the normalized concentrations of each species are given by the following expressions:

$$c'_{Co} = c_1' = \frac{c_1}{c_1 + c_2} \quad \text{and} \quad c'_{Fe} = c_2' = \frac{c_2}{c_1 + c_2}$$

where $c_1 = c_{Co}$ and $c_2 = c_{Fe}$. The decomposition of $Fe(CO)_5$ is a second order reaction and the decomposition of $Co_2(CO)_8$ is a first order reaction (Table 4.1), therefore, in order to achieve equal initial decomposition rates the following requirement is necessary:

$$k_{Fe} \cdot (c_2')^2 = k_{Co} \cdot c_1'$$

Substituting the expressions for the precursor concentrations, the following relationship is obtained:

$$\frac{k_{Fe}}{k_{Co}} = \left(\frac{c_1}{c_2}\right)^2 + \frac{c_1}{c_2}$$

Solving this quadratic equation and selecting only the positive result, the relationship between the initial concentrations of the iron and cobalt precursors can be determined. In subsequent discussions this equation will be referred to as the quadratic relationship, or the equal rates relationship.

If the initial concentration of one of the precursors is known (or is chosen), the initial concentration of the other precursor is determined, and the initial rates can be controlled to accommodate a simultaneous initial decomposition reaction of both metal carbonyls.

Table 4.1: Comparison of rate constants and reaction order for the decomposition of iron pentacarbonyl and di-cobalt octacarbonyl in pure solvents and in solutions containing polystyrene[10]

Organometallic Precursor	Reaction Order	Rate Constant
$Co_2(CO)_8$ + PS	1	$1.38 \pm 0.23 \cdot 10^{-4}$
$Fe(CO)_5$ + PS	2	$7.28 \pm 1.89 \cdot 10^{-5}$
$Co_2(CO)_8$ + PS ($+Fe(CO)_5$)	1	$1.23 \pm 0.48 \cdot 10^{-4}$
$Fe(CO)_5$ + PS ($+Co_2(CO)_8$)	2	$1.35 \pm 0.54 \cdot 10^{-4}$
$Co_2(CO)_8$ (in Toluene)	1	$1.03 \pm 0.11 \cdot 10^{-5}$
$Fe(CO)_5$ (in Ethylbenzene)	2	$8.45 \pm 0.86 \cdot 10^{-6}$

Using the equal rates relationship, known experimental rate constants for these species in polystyrene and toluene (Table 4.1), and choosing $[Co_2(CO)_8] = 2.5 \cdot 10^{-3}$ M. The appropriate molar concentration of $Fe(CO)_5$ to induce equal decomposition rates was calculated and equal to $3.78 \cdot 10^{-3}$ M. Volatility and difficulties in dissolving of the

precursors result in experimental metal carbonyl concentrations that vary from the intended concentrations. The actual metal carbonyl concentrations in solution during the decomposition were calculated using the previously described equation with the system-specific extinction coefficient ε, optical path length, and the characteristic carbonyl peak heights.

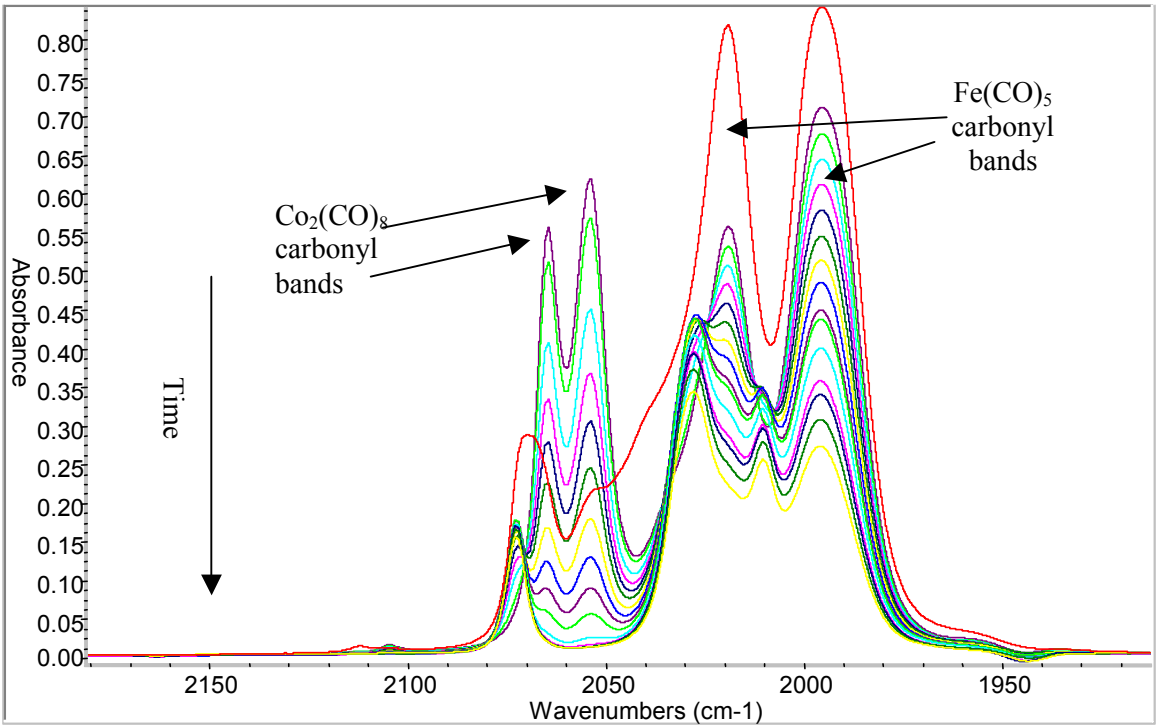

Figure 4.2: FT-IR spectra of the formation of FeCo nanoclusters via the co-decomposition of $Fe(CO)_5$ and $Co_2(CO)_8$

The actual concentrations of the metal carbonyls decomposed in this trial were $[Co_2(CO)_8] = 3.3 \cdot 10^{-3}$ M and $[Fe(CO)_5] = 7.5 \cdot 10^{-3}$ M. The characteristic carbonyl peak for $Fe(CO)_5$ is located at 1995 cm^{-1} and for $Co_2(CO)_8$ is located at 1860 cm-^{1}.[1,10,34,36]

Plotting metal carbonyl concentrations with respect to time allows calculation of reaction order and decomposition rate for the carbonyl species. A linear plot of ln (c/c_o) (where c is the carbonyl concentration and c_o is the initial carbonyl concentration)

indicates a first order process and a linear plot of $1/(c/c_o)$ indicates a second order process. The slopes of these plots provide the decomposition rate constants of these decompositions.

Comparing the decomposition rate constants of the combined carbonyl precursors

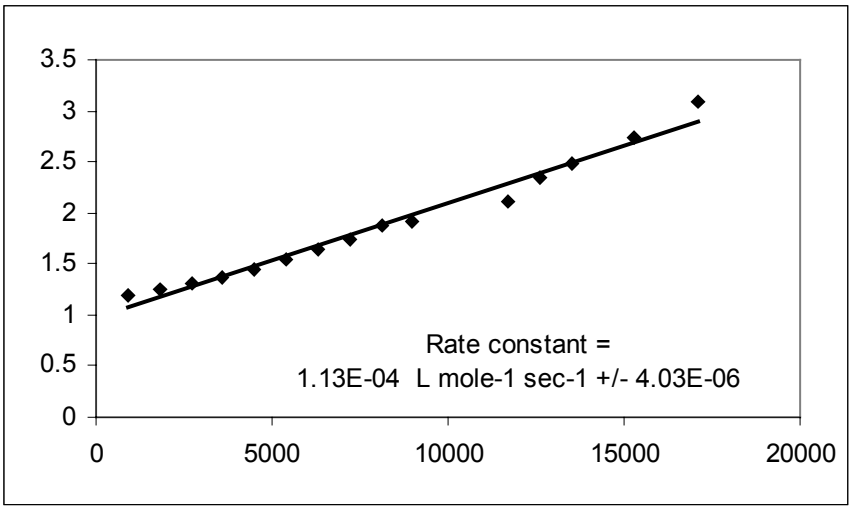

Figure 4.3: Second order decomposition of $Fe(CO)_5$ co-decomposed with $Co_2(CO)_8$

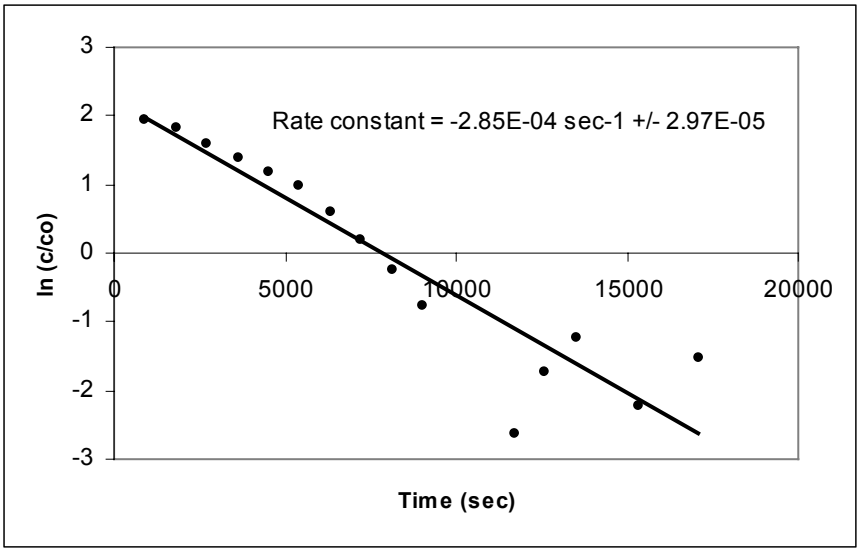

Figure 4.4: First order decomposition of $Co_2(CO)_8$ co-decomposed with $Fe(CO)_5$

to those of the individual precursors (indicated by the slopes in Figures 4.3 and 4.4, it shows that there is a slight increase in decomposition rate constants for each of these species. However, the initial decomposition rate constants are actually even more different than they were for the individual species. This indicates a difference in nucleation behavior between the two species, and means that no improvement has been made in the matching of decomposition rates, and thus it is expected that the combination of these concentrations of carbonyls would not produce thoroughly chemically mixed nanoalloys. This combination of carbonyls likely creates a core-shell structure with the quicker-decomposing cobalt carbonyl forming a core and the slower decomposing iron carbonyl forming a shell.

4.2.1 Characterization of nanoalloys with kinetic control

The nanoalloys in this study were characterized using TEM and electron diffraction to determine their size and structure. TEM images (Figure 4.5) show chain structures of nanoparticles with an average size of 10.5 ± 1.5 nm with crystalline areas (indicated by dark spots in the clusters). These dark center regions indicate

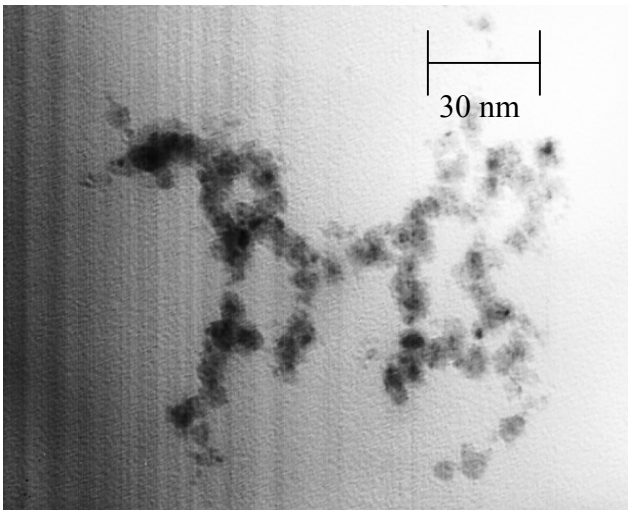

Figure 4.5: High magnification TEM micrograph of FeCo nanoclusters created by the co-decomposition of $Fe(CO)_5$ and $Co_2(CO)_8$

inhomogenaeity in the clusters, which would be expected from the difference in kinetics between the precursors. Because of the kinetic differences, it is predicted that these species have a core-shell morphology. Electron diffraction patterns, Figure 4.7, obtained from a variety of these clusters indicate a bcc structure, which matches the predicted bcc structure from the FeCo bulk binary phase diagram at this composition (calculated to be 46% Co from initial precursor concentrations).

TGA can be used as an analytical technique to examine the surface chemistry of nanoclusters. Films of these nanoalloys in polymer can be heated until the polymer decomposes, and the shape of the polymer decomposition curve gives an indication of the chemical interaction between the clusters and the polymer. These curves can be compared to curves from single metal nanoclusters to determine if their surfaces resemble those of a single type of metal with a steep decomposition slope (such as what a core-shell morphology would exhibit) or have a more gradual slope, indicating a combination of two types of metal-polymer interactions and a mixed cluster surface.

TGA of a film of these nanoalloys resembles that of the single metal species with a steep slope, indicating single metal surface chemistry and providing further support for the possibility of a core-shell morphology.

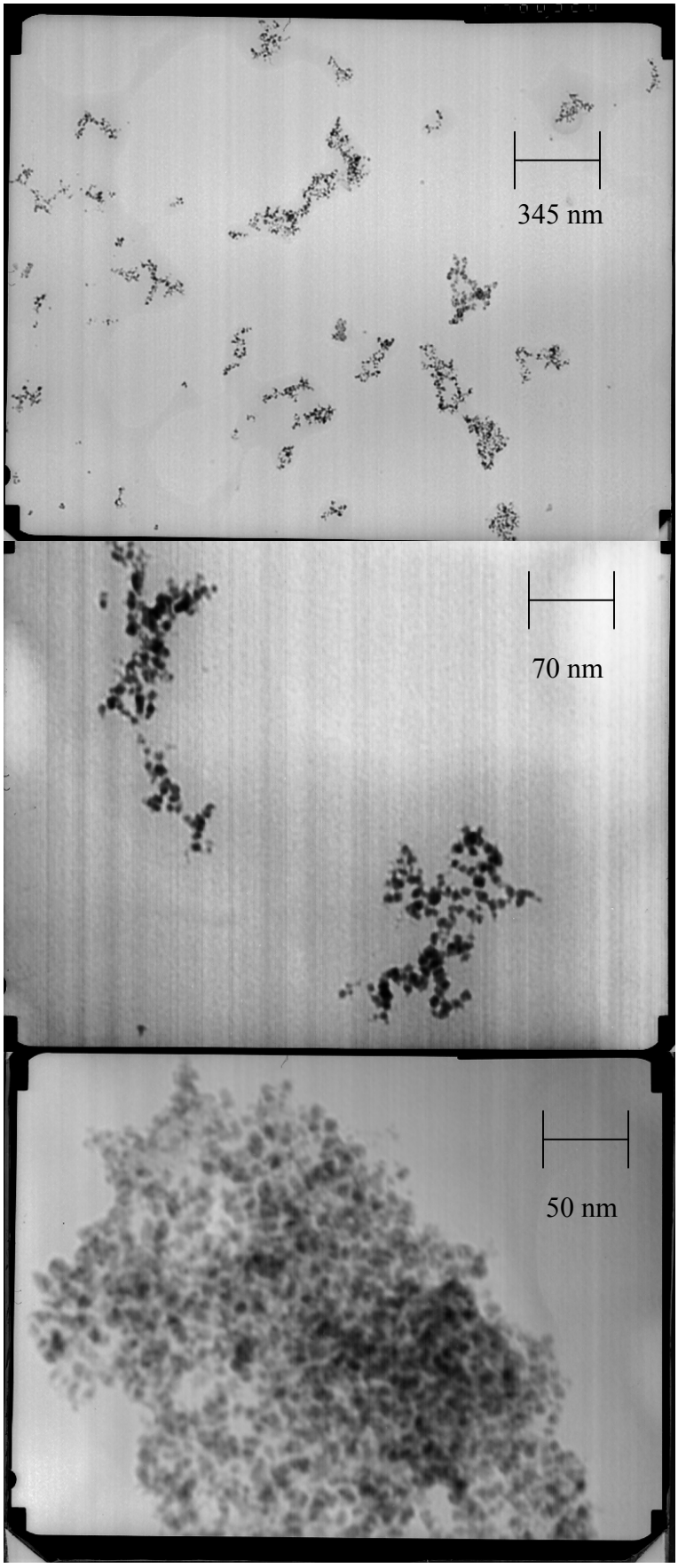

Figure 4.6: TEM micrographs of FeCo nanoclusters produced by the co-decomposition of $Fe(CO)_5$ and $Co_2(CO)_8$

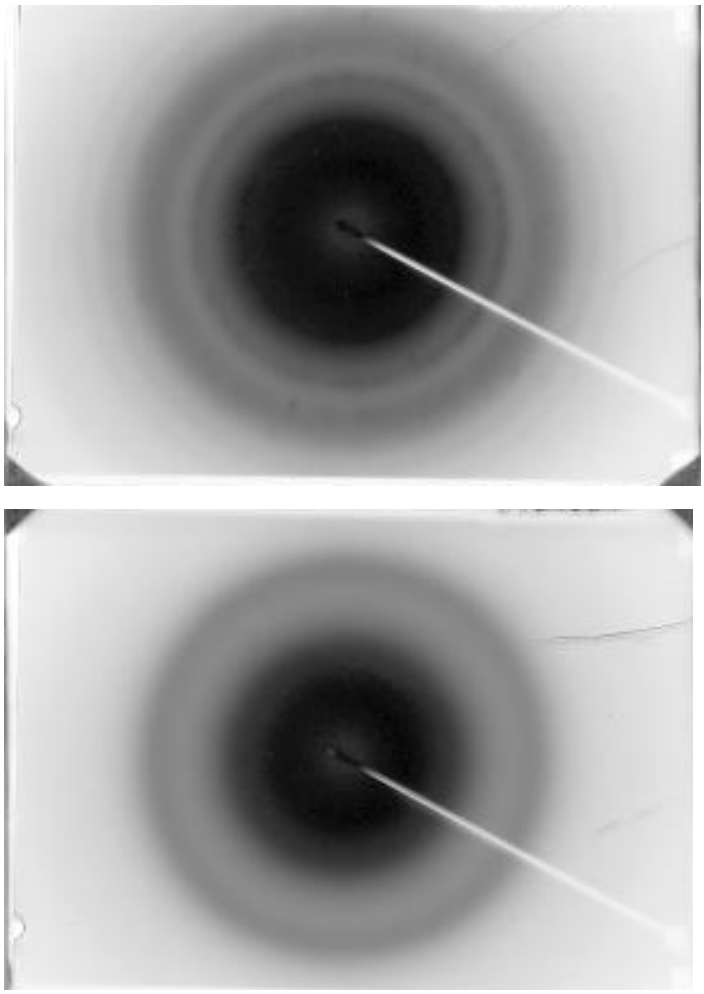

Figure 4.7: TEM diffraction patterns obtained from FeCo nanoalloys indicating a bcc structure

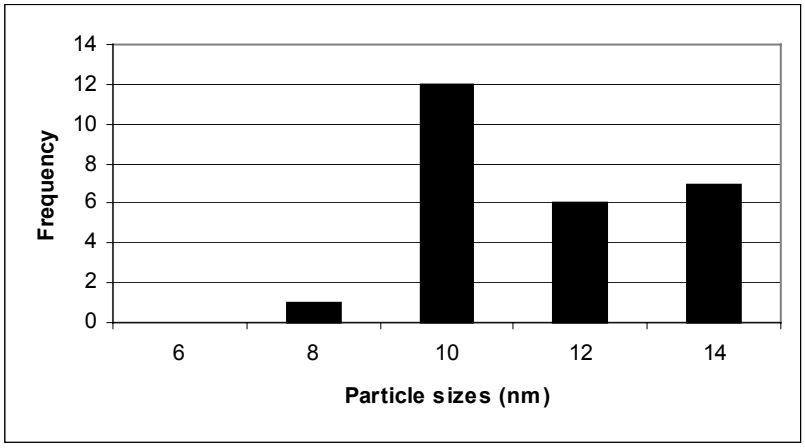

Figure 4.8: Histogram of particle sizes of FeCo nanoalloys

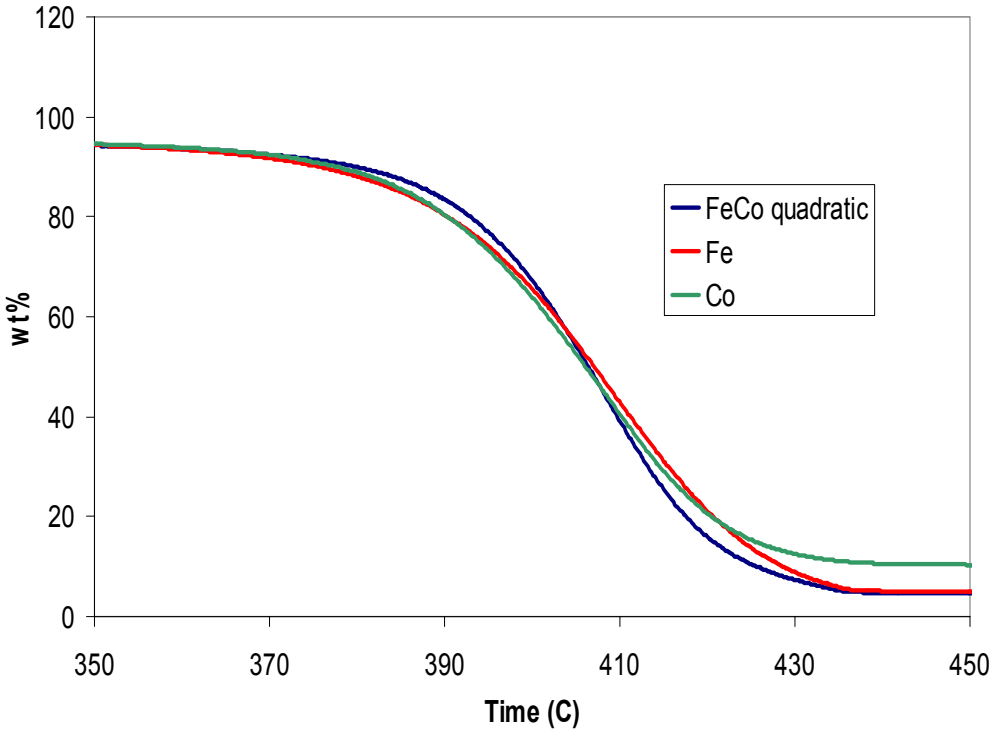

Figure 4.9: TGA curve of FeCo nanoalloys indicating a single metal shell

4.3 Formation of nanoalloys based on binary bulk phase diagrams

4.3.1 2% Fe/98% Co

In order to attempt to create nanoalloys with defined compositions from the bulk FeCo phase diagram, controlled amounts of the carbonyl precursors were co-decomposed. .014 g $Fe(CO)_5$ and 0.37933 g $Co_2(CO)_8$ were combined in a 100 ml solution of polystyrene and toluene in order to produce a solution with a metal atom ratio of 2% Fe and 98% Co as discussed in Chapter 3. Molar concentrations of metal carbonyl that were created were $[Fe(CO)_5] = 2.3 \cdot 10^{-3}$ M and $[Co_2(CO)_8] = 2.0 \cdot 10^{-2}$ M.

Kinetic analysis of the concentrations over time shows a decrease in the decomposition rate of $Fe(CO)_5$ and a decrease in the decomposition rate of $Co_2(CO)_8$ as compared to the individual decompositions of these species.

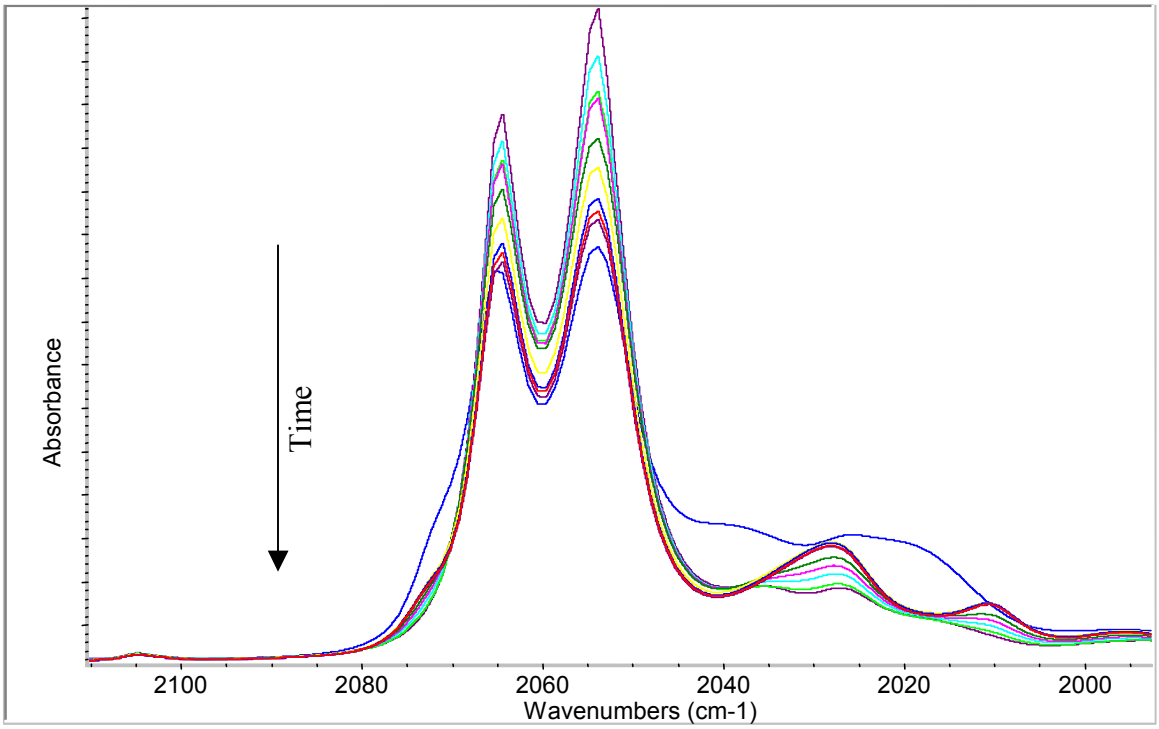

Figure 4.10: FT-IR spectra of 2% Fe/ 98% Co decomposition of $Fe(CO)_5$ and $Co_2(CO)_8$

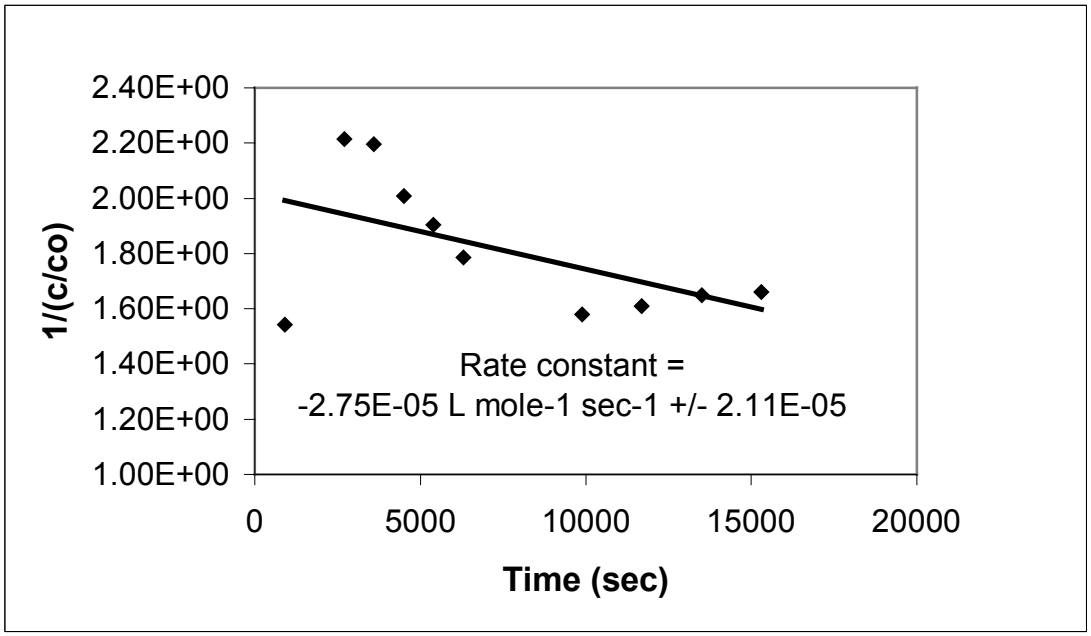

Figure 4.11: Second order decomposition kinetics of $Fe(CO)_5$ in 2%Fe/98%Co

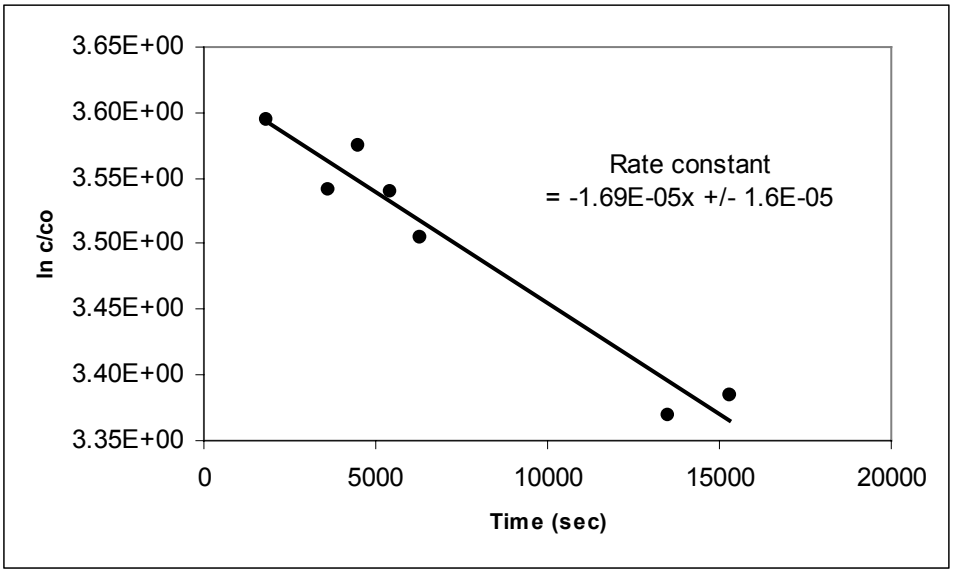

Figure 4.12: First order decomposition kinetics of $Co_2(CO)_8$ in 2%Fe/98%Co

TEM results indicate spherical clusters arranged in chain structures with an average particle size of 33.5 nm ± 8.5 nm (Figures 4.13, 4.14), and electron diffraction indicates a bcc structure with several preferential direction spots (Figure 4.16), which means there are areas of crystallinity in the clusters. This does not match the structure predicted for this composition on the bulk phase diagram (hcp), but this may be expected from the ability of nanoclusters to exhibit thermodynamically unfavorable structures. TGA curves (Figure 4.17) from a film of these clusters indicate a slope different than that of either of the single metal clusters, and with a shallower slope, indicating a mixed surface chemistry. This makes sense when observing the similarities in rate constants of the precursors (indicating that the precursors complete their decompositions concurrently), and the TEM images seem to show particles with crystalline and amorphous regions throughout the clusters but not with a core-shell morphology.

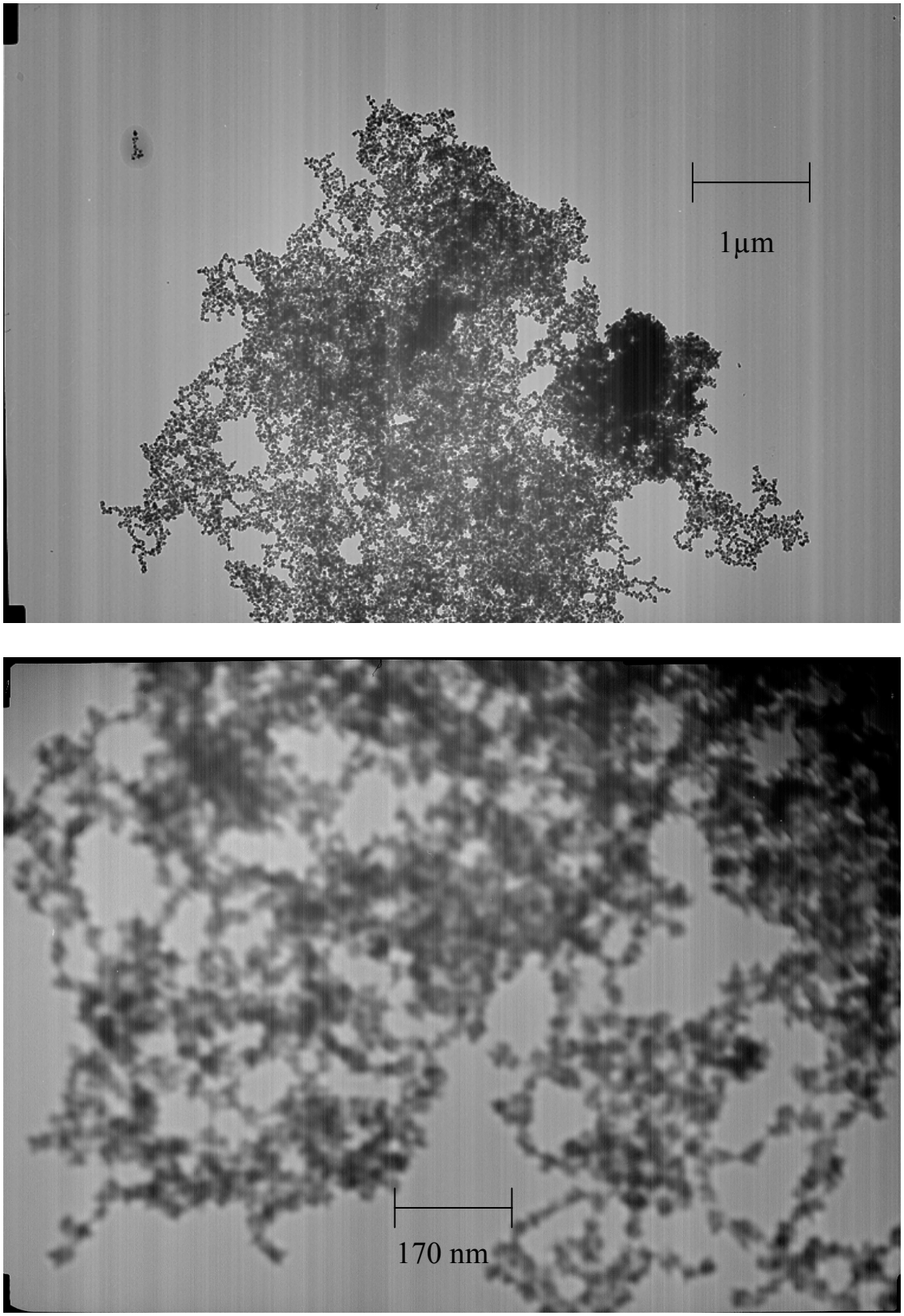

Figure 4.13: TEM micrographs of macroscale and nanoscale organization of FeCo nanoclusters produced from 2%Fe/ 98%Co

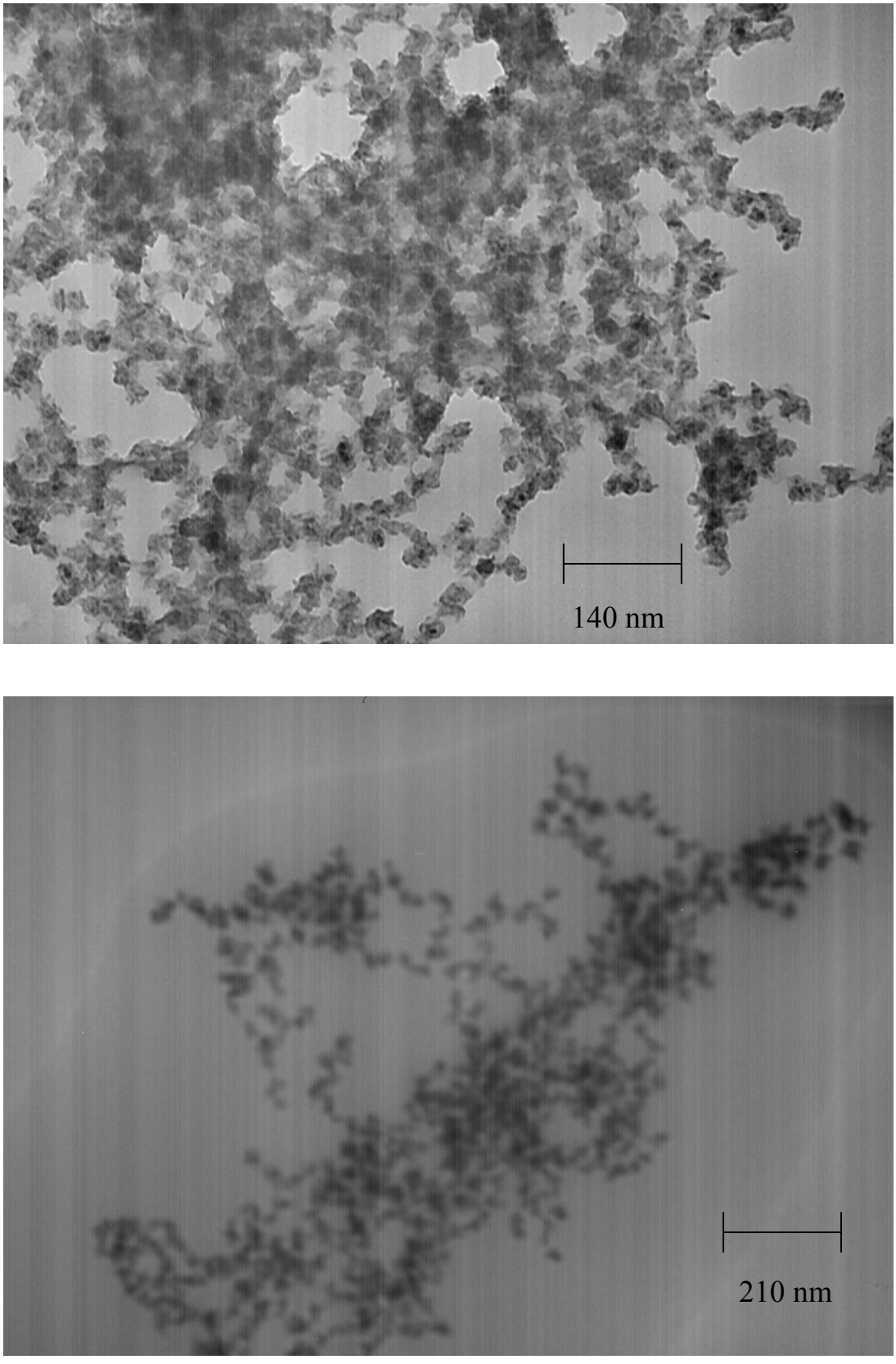

Figure 4.14: TEM micrographs of macroscale and nanoscale organization of FeCo nanoclusters produced from 2%Fe/ 98%Co

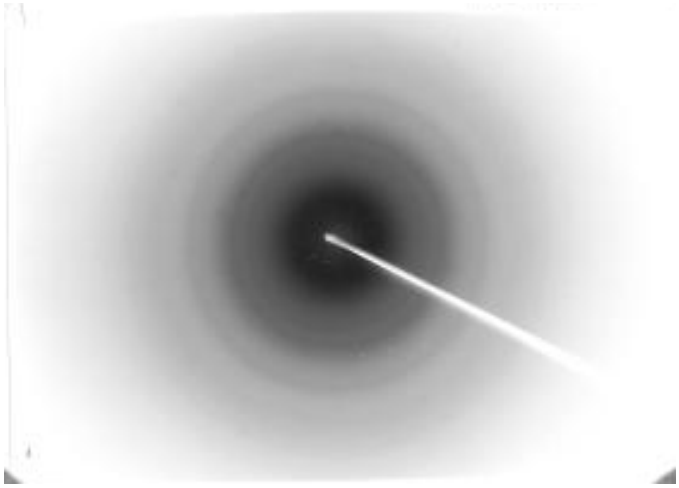

Figure 4.15: TEM diffraction pattern of FeCo nanoclusters produced via the co-decomposition of $Fe(CO)_5$ and $Co_2(CO)_8$ with 2% Fe/ 98% Co

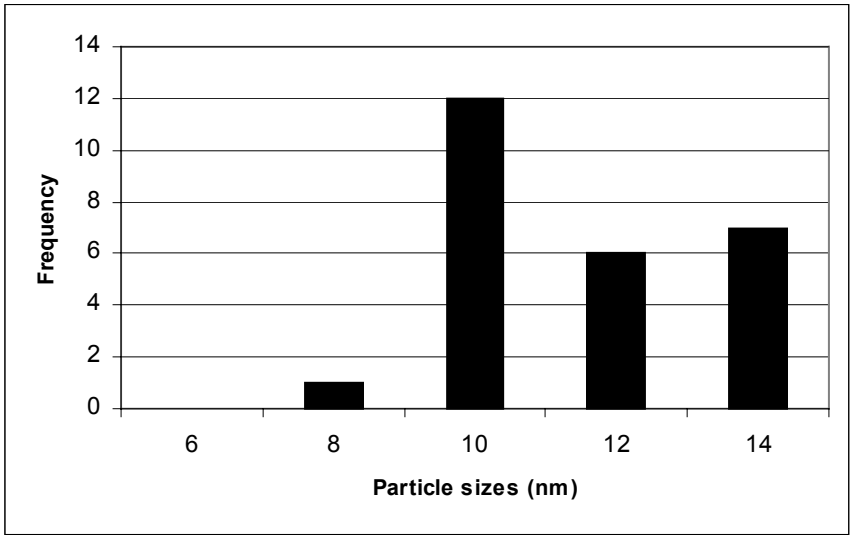

Figure 4.16: Histogram of particle sizes of FeCo nanocluster produced with 2% Fe / 98% Co

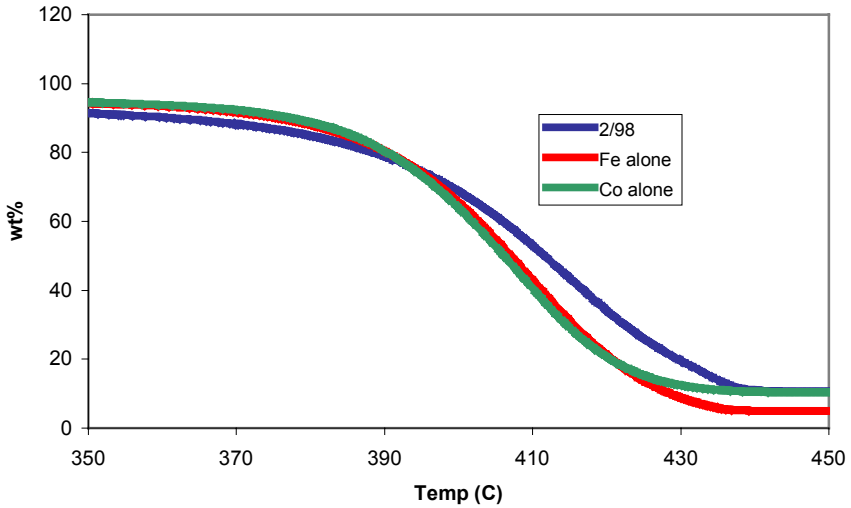

Figure 4.17: TGA curve from a film of 2% Fe / 98% Co nanoalloy indicating a mixed cluster surface

4.3.2 10% Fe/ 90% Co

.07 g $Fe(CO)_5$ and .523 g $Co_2(CO)_8$ were combined in a 100 ml solution of polystyrene and toluene in order to produce a solution with a metal atom ratio of 10% Fe and 90% Co. Actual molar concentrations in solution were $[Fe(CO)_5] = 3.8 \cdot 10^{-3}$ M and $[Co_2(CO)_8] = 1.3 \cdot 10^{-2}$ M.

Figure 4.18 shows the infrared spectra obtained from the 10%Fe/90%Co system. Kinetic analysis of the IR spectra shows the decomposition rate of $Fe(CO)_5$ to be a second order process with rate constant $4.54 \cdot 10^{-5}$ s^{-1} and the decomposition rate of $Co_2(CO)_8$ to be a first order process with rate constant $2.16 \cdot 10^{-5}$ s^{-1}.

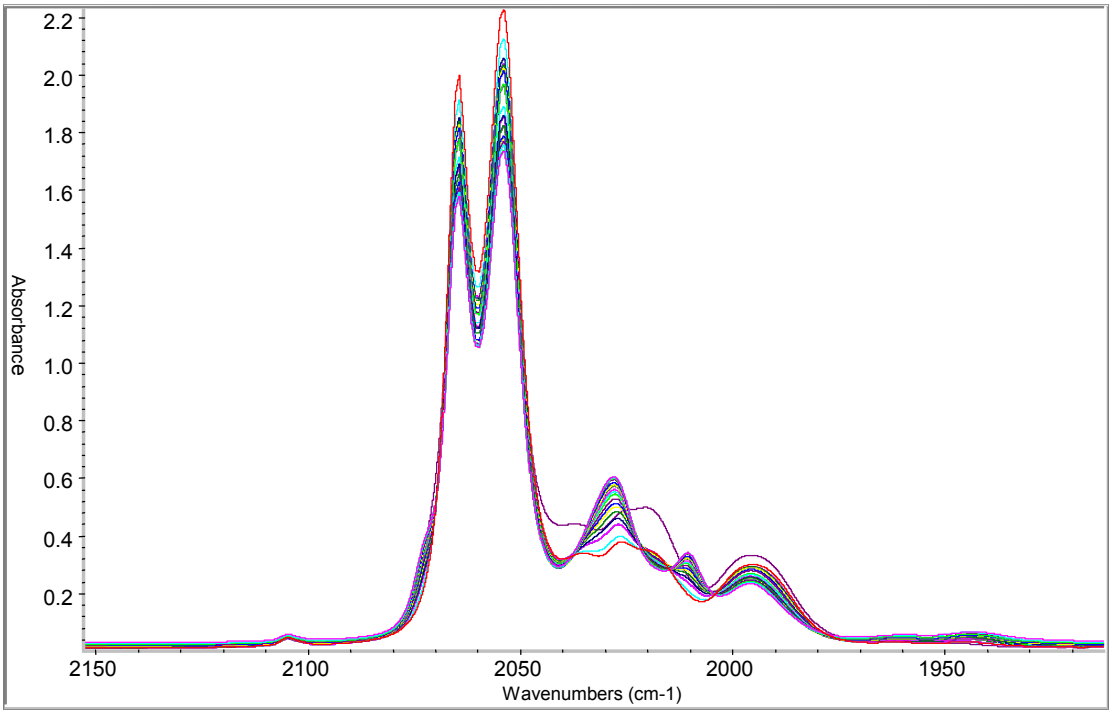

Figure 4.18: FT-IR spectra of 10% Fe / 90% Co decomposition of $Fe(CO)_5$ and $Co_2(CO)_8$

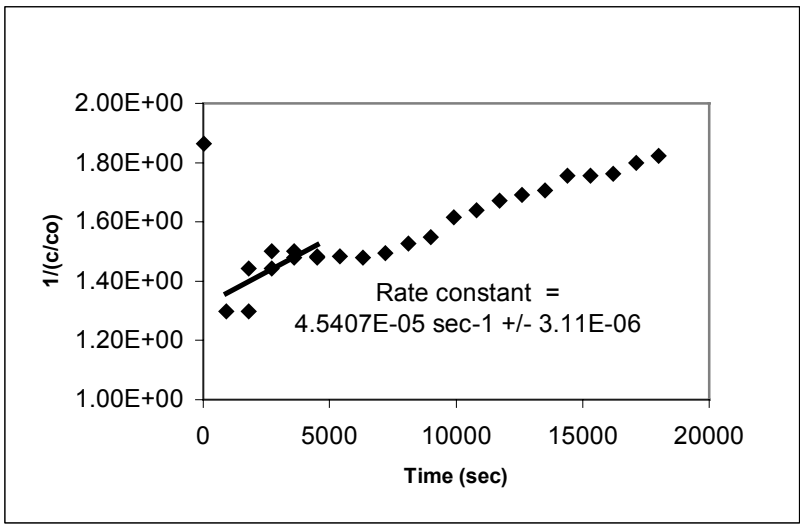

Figure 4.19: Second order decomposition kinetics of $Fe(CO)_5$ in 10% Fe/ 90% Co

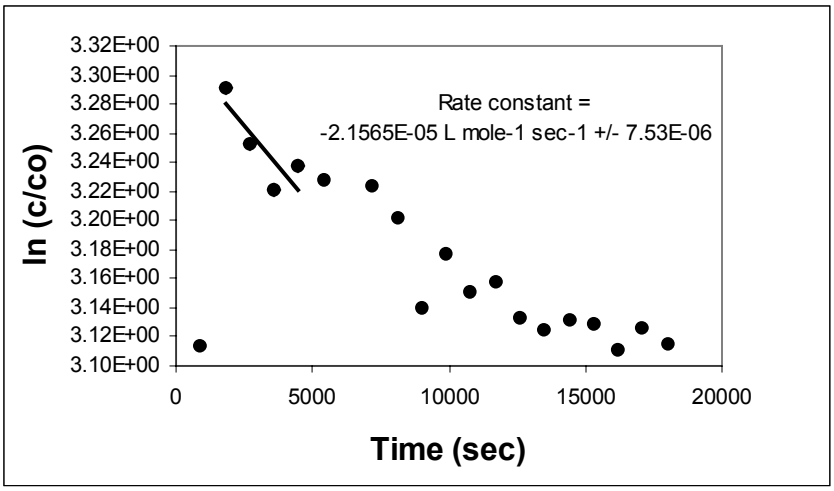

Figure 4.20: First order decomposition kinetics of $Co_2(CO)_8$ in 10% Fe/ 90% Co

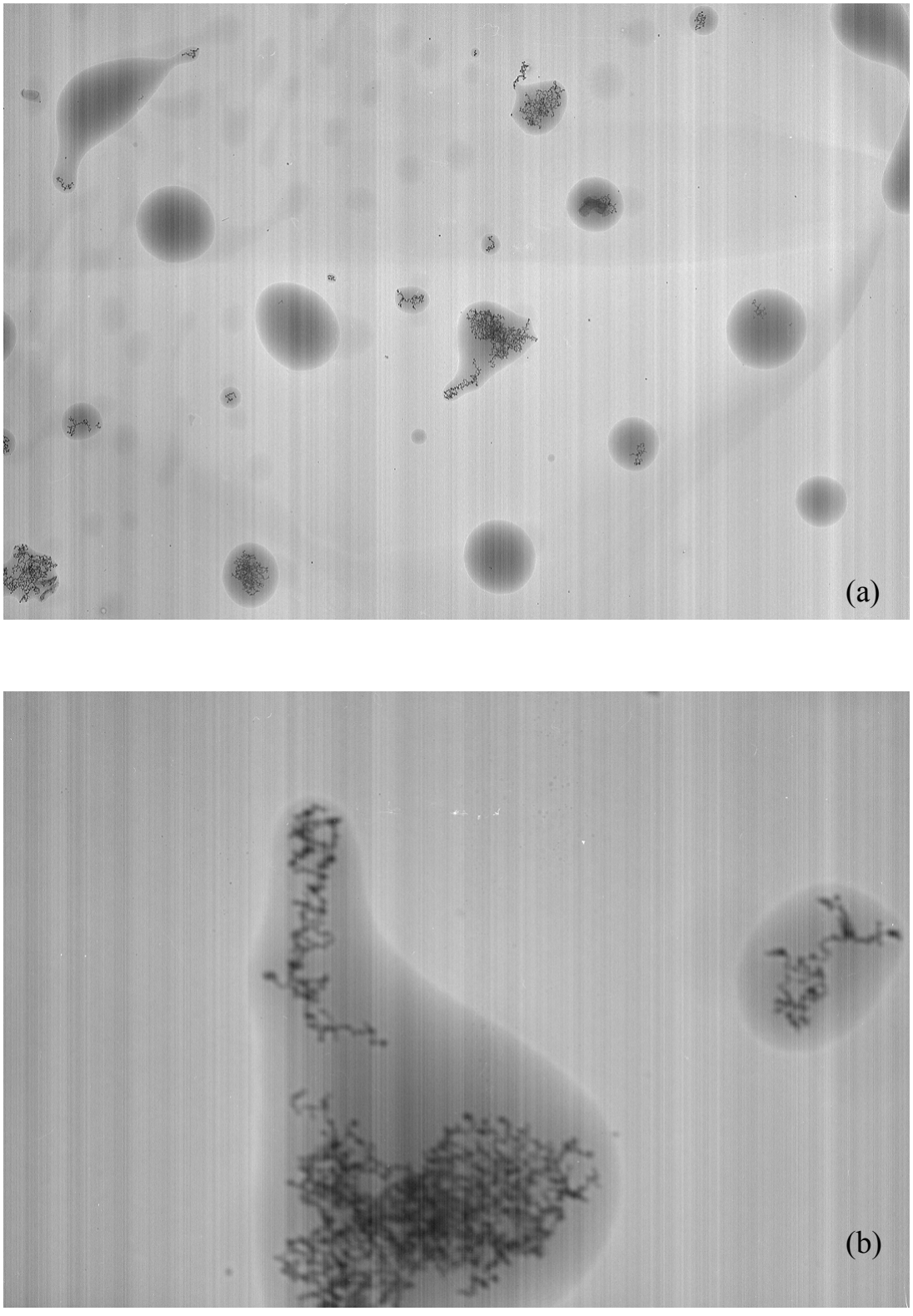

Figure 4.21: TEM micrographs showing a) an assembly of FeCo nanoalloys in “bubbles” of polymer and solvent and b) the assembly of nanoparticles inside these bubbles

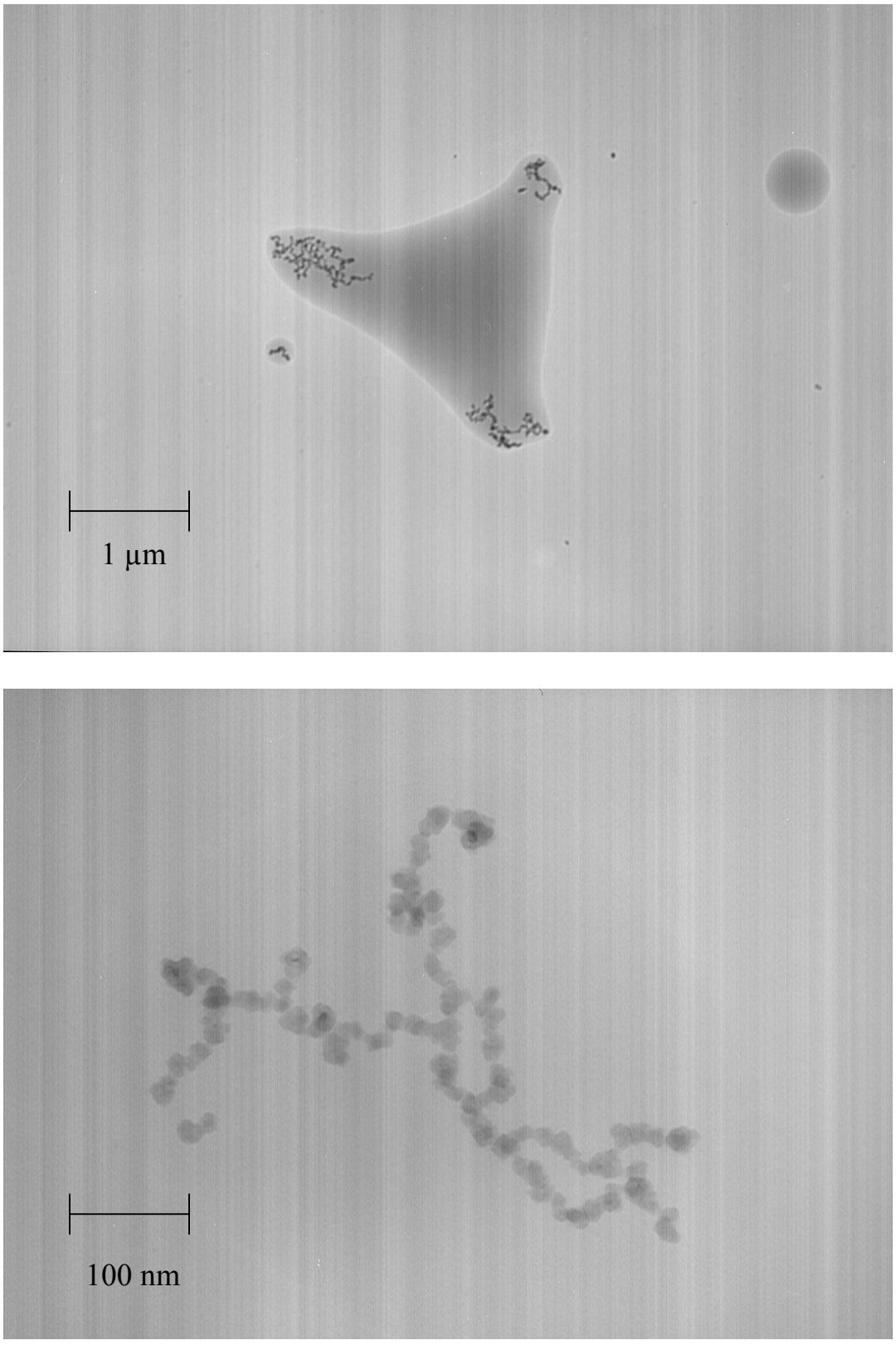

Figure 4.22: TEM micrographs showing the collection of FeCo nanoalloy chains in a bubble of solvent and polymer and the nanoscale organization of spherical nanoparticles from 10% Fe /90% Co

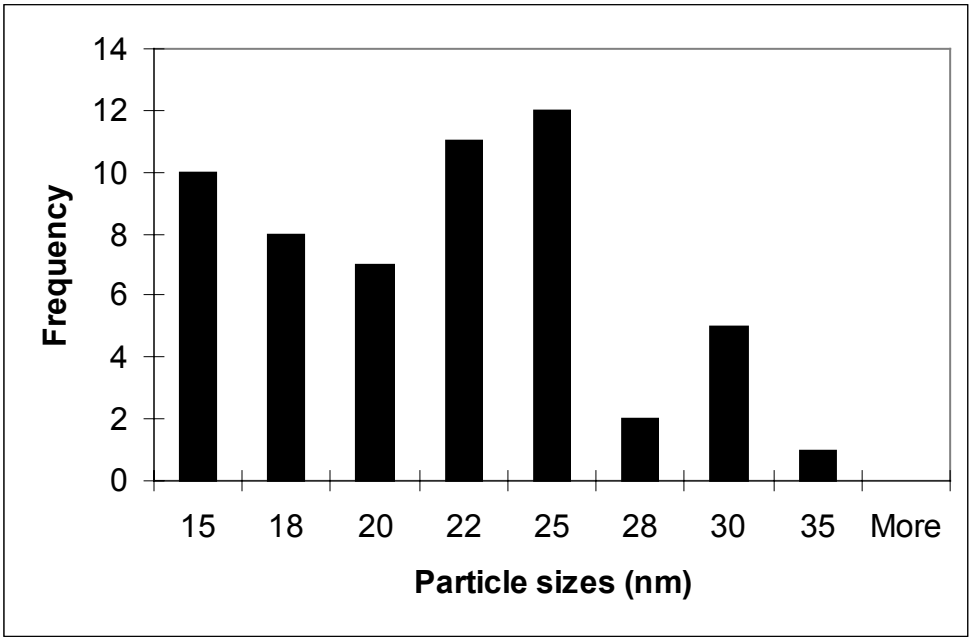

Figure 4.23: Histogram of particle sizes of FeCo nanoalloys produced using 10% Fe / 90% Co

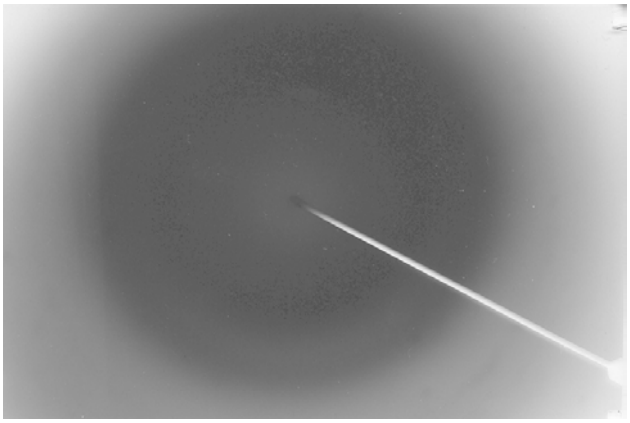

Figure 4.24: Electron diffraction of FeCo from 10% Fe/ 90% Co indicating a bcc structure

TEM results indicate an average particle size of 21.7 ± 4.9 nm (Figure 4.23) and electron diffraction indicates a bcc structure (Figure 4.24). This is not expected for this composition from the bulk phase diagram, at this iron/cobalt ratio the mixed phase α+β is predicted, though not surprising with the tendency of nanoalloys to form structures that defy the traditional bulk phase diagram. TGA (Figure 4.25) of a film of these

nanoclusters indicates surface chemistry similar to that of a single metal surface, which means there is likely a core-shell type morphology being produced with a single metal forming the surfaces of the clusters.

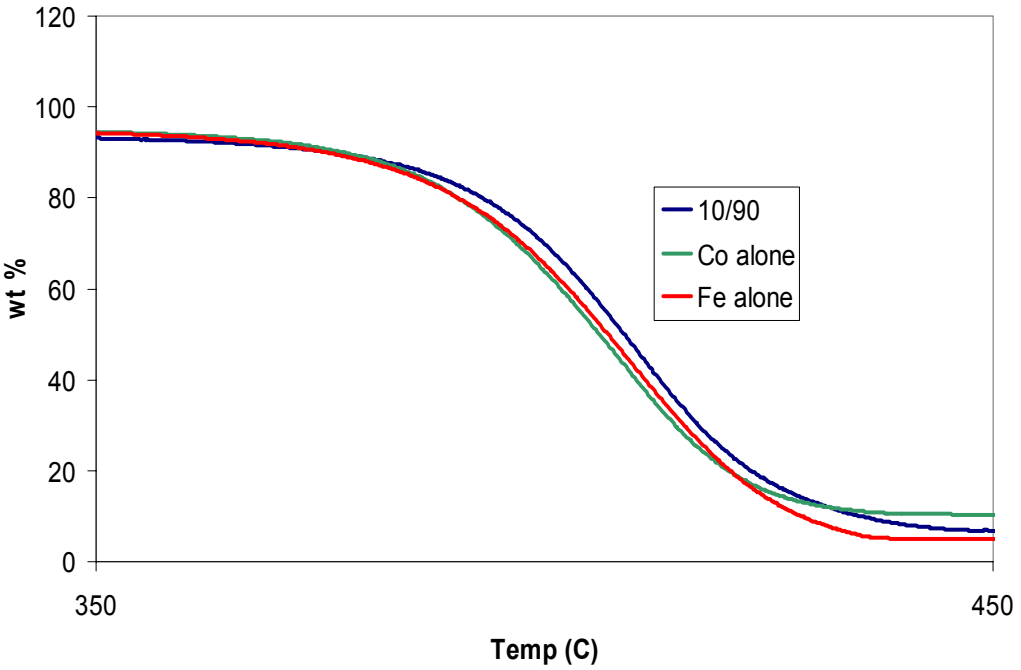

Figure 4.25: TGA curve of film of 10% Fe/90% Co nanoalloys indicating a single type of surface chemistry and a core-shell type structure

4.4 Effect of polymer composition on nanocluster formation

4.4.1 Systems in PMMA

In order to examine the effect of changing the solvent and stabilizing polymer in these systems, $Fe(CO)_5$ and $Co_2(CO)_8$ were combined in a solution of chlorobenzene (1.87 wt%) and 120,000 M_W PMMA. Studies have been previously performed on the decomposition of $Co_2(CO)_8$ in PMMA and chlorobenzene. The experimentally determined extinction coefficient for the $Co_2(CO)_8$ system was $\varepsilon = 1100$ L mol^{-1} cm-1 and the decomposition reaction was determined to be a first order process with a rate constant of $3.13 \cdot 10^{-5}$ s^{-1}.[36] The PMMA/chlorobenzene system is of interest because of PMMA's strong affinity for transition metal surfaces. The high affinity to bond to the

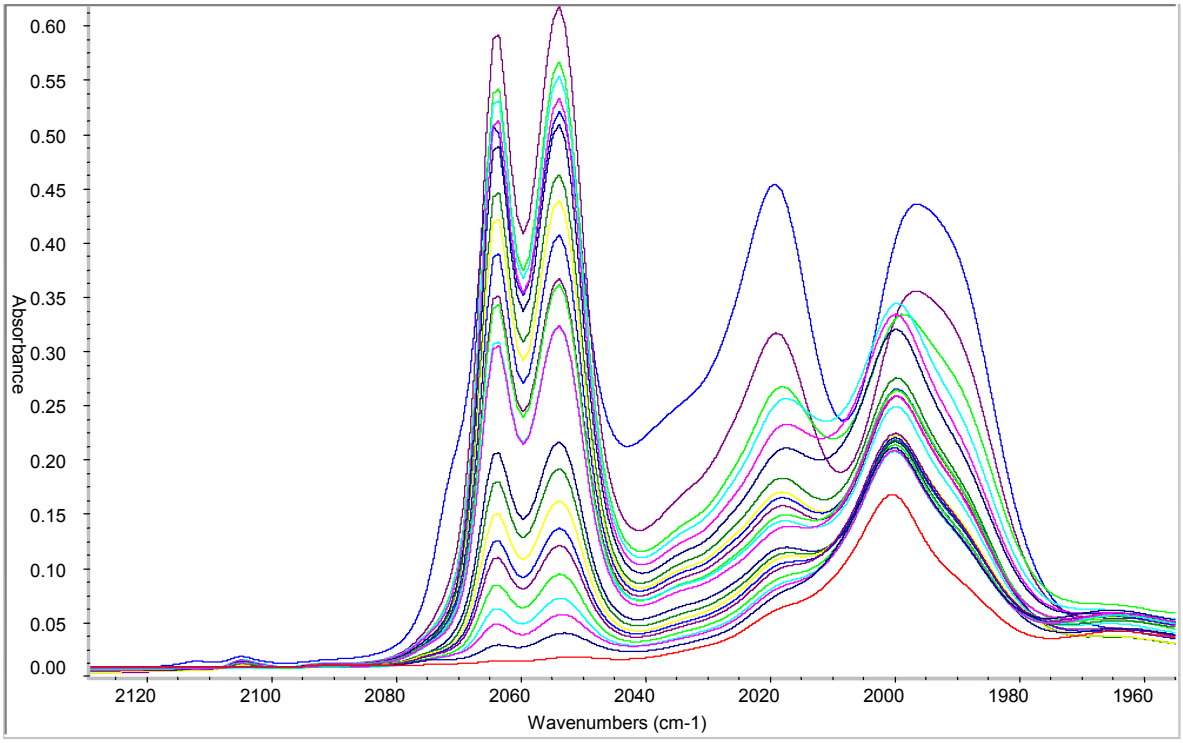

Figure 4.26: FT-IR spectra of FeCo nanoclusters created by the decomposition of equal amounts of $Fe(CO)_5$ and $Co_2(CO)_8$ in PMMA and chlorobenzene

metal surface leads to nanoclusters that exhibit relatively complete polymer coverage and

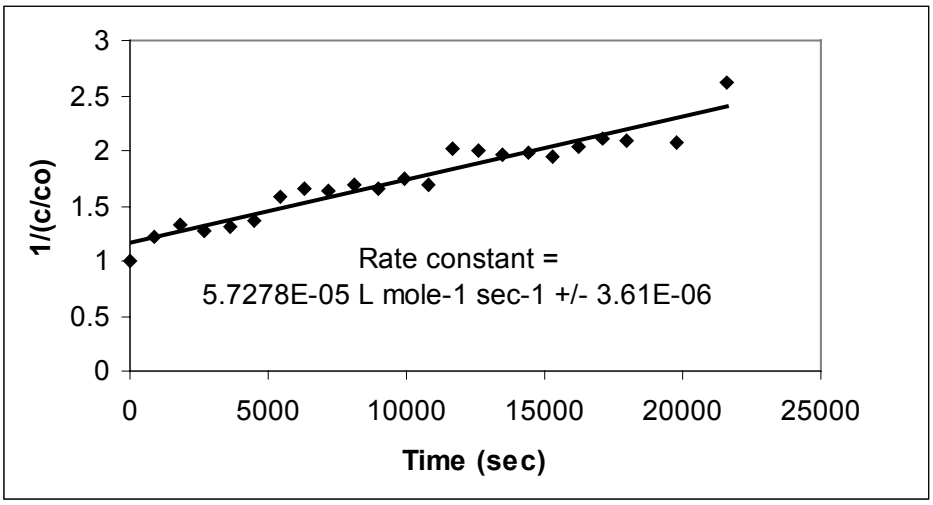

Figure 4.27: Second order decomposition kinetics of $Fe(CO)_5$ co-decomposed with $Co_2(CO)_8$ in PMMA

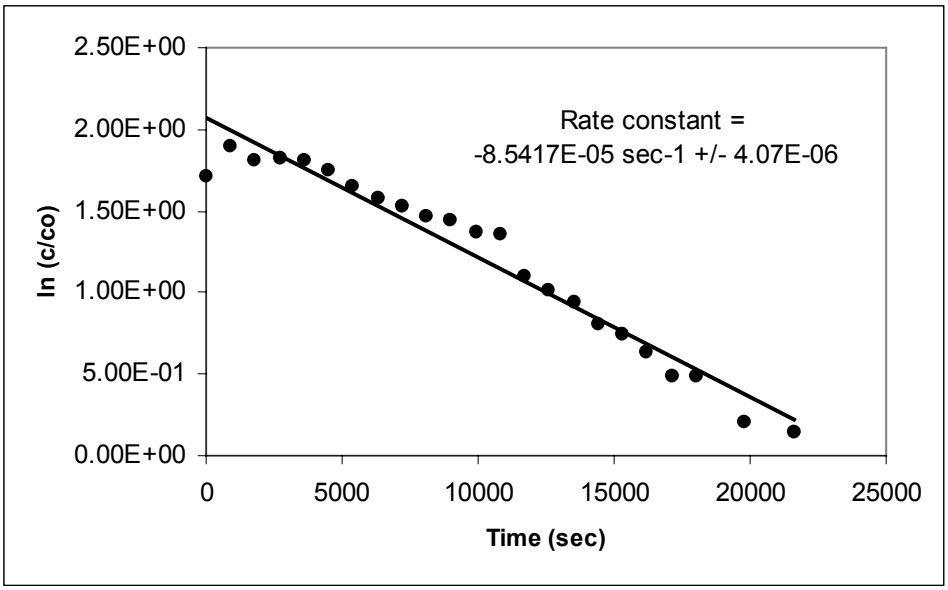

Figure 4.28: First order decomposition kinetics of $Co_2(CO)_8$ co-decomposed with $Fe(CO)_5$ in PMMA

spherical particles.[38]

In order to explore the kinetics of FeCo nanocluster formation in PMMA and chlorobenzene, the kinetics of $Fe(CO)_5$ in this system was determined. The extinction coefficient of this species was determined by measuring the height of the carbonyl bands

of four $Fe(CO)_5$/PMMA/chlorobenzene samples with known concentrations. Absorbance was plotted versus the product of concentration and path length. The slope of the line was used to determine the extinction coefficient. An extinction coefficient of 4098 L mol^{-1} cm^{-1} was determined for this system. Next, a $6.28 \cdot 10^{-3}$ M solution of $Fe(CO)_5$ was decomposed and monitored with FT-IR. The decomposition kinetics was analyzed and the decomposition was determined to be a second order process with $k_{dec} = 5.58 \cdot 10^{-5} s^{-1}$.

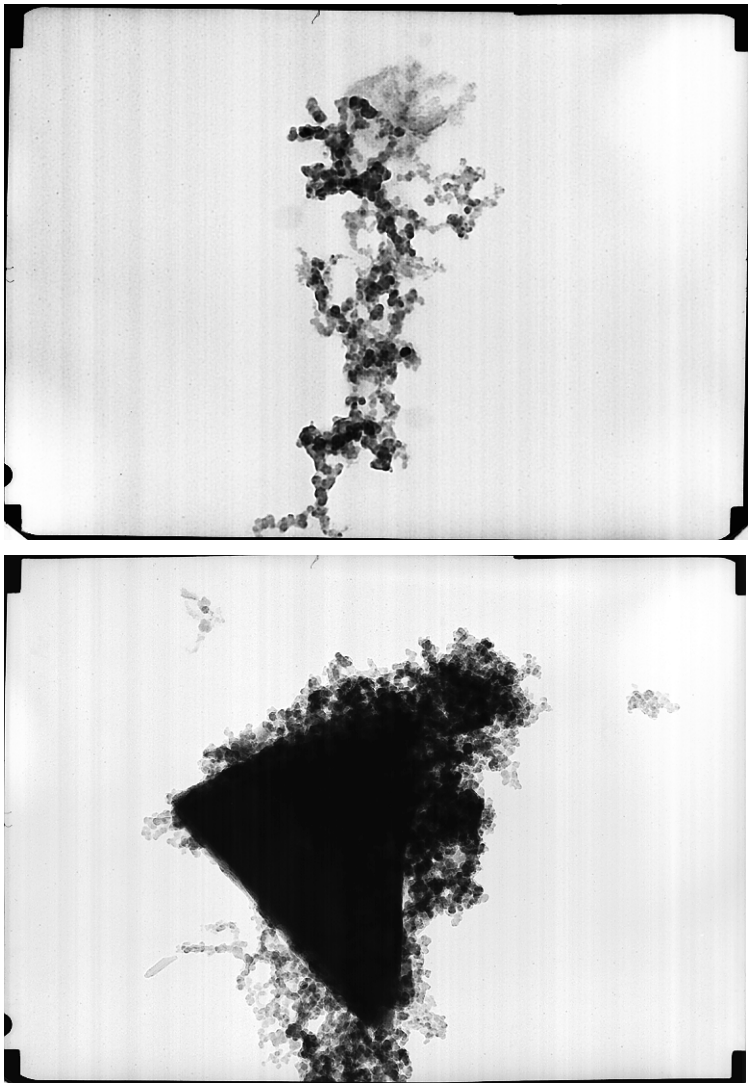

Figure 4.29: TEM micrographs showing the assembly and nanostructure of FeCo nanoparticles synthesized from $Fe(CO)_5$ and $Co_2(CO)_8$ in PMMA and chlorobenzene

In order to examine the mutual influence of the decompositions of $Fe(CO)_5$ and $Co_2(CO)_8$ in this system, a decomposition was performed with equal concentrations of $Fe(CO)_5$ and $Co_2(CO)_8$ in a PMMA/chlorobenzene solution. Actual experimentally-determined metal carbonyl concentrations produced in solution were $[Fe(CO)_5] = 5.2 \cdot 10^{-3}$

M and $[Co_2(CO)_8] = 6.9 \cdot 10^{-3}$ M. Examining the decomposition kinetics of these species (Figures 4.27 and 4.28) and comparing them to the individual decomposition kinetics, it is shown that the decomposition rate constant of $Fe(CO)_5$ increases from $5.56 \cdot 10^{-5}$ s-^{1} in the pure system to $7.18 \cdot 10^{-5}$ s^{-1}. The decomposition rate constant of $Co_2(CO)_8$ increases to $5.48 \cdot 10^{-5}$ s^{-1}, indicating the interaction of these species in solution and the positive mutual influence of their decompositions. Comparing these rate constants of decomposition to those of the individual components, it appears that the decomposition rate of $Fe(CO)_5$ has increased, indicating an improvement when trying to match initial decomposition rate of the two species.

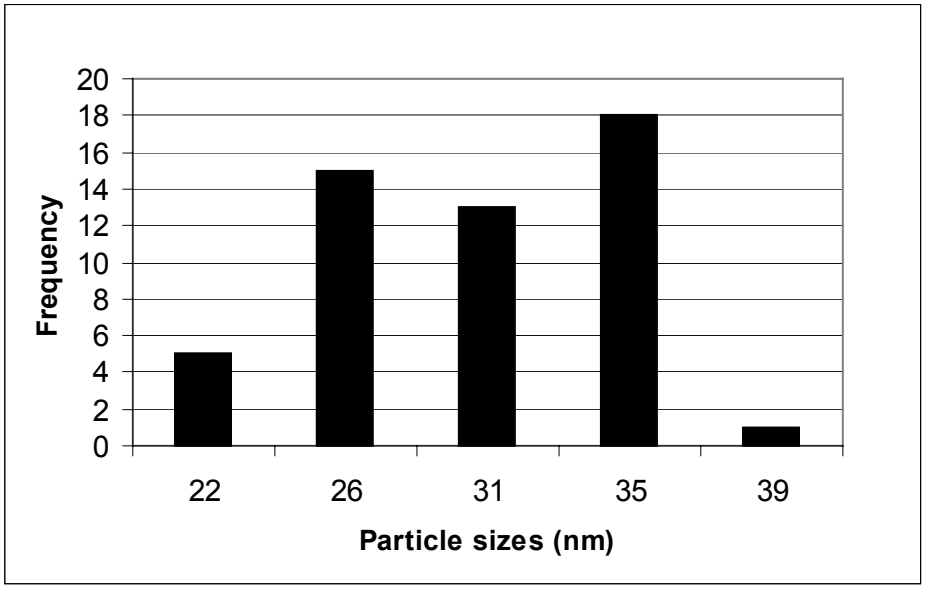

Figure 4.30: Histogram of particle sizes of FeCo nanoclusters created with equal amounts of $Fe(CO)_5$ and $Co_2(CO)_8$ in PMMA and chlorobenzene

TEM was performed on the nanoalloys produced with this system (Figure 4.29). TEM micrographs indicate a spherical cluster shape and individual clusters of size 29.8 ±

4.5 nm. The synthesized clusters are spherical as expected using PMMA as a stabilizer, but it does not produce the expected separation of individual clusters. This may be attributed to the relatively high concentrations of metal carbonyls in the solution. In addition to the regularly shaped spherical particles, there are areas of large aggregates and collections of metal, indicating incomplete cluster polymer coverage. The chain structure produced will be further discussed in Chapter V. Electron diffraction (Figure 4.31) indicates a hcp structure, which is not expected from the bulk phase diagram for this composition (the original solution contained 72% Co, 28% Fe), but is indicative of the presence of zero-valent cobalt in the cores of these nanoclusters. This supports the assumption that these nanoalloys have a core-shell structure with a cobalt core due to the different kinetics of their precursors.

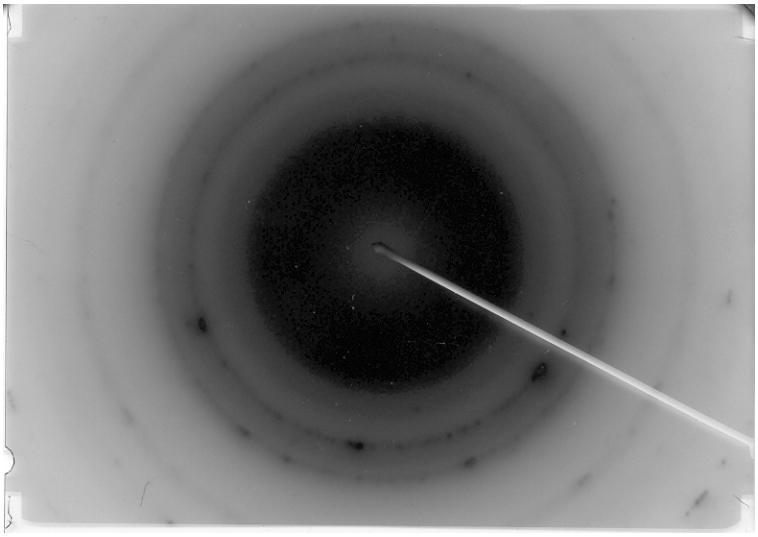

Figure 4.31: Electron diffraction pattern indicating a hcp structure

Using the individual decomposition rates of the carbonyl species in the PMMA/chlorobenzene system, the "equal rates" relationship was constructed as previously discussed.

$$\frac{k_{Fe}}{k_{Co}} = \left(\frac{c_1}{c_2}\right)^2 + \frac{c_1}{c_2}$$

Using the individual metal carbonyl rate constants and an initial $Co_2(CO)_8$ concentration of $5 \cdot 10^{-3}$ M, the appropriate concentration of $Fe(CO)_5$ as $4.63 \cdot 10^{-3}$ M was determined for this system. Experimentally determined initial concentrations were $[Co_2(CO)_8] = 7.82 \cdot 10^{-3}$ M and $[Fe(CO)_5] = 6.25 \cdot 10^{-3}$ M.

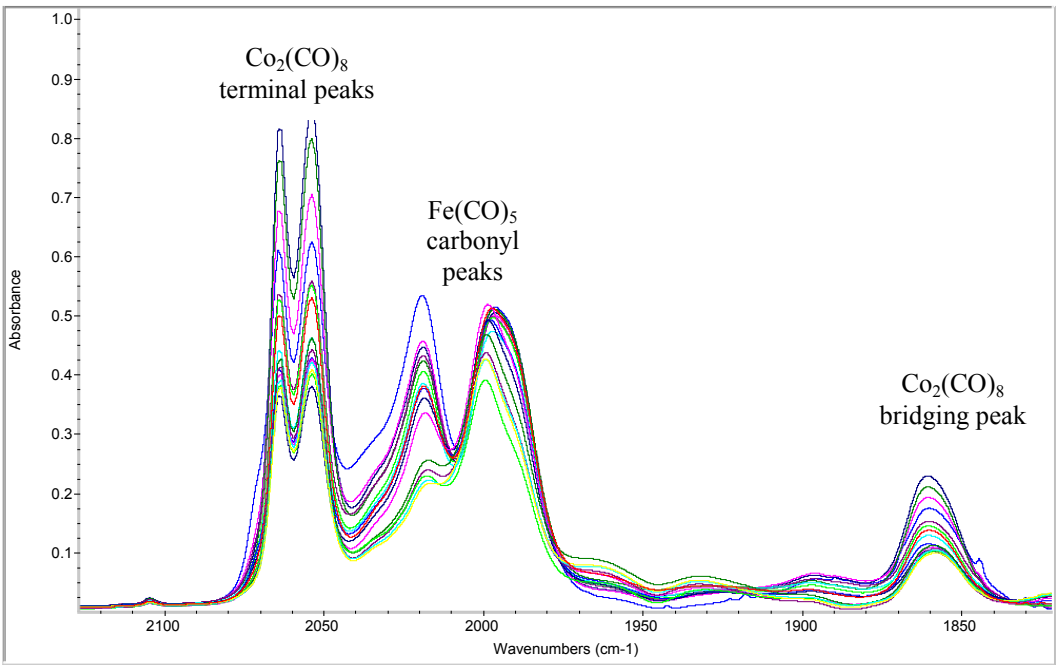

Figure 4.32: FT-IR spectra of $Fe(CO)_5$ and $Co_2(CO)_8$ using "equal rates" method in PMMA

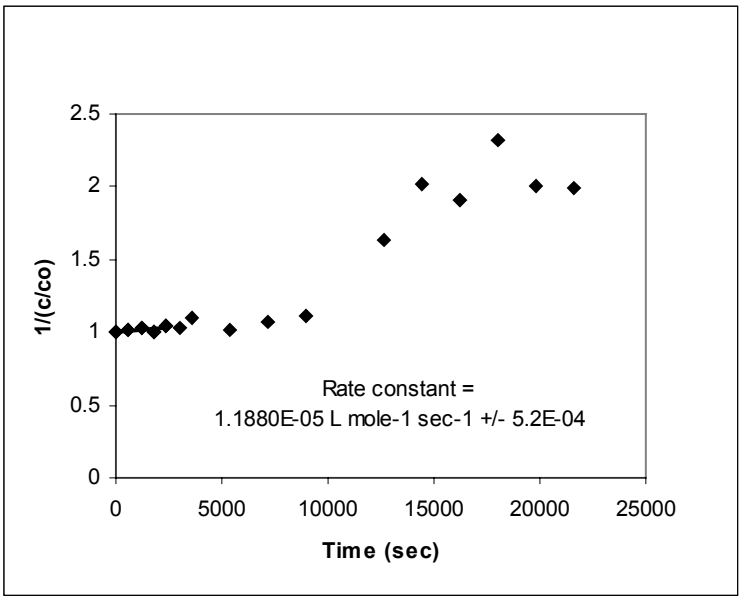

Figure 4.33: Second order decomposition of $Fe(CO)_5$ co-decomposed with $Co_2(CO)_8$ in PMMA

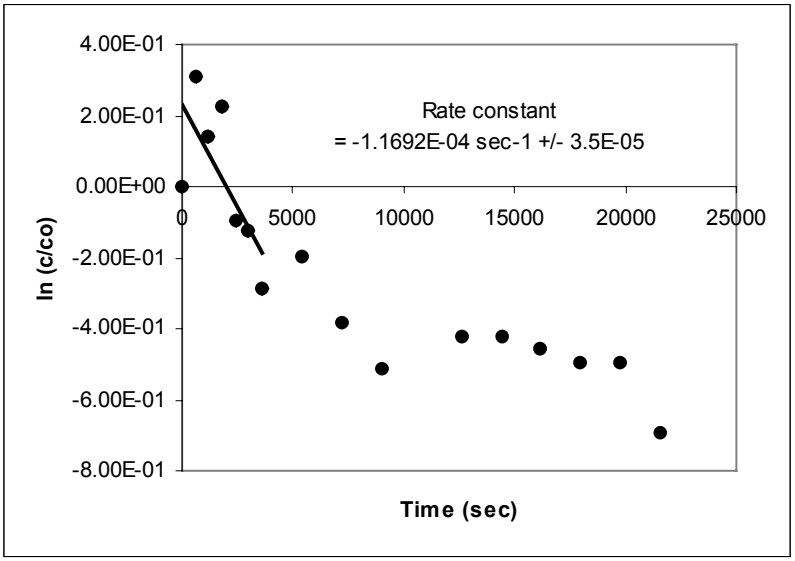

Figure 4.34: First order decomposition of $Co_2(CO)_8$ co-decomposed with $Fe(CO)_5$ in PMMA

Figures 4.33 and 4.34 show the decomposition rate analysis for each component in the mixed system. There is a great deal of scatter in the data, but an order of magnitude analysis is effective to determine whether or not the rate constants in the mixed system are similar and therefore, beneficial conditions for mixed-cluster formation. Examining the

co-decomposition kinetics, it appears that the decomposition rate constant of $Fe(CO)_5$ has decreased (indicating a slower reaction rate) and the decomposition rate constant of $Co_2(CO)_8$ has increased. The rates of the individual metal carbonyls were different by

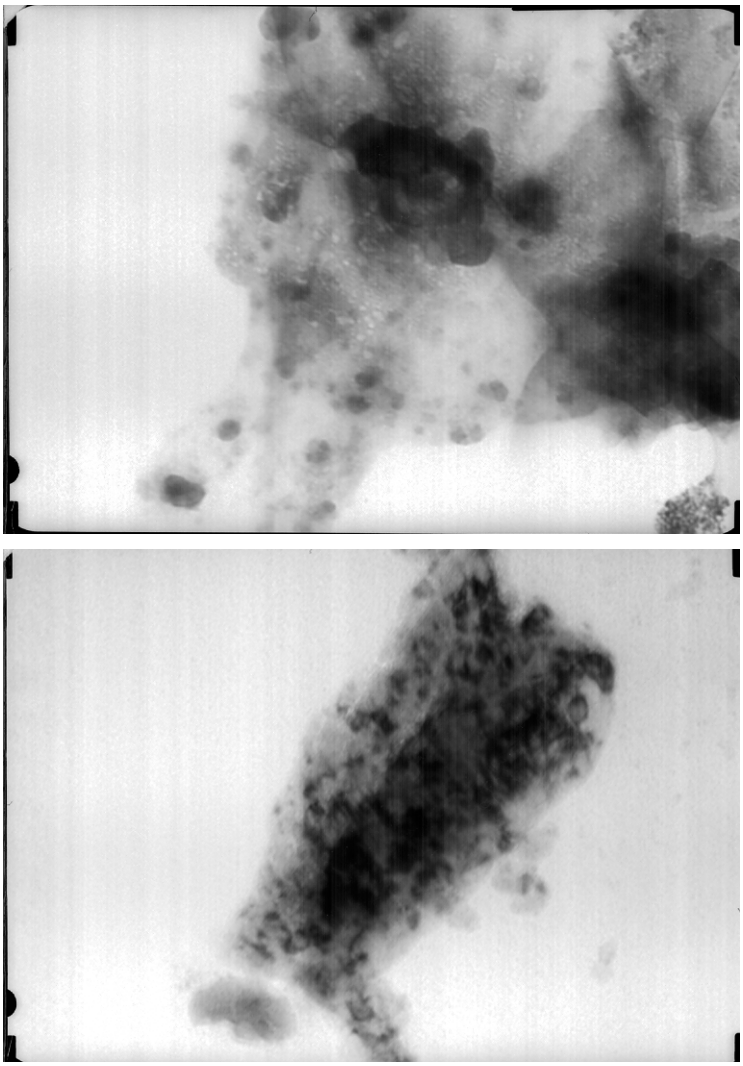

Figure 4.35: TEM micrographs showing the agglomeration of FeCo clusters formed using the "equal rates" method in PMMA

approximately an order of magnitude. Because the difference in decomposition rates has actually increased, it is expected that this method would not produce thoroughly mixed nanoalloys.

The nanoclusters produced with this method seem to have very irregular size and shape, average size 15 ±. 3.5 nm (Figure 4.35). Electron diffraction (Figure 4.36) of these nanoclusters indicate a bcc structure, which is expected for the FeCo bulk alloy with this metal ratio (69.7% Co, 20.7% Fe), but this composition is also near the edge of the transition between bcc and α+β. This could be an explanation for the disorder in the nanoalloy structure; the structure of a nanoalloy at this composition is not stable.

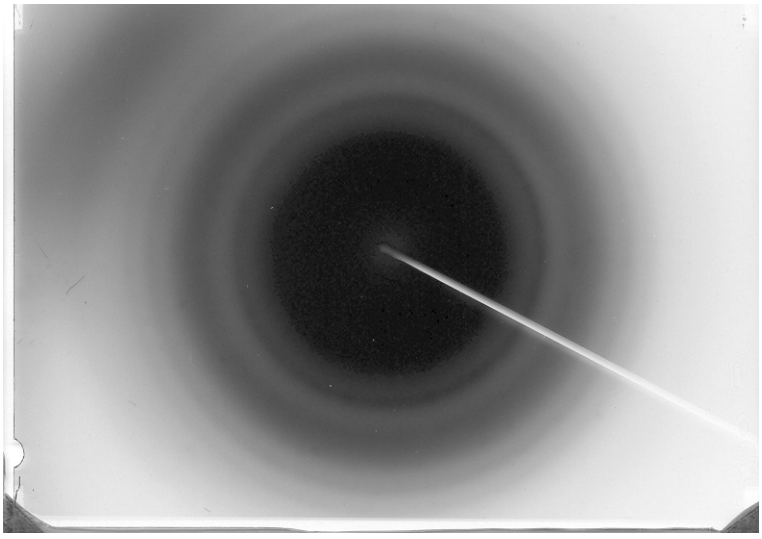

Figure 4.36: Electron diffraction pattern showing a bcc structure

4.5 "Cold synthesis" method in PVF_2/DMF solutions

The decomposition of $Fe(CO)_5$ and $Co_2(CO)_8$ in PVF_2 and DMF was performed in an attempt to create nanoclusters of a novel size and shape, showing the influence of changing the stabilizing polymer on the shape of the resulting nanoclusters. This cold synthesis method for the production of metal oxide nanoclusters has produced Fe_2O_3 clusters of very regular shape in previous studies.[38] In this study, the combination of two

metal carbonyl precursors and polymer/solvent ratio, along with this method of processing, forms spherical FeCo oxide clusters that link in chains. The clusters are slightly longer in the direction in which they link together, and the metal that links them together is clearly visible, Figure 4.38. They are of average diameter 154.3 ± 14.5 nm.

These results are expected from this system. If the iron precursor is decomposed after it is already stabilized in a dried polymer film ("cold method"), such as in this experiment, there will be two important aspects to cluster formation.[38] First, the nucleation sites for the clusters will not be homogeneously dispersed.[38] Thus, particles form in some areas and not in others. Second, since the particles that do form are very close in proximity, there are very strong attractive forces. [38] These van der Waals forces cause continued agglomeration despite the polymer cap, and bridges of iron and cobalt oxide form between the clusters.[38] This causes the chain morphology.

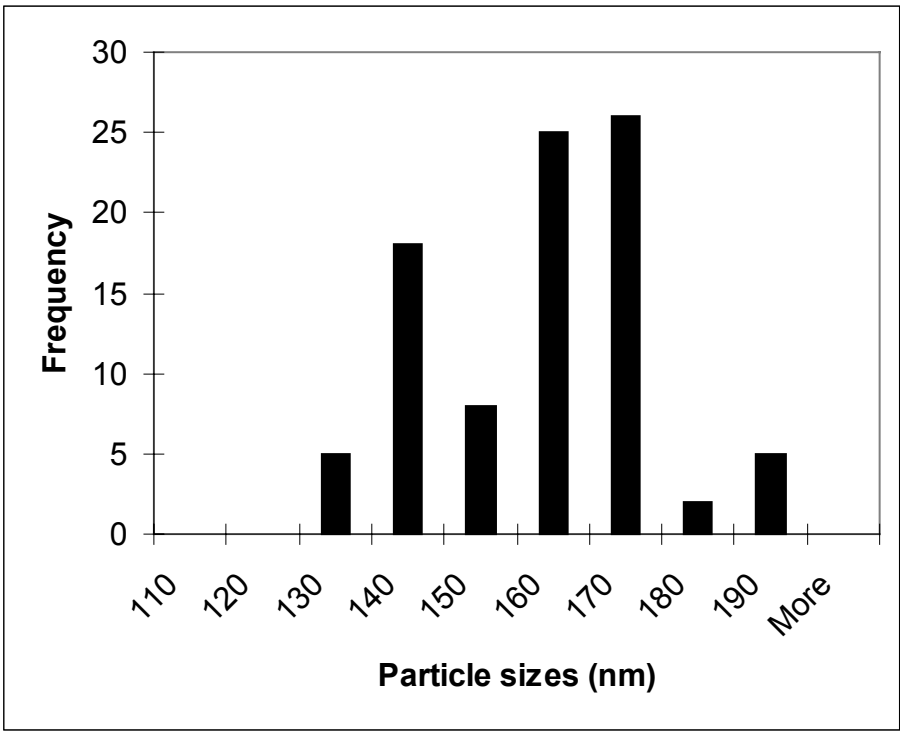

Figure 4.37: Histogram of particle sizes of FeCo oxides formed by the co-decomposition of $Fe(CO)_5$ and $Co_2(CO)_8$

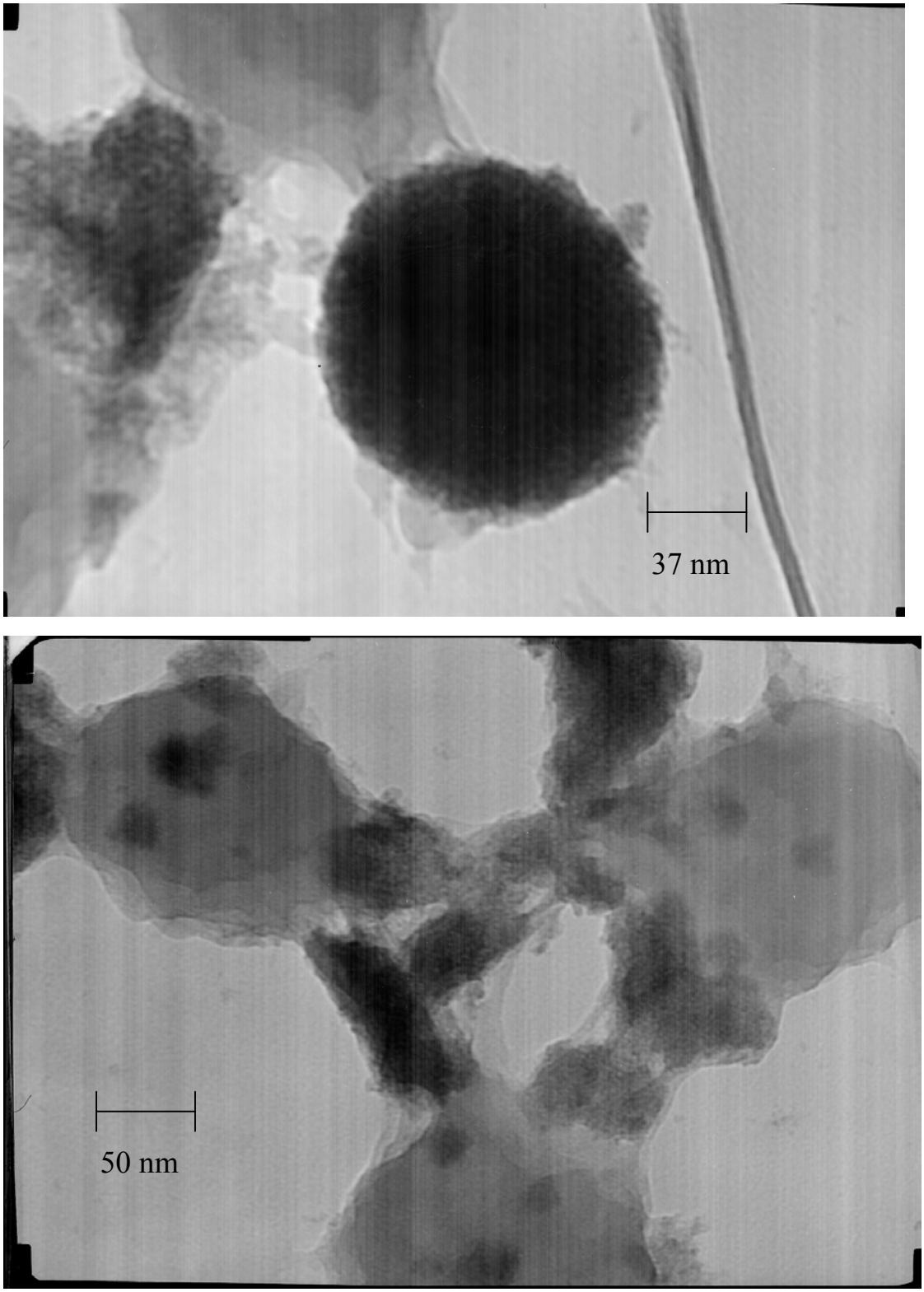

Figure 4.38: Nanoscale structure of FeCo oxides created with $Fe(CO)_5$ and $Co_2(CO)_8$ in PVF_2 and DMF

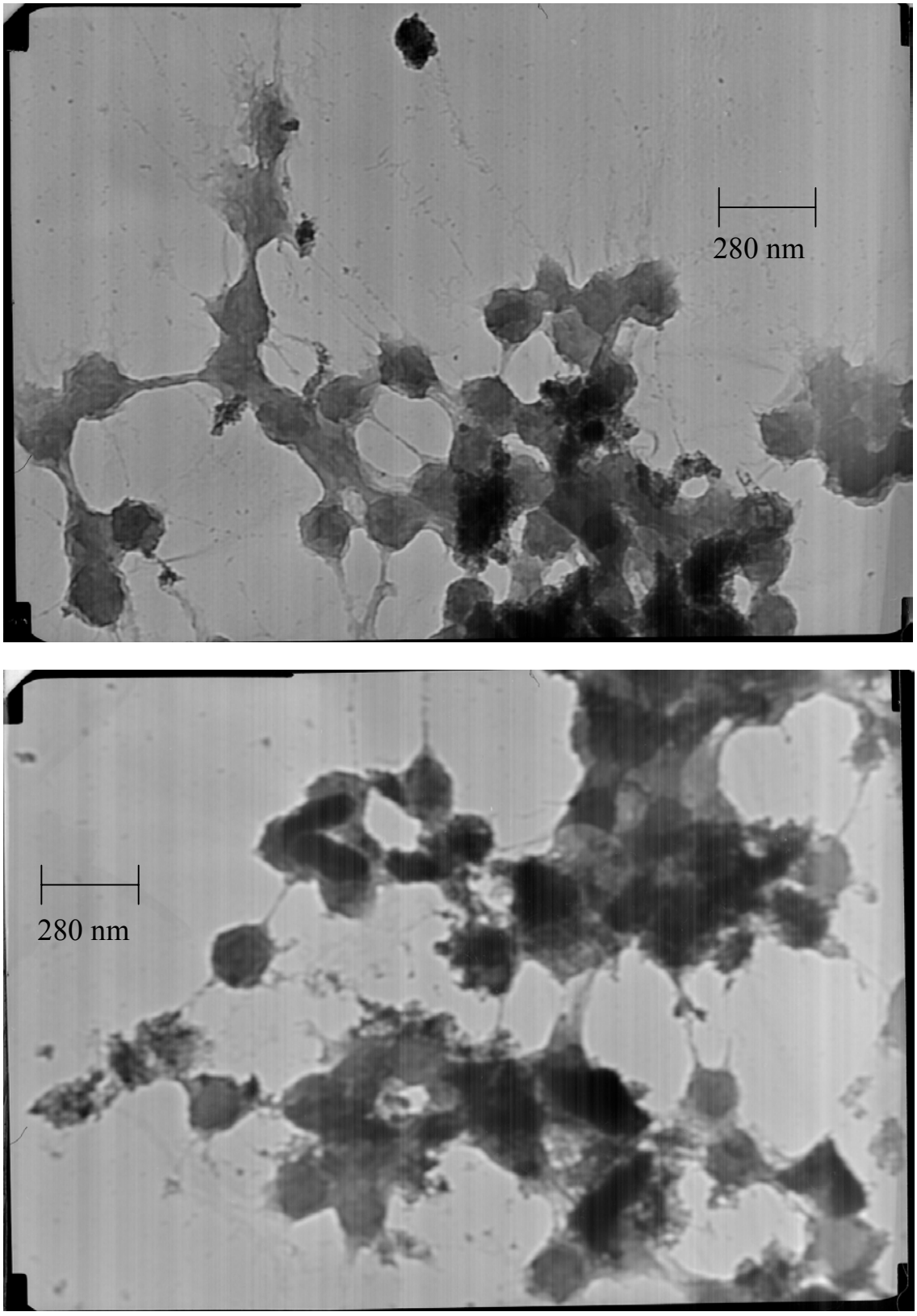

Figure 4.39: Macroscale assembly of FeCo oxide clusters created with $Fe(CO)_5$ and $Co_2(CO)_8$ in PVF_2

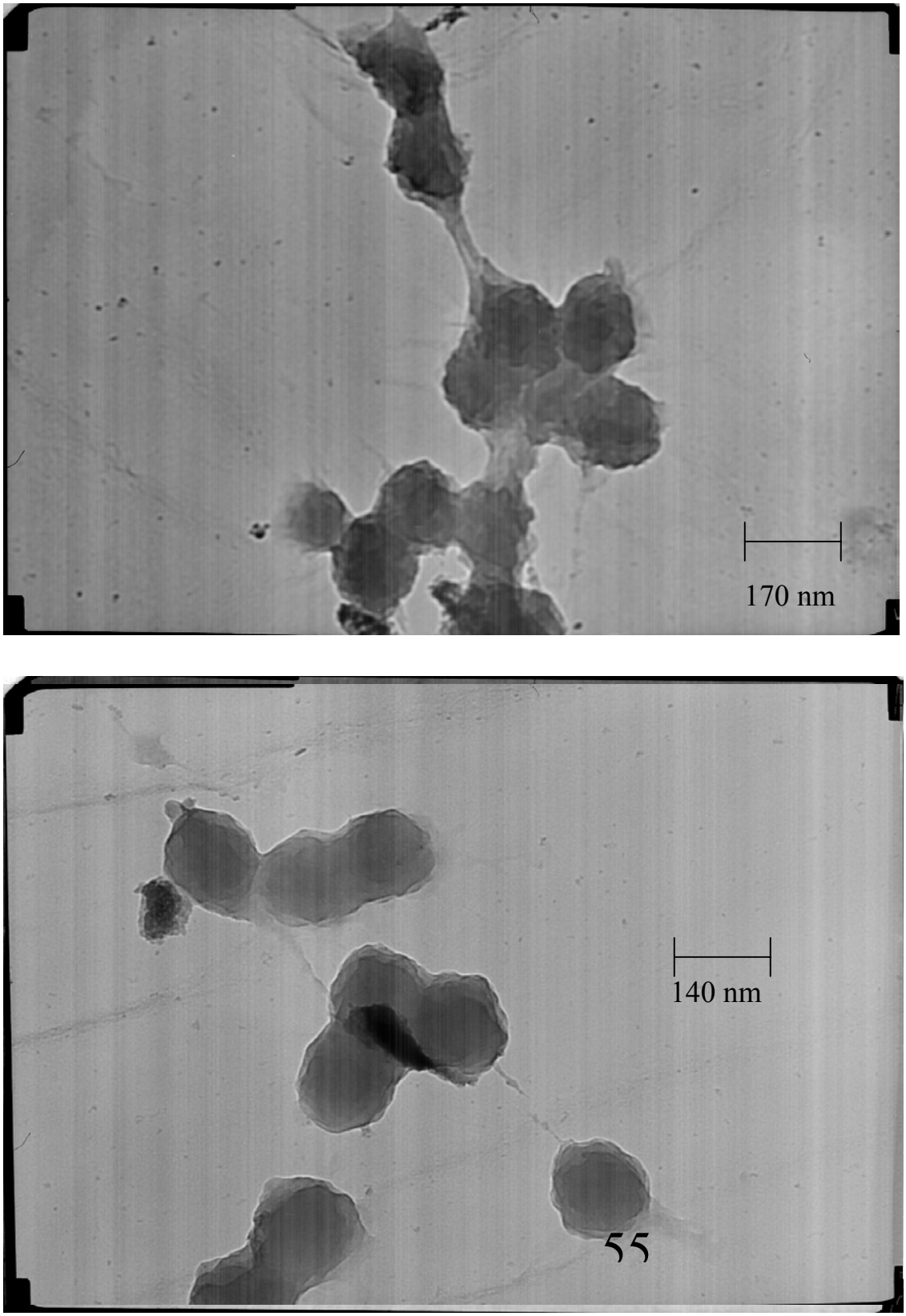

Figure 4.40: Nanoscale structure of FeCo oxide clusters created with $Fe(CO)_5$ and $Co_2(CO)_8$ in PVF_2

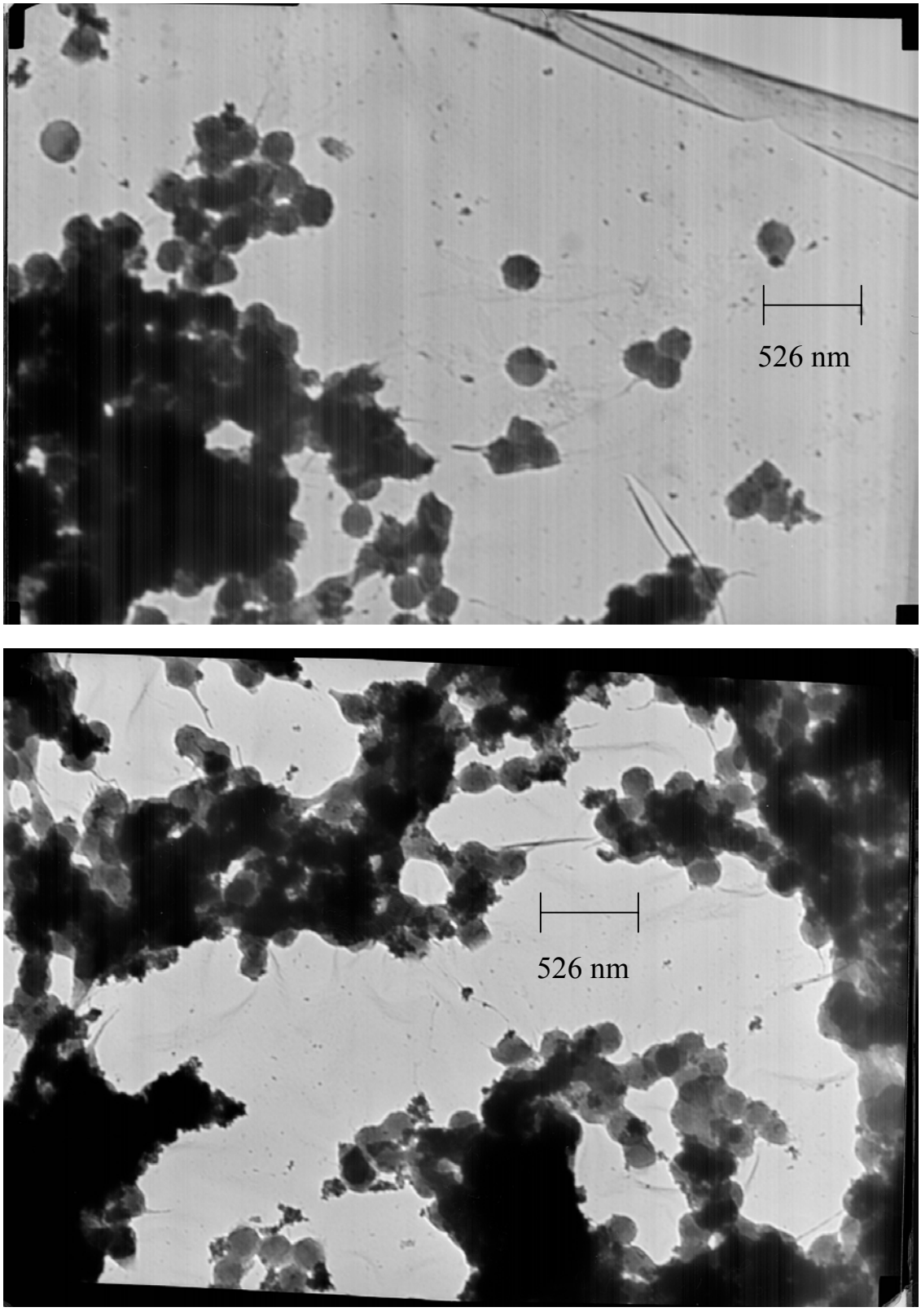

Figure 4.41: Macroscale assembly of FeCo oxide clusters created with $Fe(CO)_5$ and $Co_2(CO)_8$ in PVF_2

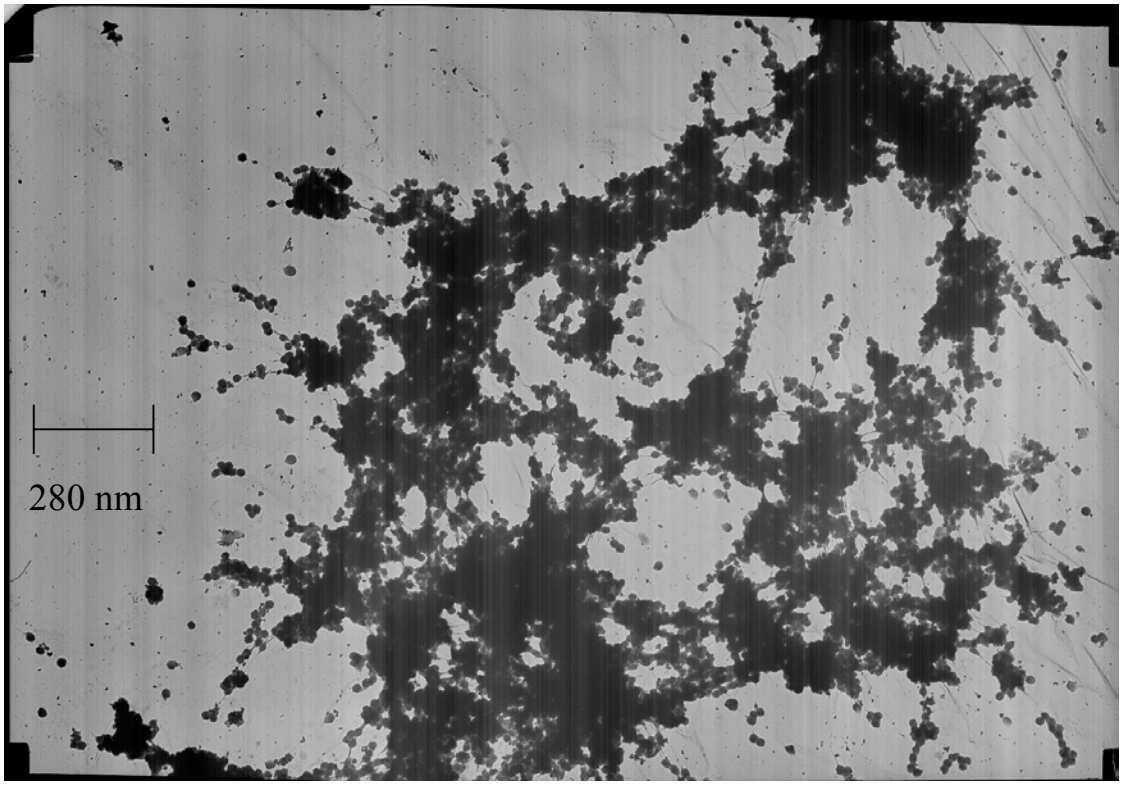

Figure 4.42: Macroscale organization of FeCo oxide clusters created with $Fe(CO)_5$ and $Co_2(CO)_8$ in PVF_2

Analysis of TEM diffraction patterns of these clusters indicate a hcp structure with amorphous regions.

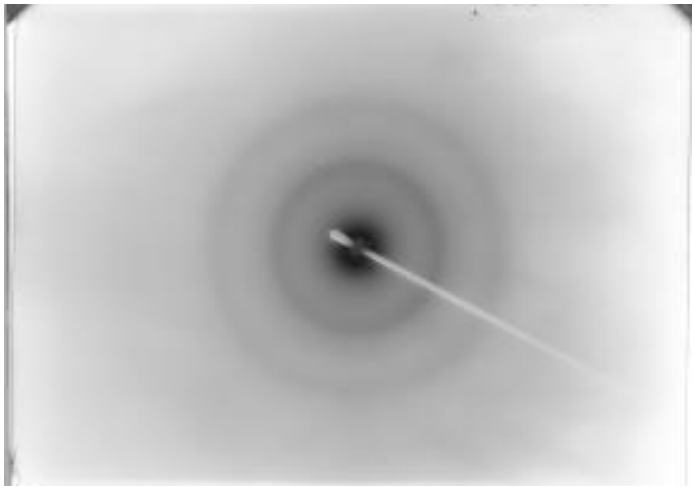

Figure 4.43: TEM diffraction pattern of a sample of FeCo oxides

4.6 Summary of $Fe(CO)_5$ and $Co_2(CO)_8$ based systems

Various methods have been employed to attempt to control the composition and shape of FeCo nanoclusters synthesized with $Fe(CO)_5$ and $Co_2(CO)_8$. These methods were employed with limited success, however, because the decompositions of $Fe(CO)_5$ and $Co_2(CO)_8$ are very different in rate constant magnitude and reaction order. Several of these decompositions produce structures not normally present in the bulk at their compositions, but it is common to see thermodynamically unfavorable structures produced at the nanoscale.

CHAPTER 5

$Fe(CO)_5$ and $Co_4(CO)_{12}$ Based Systems

5.1 Overview

As emphasized in previous chapters, in order to synthesize well-mixed FeCo nanoalloys, the kinetics of both the iron and the cobalt precursors need to be considered. When examining the decomposition rates of $Co_2(CO)_8$ and $Fe(CO)_5$, it was determined that their decomposition kinetics vary greatly in both reaction order and rate. In order to produce true mixed-composition nanoalloys it is necessary that the initial precursor decomposition rates be similar in rate. In Chapter 4, methods were attempted to manipulate the kinetics of the carbonyl species to induce similar initial decomposition rates. Even more beneficial would be to use two metal carbonyls that have similar initial decomposition kinetics, without the need for kinetic manipulation. As a result, this study includes the examination of the possible use of $Co_4(CO)_{12}$ as an alternate cobalt carbonyl precursor.

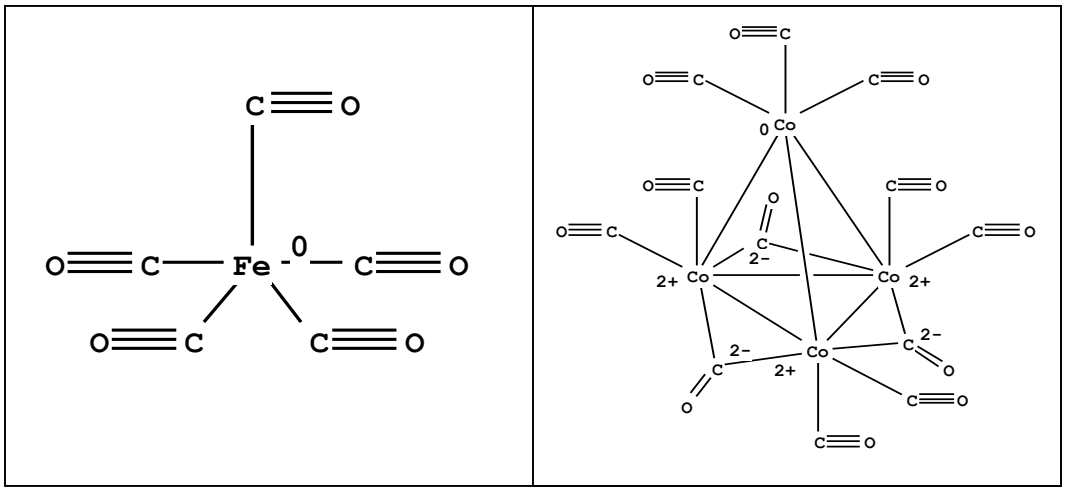

Figure 5.1: $Fe(CO)_5$ and $Co_4(CO)_{12}$, the metal carbonyls used in this section of the study

This work includes a kinetic study of the independent decomposition of $Co_4(CO)_{12}$ and determination of the influence of its presence on the decomposition of $Fe(CO)_5$ in stabilizing conditions. From previous work[10,11], we would expect that low concentration metal carbonyls would not have a strong mutual influence on their rates of reaction in these dilute and stabilized systems, partially due to the different diffusional patterns that the metal carbonyl precursors would experience in the presence of polymer chains. Moreover, the ability of polymer chains to strongly adsorb onto the surface of the growing clusters, reduces surface energy of the cluster, and as a result, reduces the energy of nucleation for both metals.

In pursuit of the above-mentioned goals, several different experiments were performed. Section 5.2 contains a kinetic analysis of the $Co_4(CO)_{12}$ alone. Section 5.3 shows kinetic analysis of mixed systems with equal concentrations of both carbonyls. Section 5.4 investigates systems with initial concentrations which satisfy the 'quadratic relationship' for determining the appropriate concentration of precursors to induce equal initial decomposition rates. Section 5.5 and 5.6 include the analysis needed to determine the effect of concentration on the kinetic rate constant for each carbonyl.

5.2 Kinetic analysis of $Co_4(CO)_{12}$

In order to obtain kinetic data for the cobalt precursor alone, $Co_4(CO)_{12}$ was allowed to decompose in a solution containing polystyrene (PS), M_W = 100,000 g/mol. Polystyrene was dissolved in 150 mL of toluene solvent (Fisher) to obtain a solution with polymer concentration just below c* (critical coil overlap, 1.86 wt % for this molecular weight and toluene solvent combination).

After the initial spectrum of the polystyrene solution was measured, $Co_4(CO)_{12}$ was added to the three-neck flask in order to produce a $4.35 \cdot 10^{-3}$ M carbonyl solution. The solution was flushed with nitrogen while the carbonyl was added and the mixture was continuously heated at 90ºC. An initial sample of the $Co_4(CO)_{12}$ in polystyrene and toluene was removed via the rubber stopper neck. A spectrum of the initial metal carbonyl solution was measured and the cell was subsequently flushed and cleaned as previously described. Aliquots were removed every 15 min and their infrared spectra were recorded. After the characteristic cobalt carbonyl bands (for this precursor, these bands appear at 2200 cm^{-1})[43] on the spectrum had completely disappeared, the reaction was stopped and the solution was stored in vials under nitrogen.

The extinction coefficient (ε) of $Co_4(CO)_{12}$ was experimentally determined by measuring the characteristic carbonyl bands of 4 known concentration solutions of $Co_4(CO)_{12}$ in c* polymer concentrations. As previously discussed, the extinction

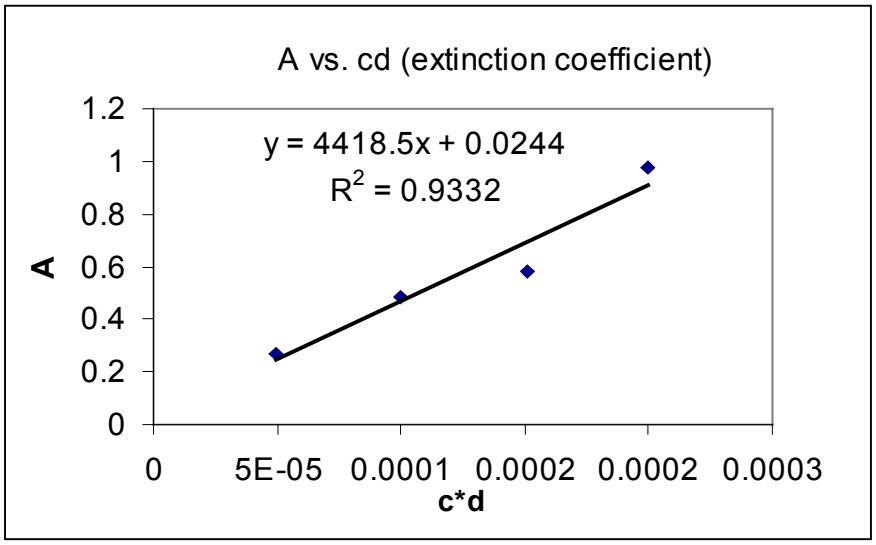

Figure 5.2: Calculation of extinction coefficient of $Co_4(CO)_{12}$

coefficient, ε=4418 L mol^{-1} s^{-1}, was determined from the slope of a linear plot of

absorbance versus the product of concentration and path length, Figure 5.2.

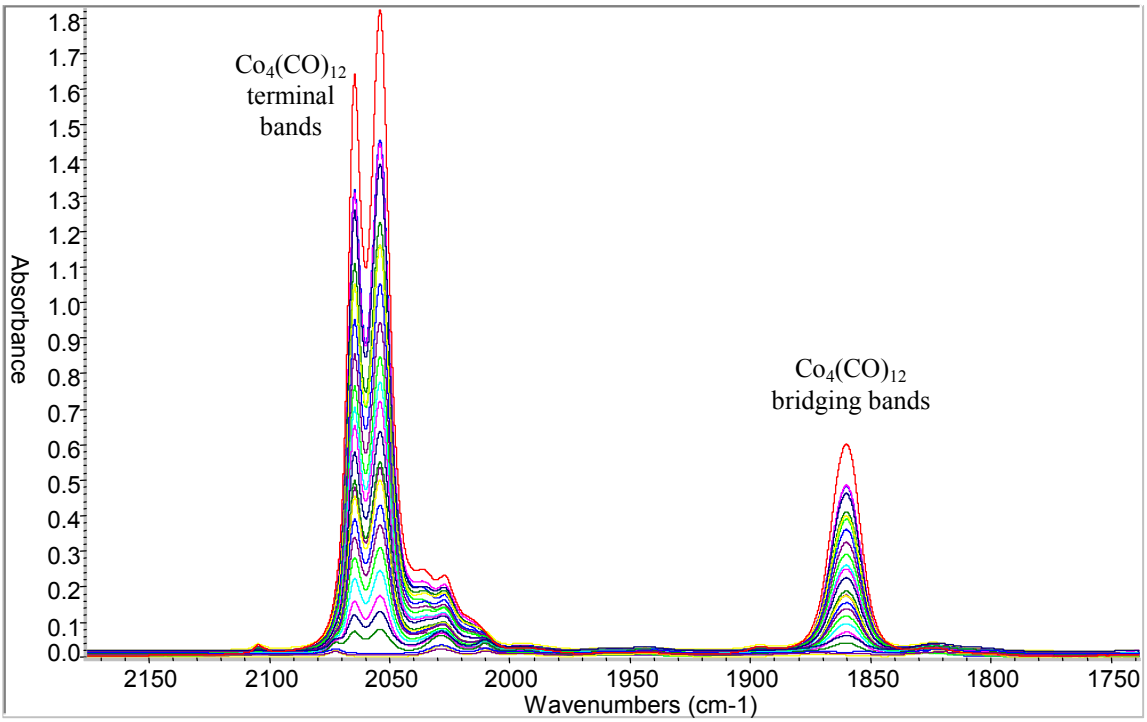

Figure 5.3: FT-IR spectra of $Co_4(CO)_{12}$

Examining the decomposition kinetics, Figure 5.4, the decomposition of $Co_4(CO)_{12}$ appears to be a first-order process with a rate constant of $1.25 \cdot 10^{-4}$ s^{-1}. This rate is very similar to that of $Co_2(CO)_8$ ($1.34 \cdot 10^{-4}$ s^{-1}), which is not entirely unexpected, Table 5.1. The decomposition of $Co_2(CO)_8$ produces $Co_4(CO)_{12}$ as an intermediate in its formation of Co and $CO_{(g)}$.[36] Observing the similarities in decomposition rates of these species, it is determined that the decomposition of the intermediate, $Co_4(CO)_{12}$, is the rate determining step in the $Co_2(CO)_8$ decomposition.

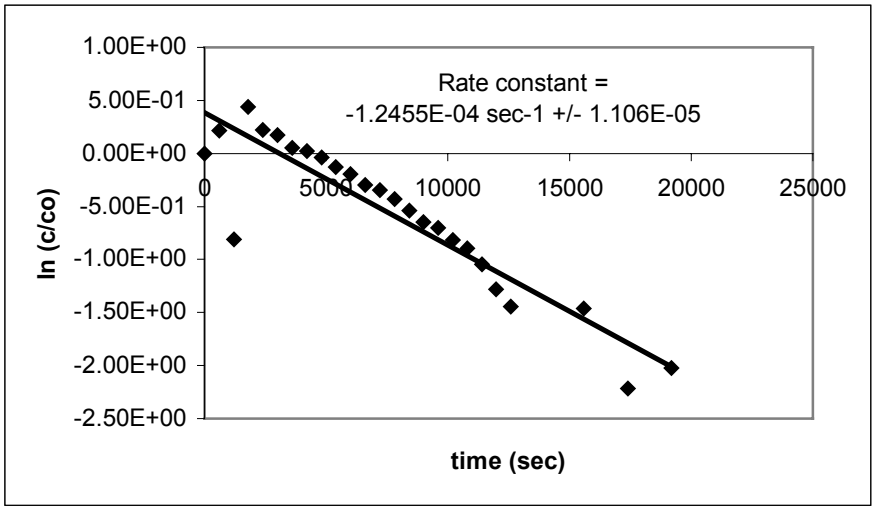

Figure 5.4: First-order kinetics of the decomposition of $Co_4(CO)_{12}$

Table 5.1: Comparison of rate constants of $Co_2(CO)_8$ and $Co_4(CO)_{12}$

Precursor	Rate Constant (s^{-1})
$Co_2(CO)_8$	$1.38 \cdot 10^{-4}$
$Co_4(CO)_{12}$	$1.25 \cdot 10^{-4}$

TEM micrographs were obtained from nanoclusters formed via the decomposition of $Co_4(CO)_{12}$ alone in polystyrene. Solutions of the clusters are gray in color with visible agglomerations of solids present in the solutions. Resulting images indicate chain structures and nanoscale (25.4 ± 4.3 nm) spherical features. Diffraction patterns indicate an hcp structure, commonly found in zero-valent cobalt. Chain structures are common in

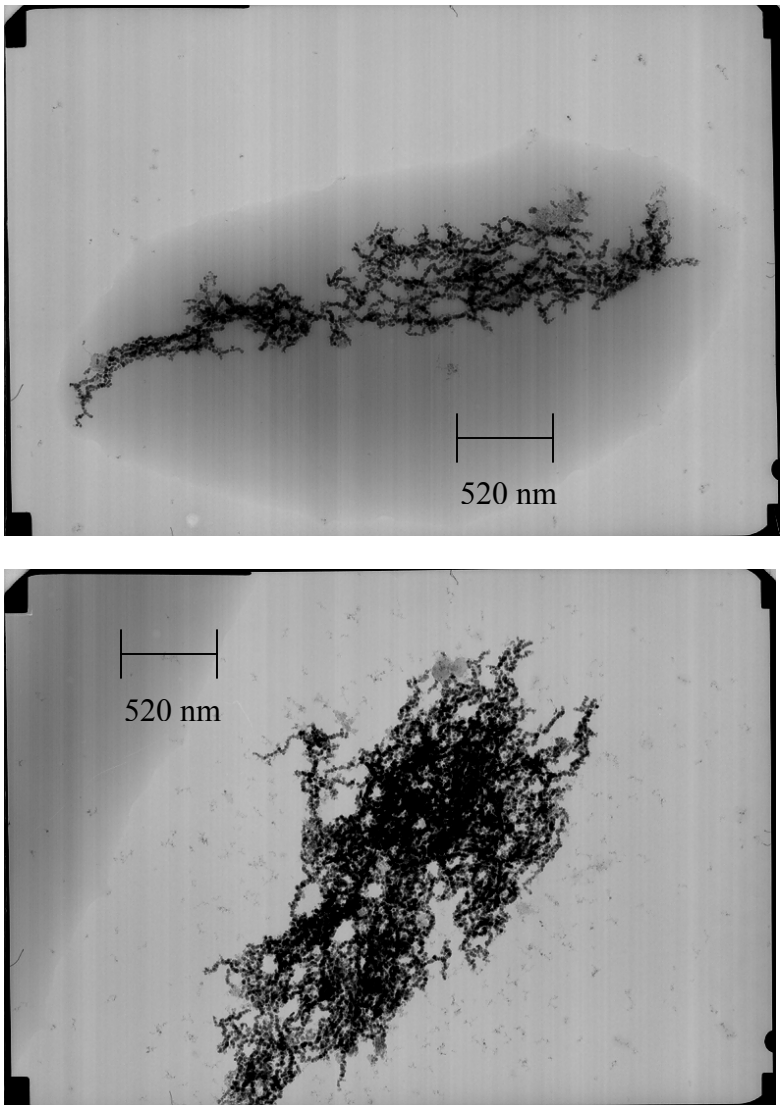

Figure 5.5: TEM micrographs showing the bulk structure of Co nanoclusters formed from $Co_4(CO)_{12}$

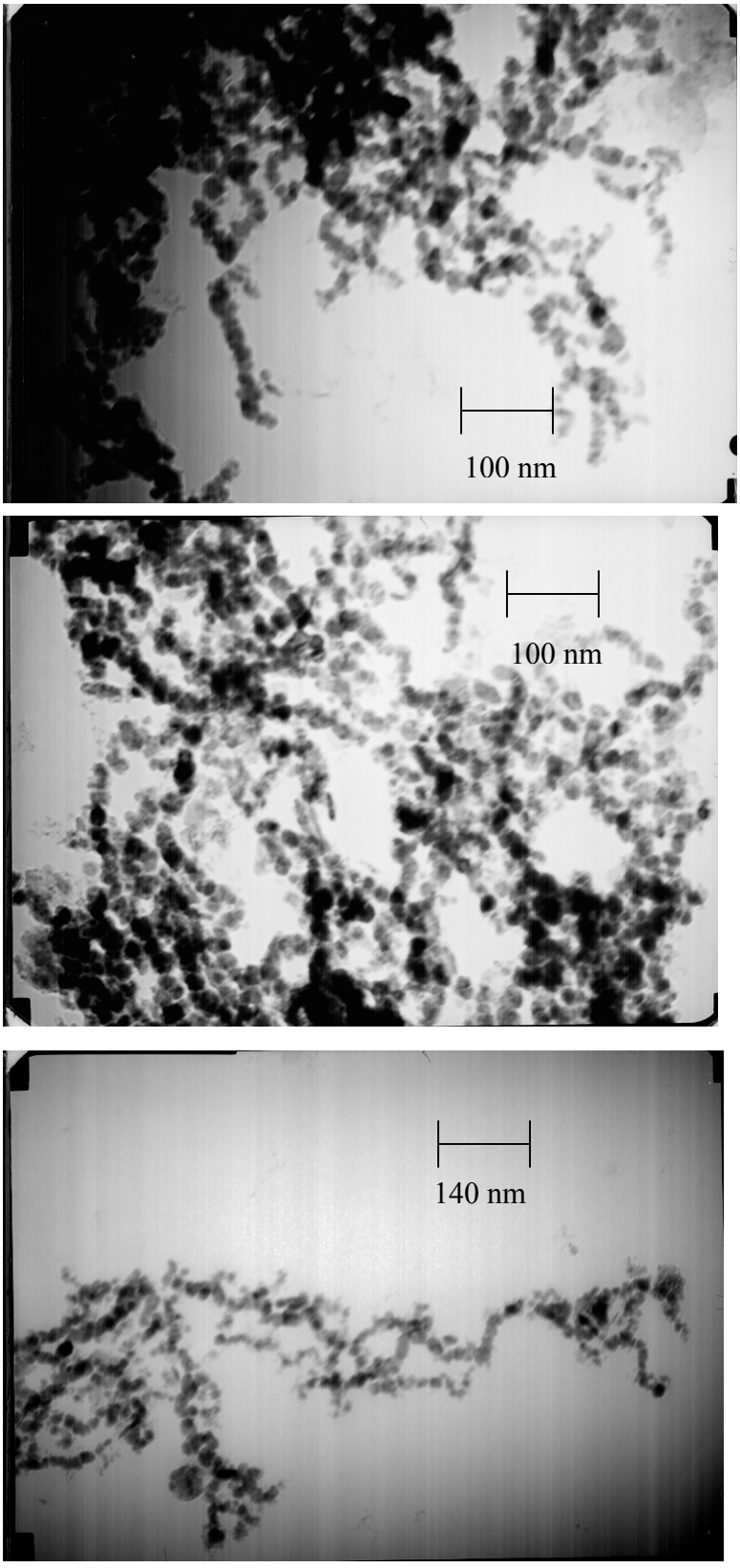

Figure 5.6: TEM micrographs showing the organization of Co nanoclusters formed via the decomposition of $Co_4(CO)_{12}$

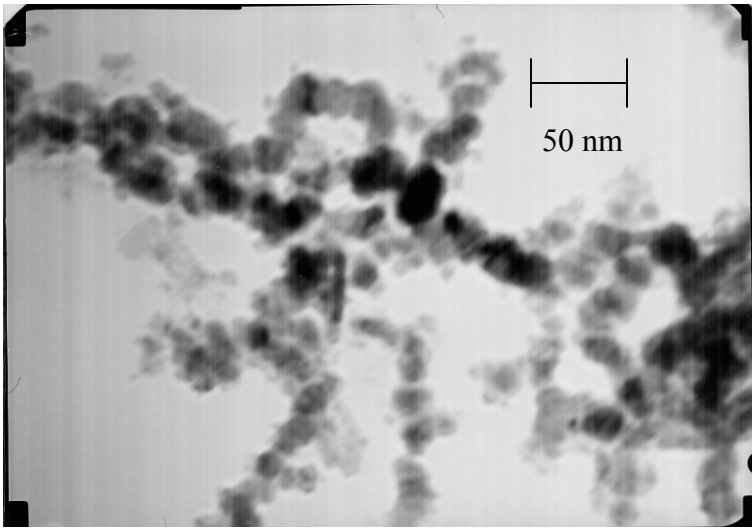

Figure 5.7: TEM micrograph showing the chain structure of Co nanoparticles formed via the decomposition of $Co_4(CO)_{12}$

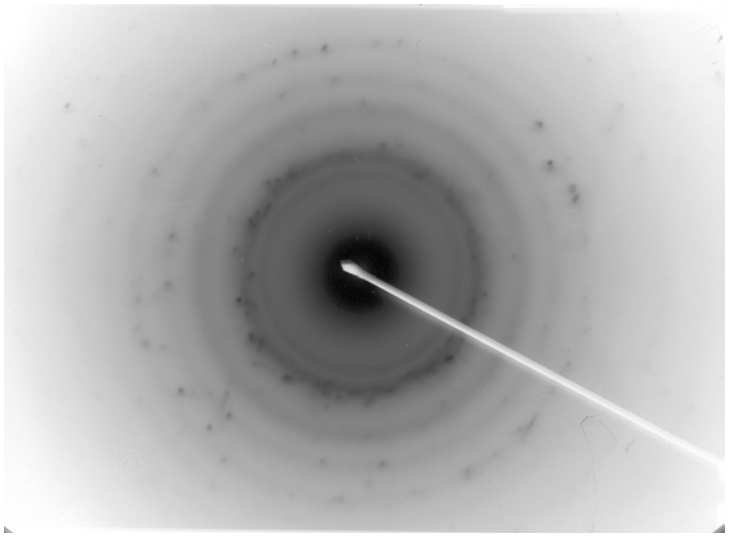

Figure 5.8: Electron diffraction pattern of Co nanoparticles with hcp structure

polystyrene-stabilized systems as polystyrene is relatively weakly bonded to the metal surfaces (via its aromatic ring).[38,39] Because this bonding is weak, the polymer chain does

not closely adhere to the cluster and sterically block the metal surface, leaving bare cluster area exposed and allowing the clusters to approach each other and grow together.

The magnetic nature of these clusters also provides an explanation for the chain structure that is produced. At the nanoscale, transition metal nanoclusters may exhibit single domain magnetism, with a very strong magnetic moment in a single direction. In a

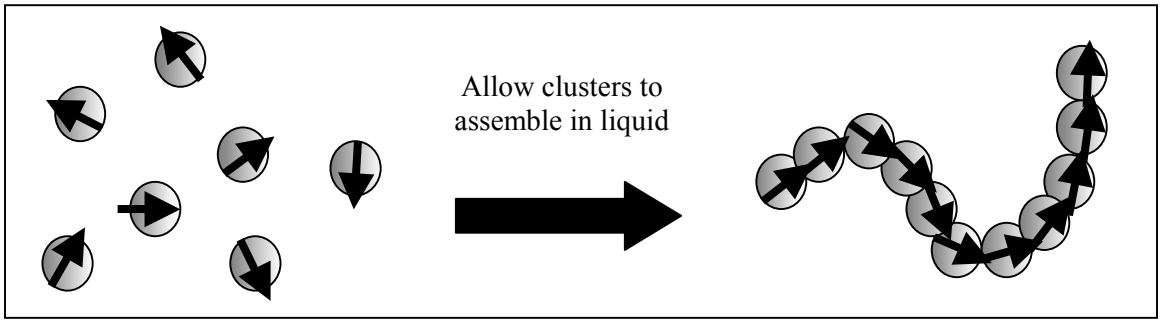

Figure 5.9: Schematic of formation of chain structures with single-domain nanoparticles in a fluid

liquid solution, the nanoparticles will be free to agglomerate and organize in a structure that will align their magnetic moments and minimize the overall system energy. In order to reduce their overall energy, the nanoparticles will align in chains.

5.3 Kinetic analysis of mixed (1:1) system with $Fe(CO)_5$ and $Co_4(CO)_{12}$

Despite the similarities in the decomposition rates of $Co_4(CO)_{12}$ and $Co_2(CO)_8$, it was necessary to further investigate the use of $Co_4(CO)_{12}$ as a possible cobalt precursor. In order to determine the mutual influence of the decompositions of $Fe(CO)_5$ and $Co_4(CO)_{12}$, an attempt was made to co-decompose a solution that contained $5 \cdot 10^{-3}$ M $Fe(CO)_5$ and $5 \cdot 10^{-3}$ M $Co_4(CO)_{12}$. Due to volatility and solubility problems, the actual molar concentrations (as determined by manipulating the experimentally-determined extinction coefficient and the absorbance of the characteristic carbonyl peaks) produced

were $[Co_4(CO)_{12}]$ = $2.69 \cdot 10^{-3}$ M and $[Fe(CO)_5]$= $4.66 \cdot 10^{-3}$M.

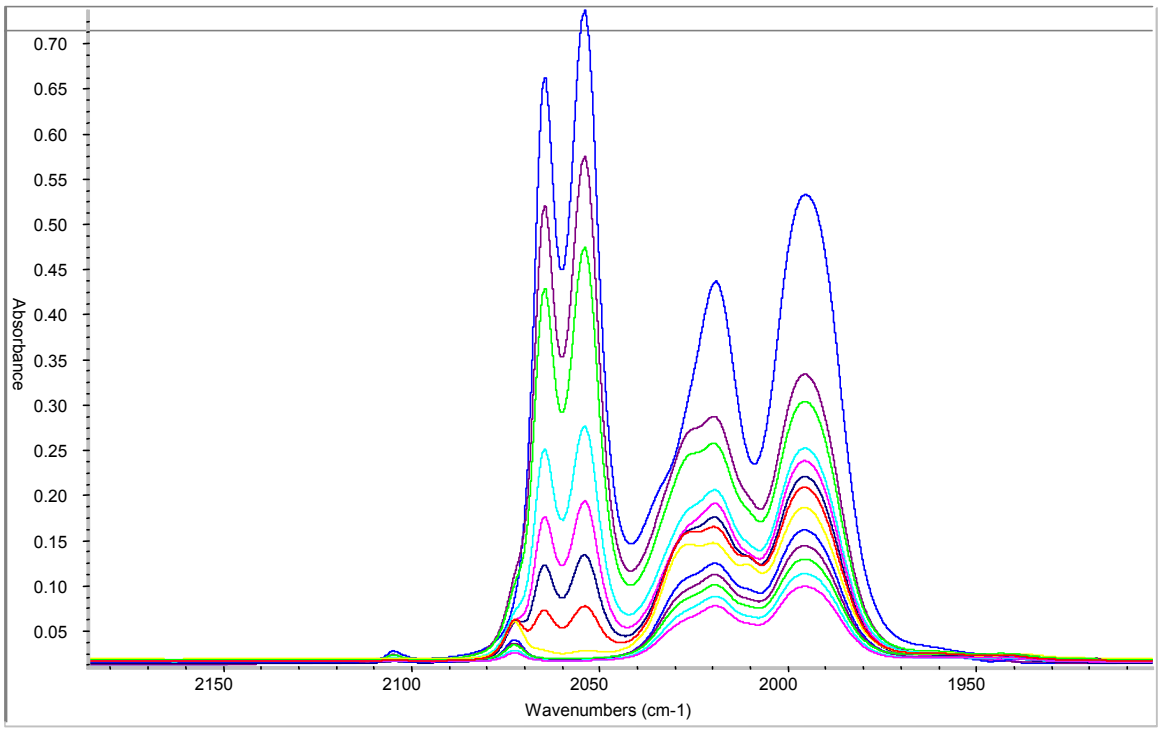

Figure 5.10: FT-IR spectra of equal amounts of $Fe(CO)_5$ and $Co_4(CO)_{12}$

When the initial decomposition rates of these species were calculated, it was found that the presence of $Co_4(CO)_{12}$ in the solution has an influence on the decomposition rate of $Fe(CO)_5$. The normalized decomposition rate of the $Co_4(CO)_{12}$ remains similar to that of its individual decomposition, but the normalized decomposition rate of the $Fe(CO)_5$ increases from $6.90 \cdot 10^{-5}$ s^{-1} to $2.80 \cdot 10^{-4}$ s^{-1}, which represents a 30%

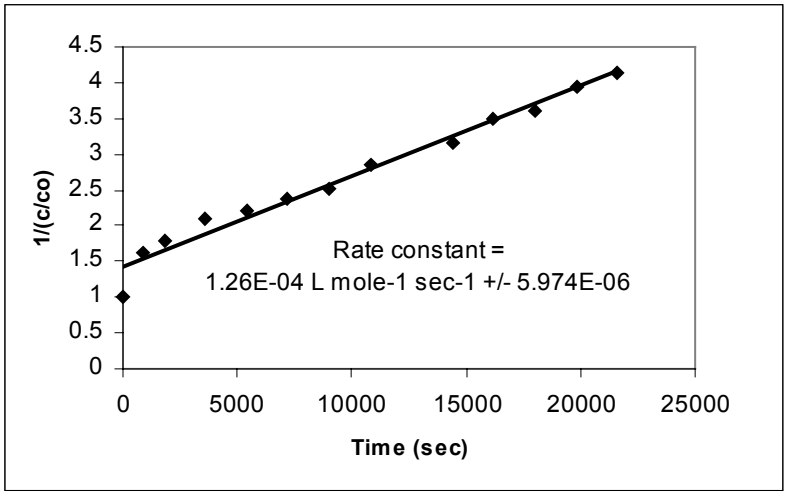

Figure 5.11: Second order decomposition kinetics of $Fe(CO)_5$ with $Co_4(CO)_{12}$

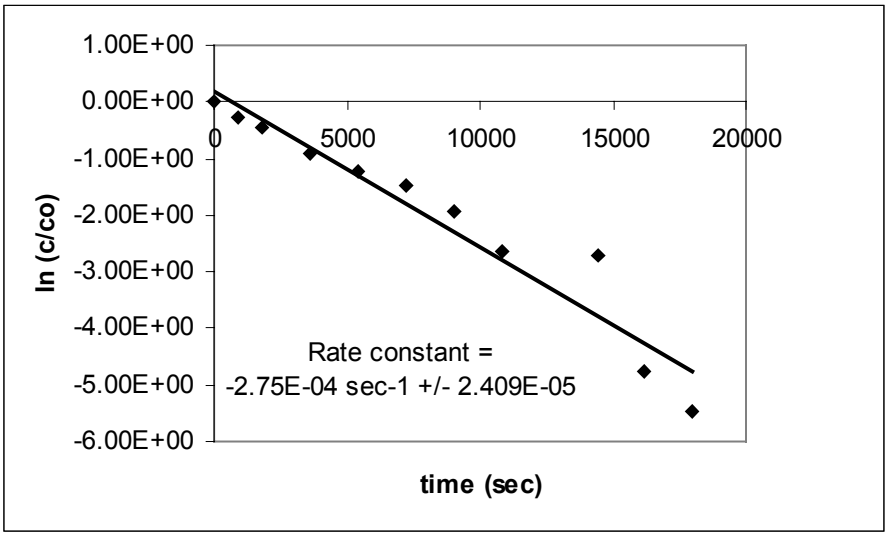

Figure 5.12: First order decomposition kinetics of $Co_4(CO)_{12}$ with $Fe(CO)_5$

increase in the rate constant, Figures 5.11 and 5.12. The decomposition of $Fe(CO)_5$ is, therefore, clearly manipulated by the presence of $Co_4(CO)_{12}$ in the system.

TEM micrographs of nanoclusters created using this method indicate chains of nanoclusters with average size 22.8 ± 4.1 nm, Figures 5.13-5.14. In the solutions of these nanoclusters there are visible agglomerations of clusters, and when placed on a stir plate these agglomerations move in response to the applied magnetic field. This indicates that the clusters are highly magnetic, which also explains the presence of chain structures.

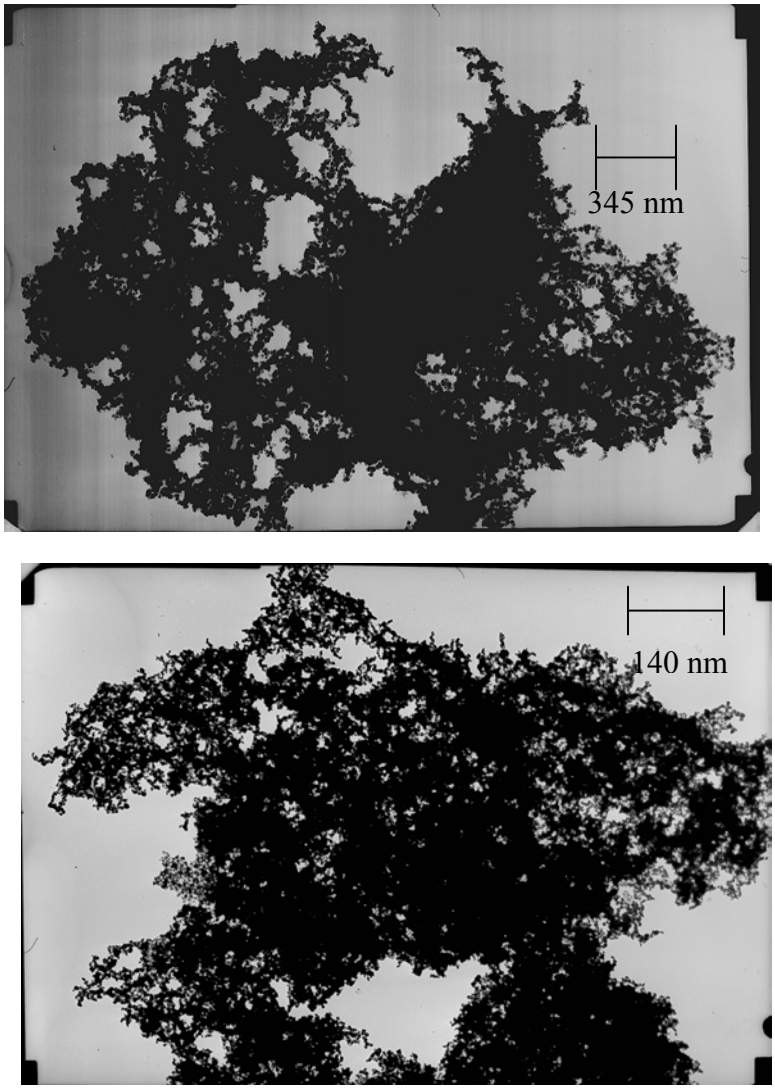

Figure 5.13: TEM micrographs showing the macroscale structure of an assembly of FeCo nanoparticles formed from equal molar amounts of precursors

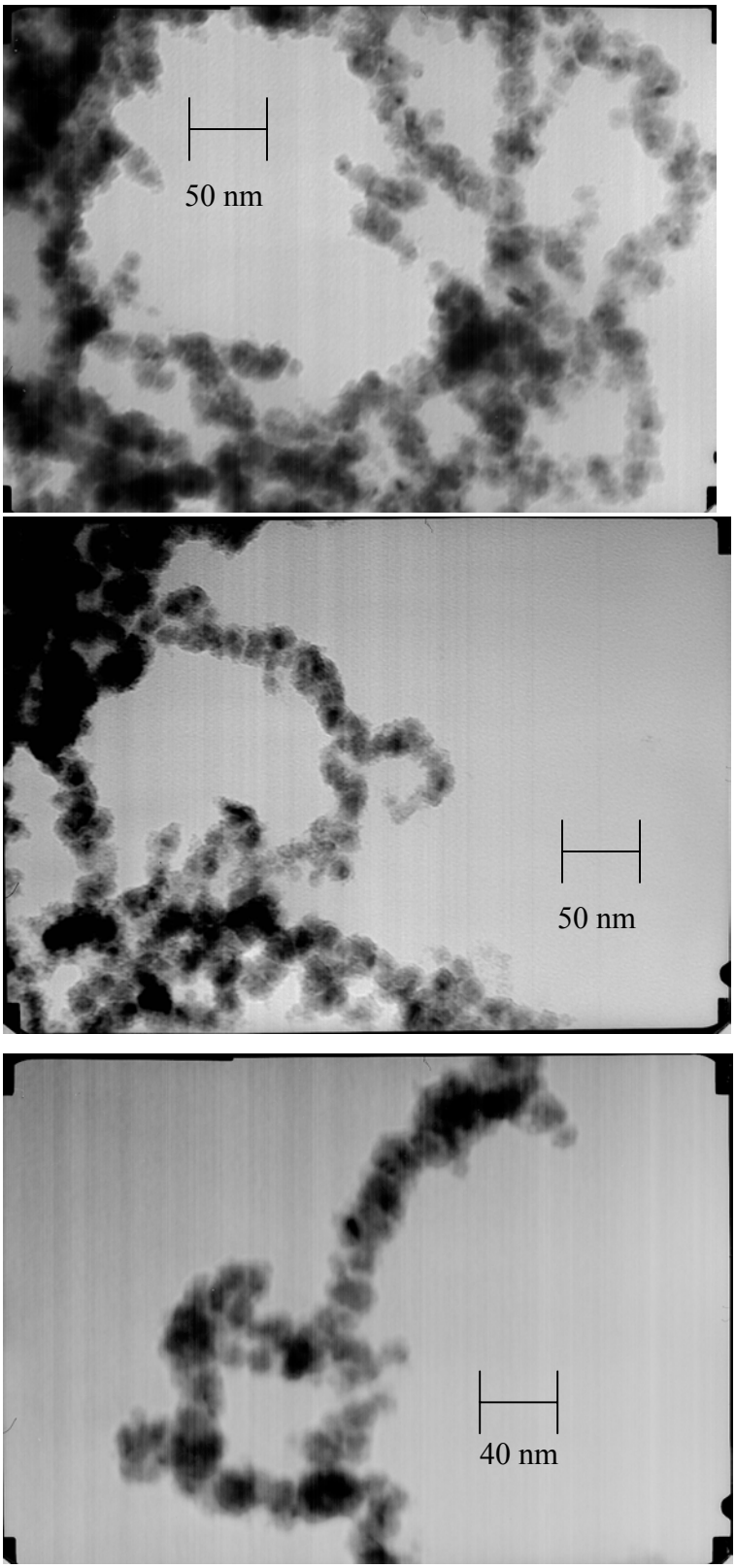

Figure 5.14: TEM micrograph showing the detailed chain structure of FeCo nanoclusters formed via the decomposition of equal amounts of metal carbonyl precursors

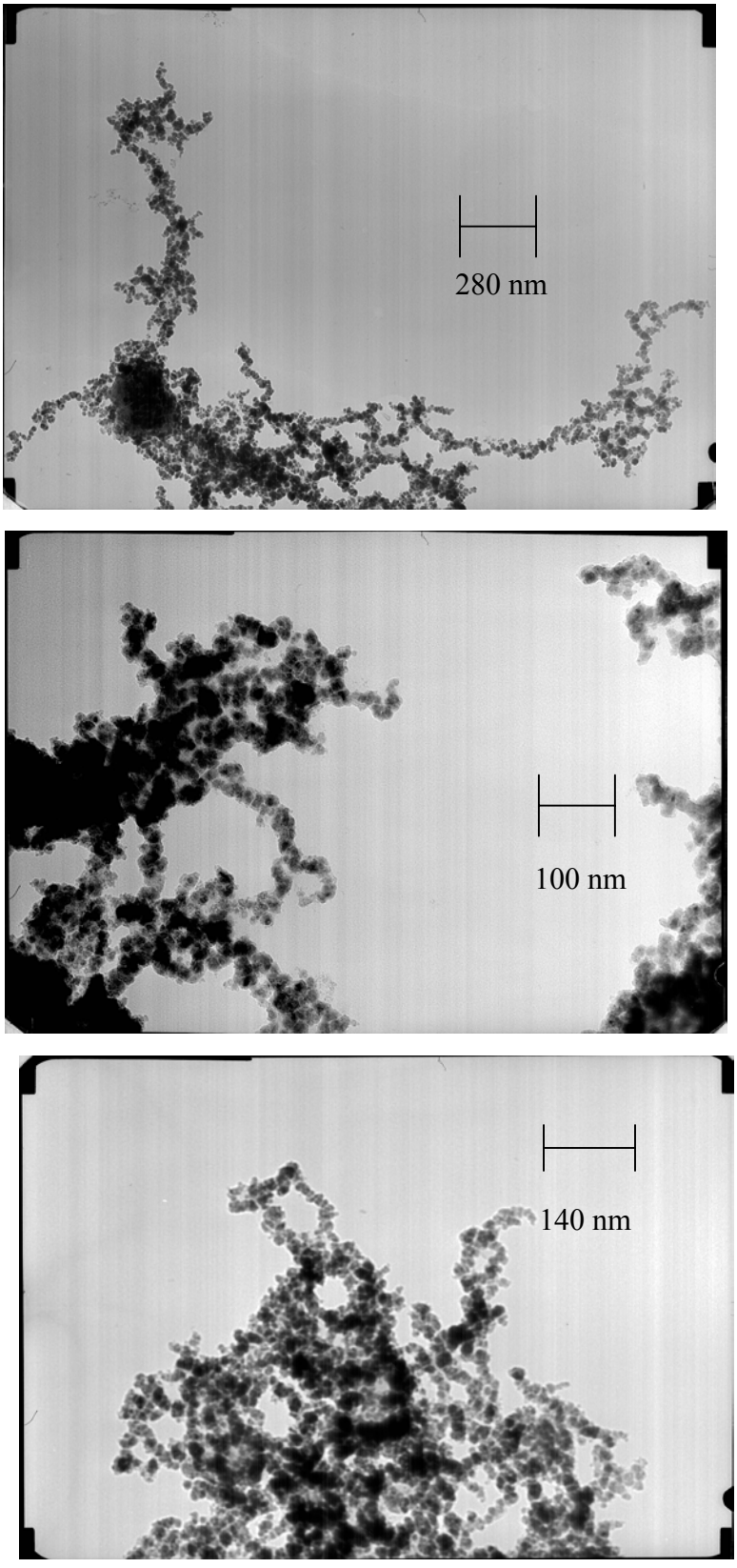

Figure 5.15: TEM micrographs showing the chain structure formed with FeCo nanoclusters synthesized using equal amounts of carbonyl precursors

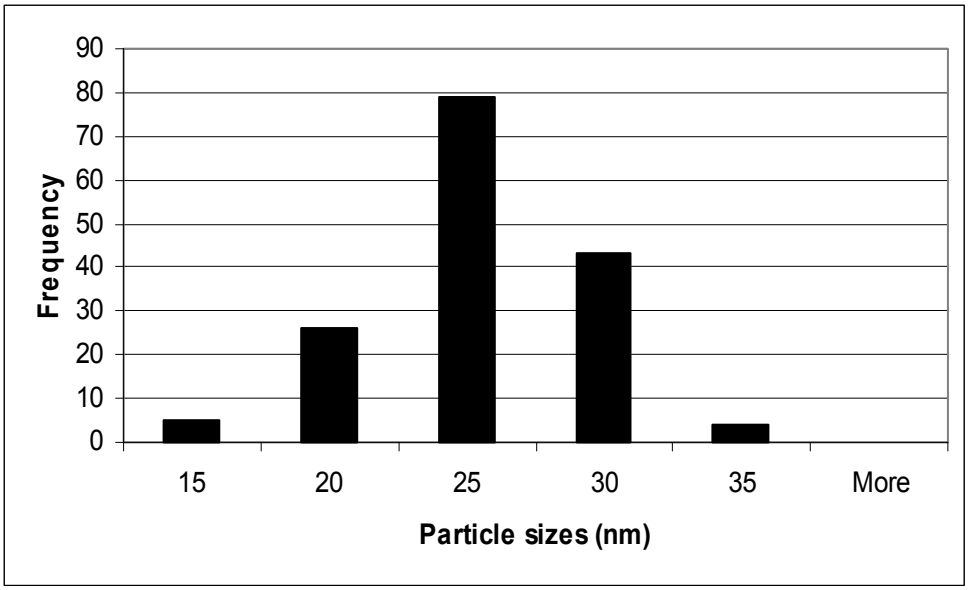

Figure 5.16: Histogram of particle sizes from equal amounts of $Fe(CO)_5$ and $Co_4(CO)_{12}$

Electron diffraction was performed on these nanoalloys, and the resulting patterns indicate a bcc crystal structure (Figure 5.17). This crystal structure is expected from the bulk phase diagram for the initial cobalt/iron ratio in the solution (70% Co, 30% Fe).

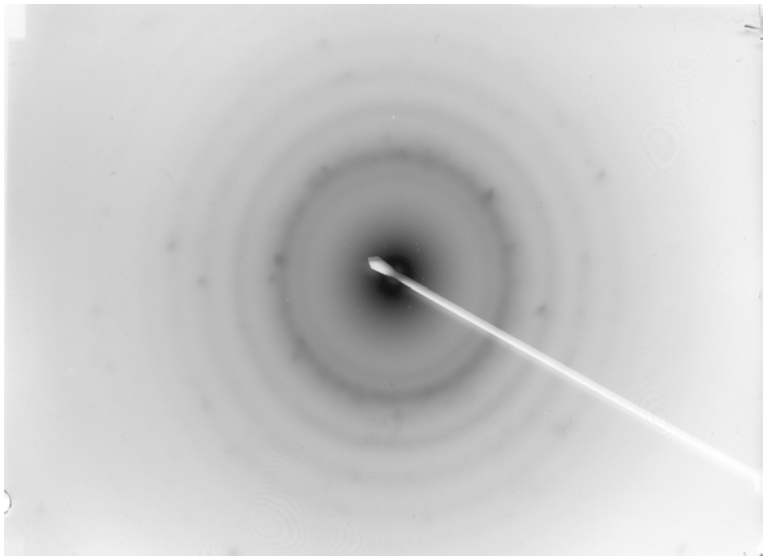

Figure 5.17: Electron diffraction pattern of FeCo from equal amounts of $Fe(CO)_5$ and $Co_4(CO)_{12}$ indicating a bcc structure

TGA was conducted on a film of these nanoalloys in polystyrene in order to investigate the surface chemistry of the clusters. Comparing the polymer decomposition slope to the decomposition of the pure polymer and the clusters produced from only $Co_4(CO)_{12}$ or from $Fe(CO)_5$, it should be noted that the slope of the mixed clusters is slightly different than both of these. Since the interaction of the polymer with the metal cluster surface can alter the temperature of the polymer burnoff, and this curve is different than the single metal cluster TGA curves, we can assume that the polymer is burning off of mixed composition cluster surfaces (a combination of the two types of metal surfaces).

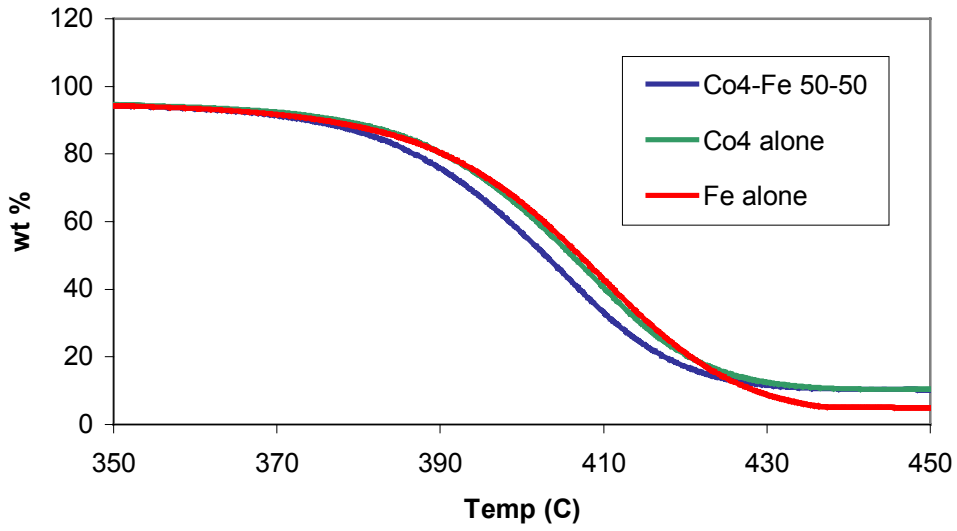

Figure 5.18: TGA of Co clusters, Fe clusters, and FeCo nanoalloys created with $Fe(CO)_5$ and $Co_4(CO)_{12}$

5.4 Mixed clusters from $Fe(CO)_5$ and $Co_4(CO)_{12}$ using "equal rates" relationship

In order to attempt to create nanoalloys with the best possible atomic mixing, there was a reconstruction of the quadratic relation ("equal rates") between reaction rates and carbonyl concentrations as previously used.

$$\frac{k_{Fe}}{k_{Co}} = \left(\frac{c_1}{c_2}\right)^2 + \frac{c_1}{c_2}$$

The initial concentration of $Co_4(CO)_{12}$ was chosen as $2.5 \cdot 10^{-4}$ M for this system. Calculation of the appropriate concentration of $Fe(CO)_5$ based on rate constants and the quadratic relationship generates a required concentration of $6.94 \cdot 10^{-3}$ M. Actual concentrations in solution were $[Co_4(CO)_{12}] = 2.85 \cdot 10^{-3}$ M and $[Fe(CO)_5] = 7.28 \cdot 10^{-3}$ M.

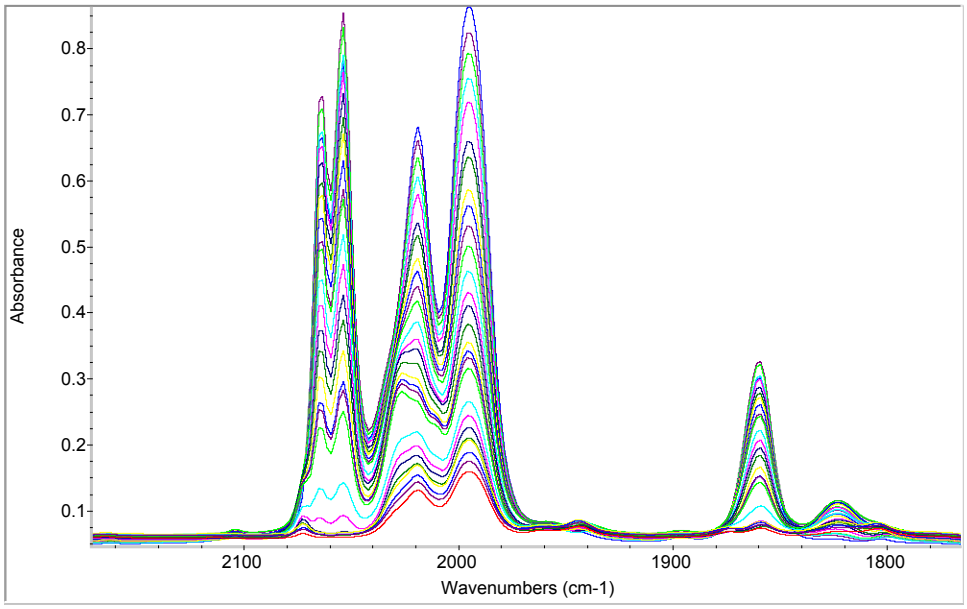

Figure 5.19: FT-IR spectra of "equal rates" method with $Fe(CO)_5$ and $Co_4(CO)_{12}$

The decomposition of $Co_4(CO)_{12}$ in the case is a first order reaction with initial rate constant $8.85 \cdot 10^{-5}$ s^{-1} and the decomposition of $Fe(CO)_5$ is a second order process with rate constant $1.56 \cdot 10^{-4}$ s^{-1}. Calculating the normalized initial decomposition rates (c/co) of these species, it is shown that the decomposition rate of $Co_4(CO)_{12}$ does not change significantly as compared to its decomposition rate alone (Figure 5.21) and the decomposition rate of $Fe(CO)_5$ also is not significantly altered (Figure 5.20). It is predicted that with a large difference in initial decomposition rates, the nanoclusters produced using these precursor concentrations would not have ideal atomic mixing and the cobalt species would decompose much more quickly than the iron species. It is predicted that these nanoalloys will exhibit a core-shell structure.

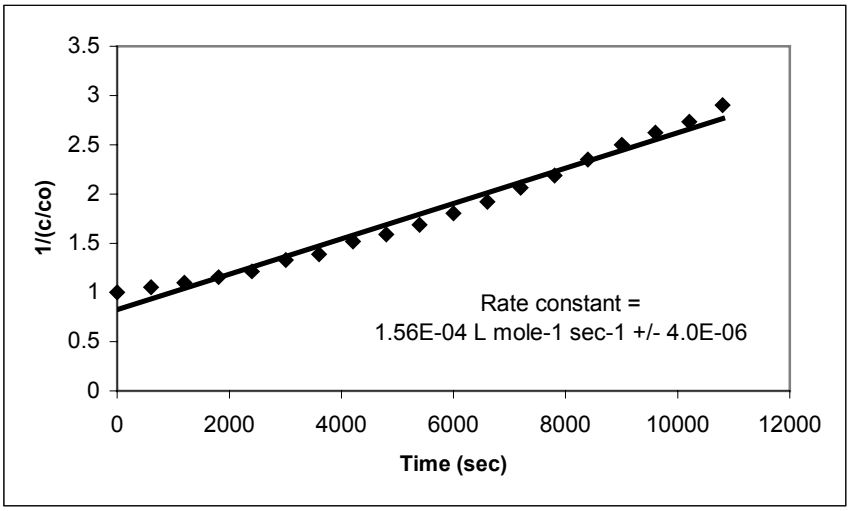

Figure 5.20: Second order decomposition of $Fe(CO)_5$ with $Co_4(CO)_{12}$ with equal rates

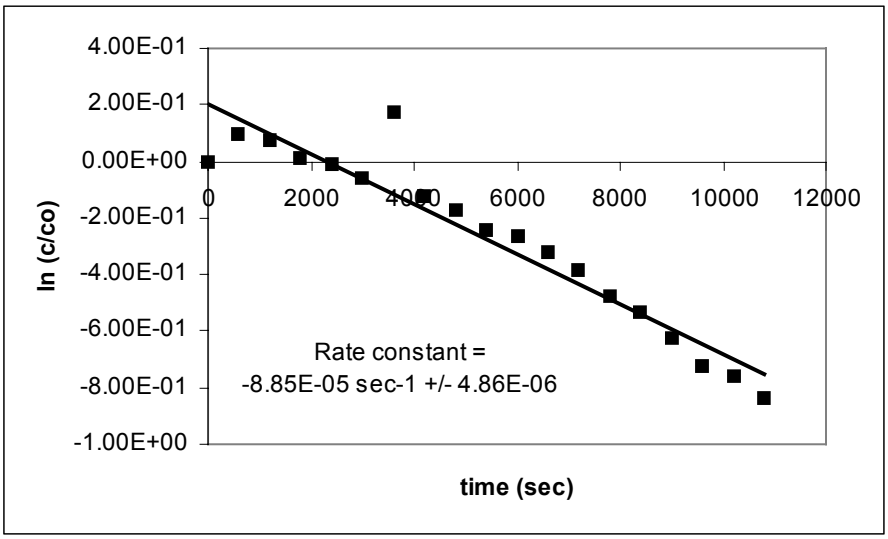

Figure 5.21: First order decomposition of $Co_4(CO)_{12}$ with $Fe(CO)_5$ with equal rates

TEM micrographs (Figure 5.22 and 5.23) of the resulting clusters indicate irregular shapes, but the majority of clusters are spherical with dark spots near their centers. The clusters form chains and are of average size 20.1± 2.7 nm. Electron diffraction (Figure 5.24) of these nanoalloys indicates a bcc structure. The initial iron/cobalt ratio was 61% Co/49% Fe. The bulk phase diagram indicates a bcc structure at that composition, so the resulting nanoalloys having this structure is reasonable.

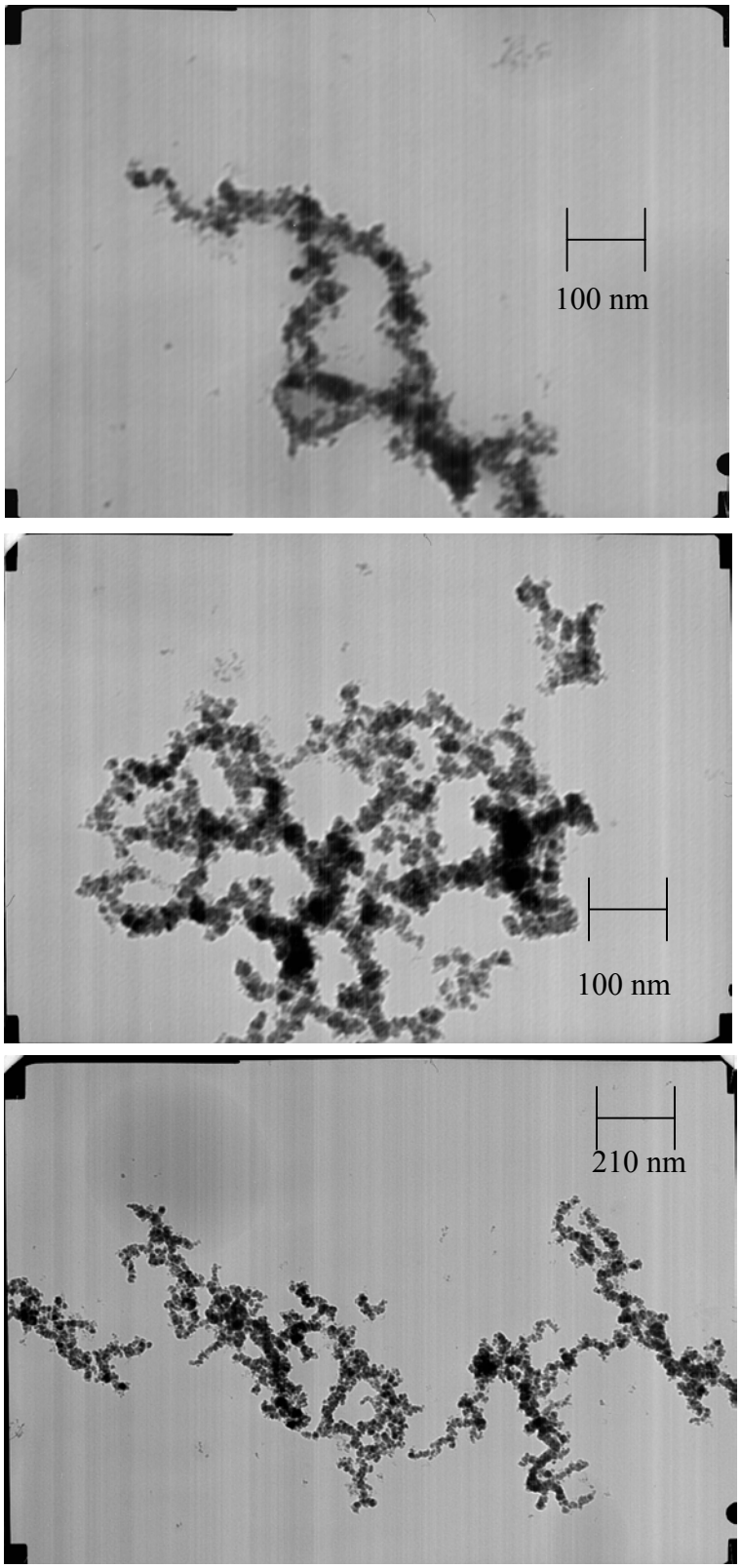

Figure 5.22: TEM micrographs of the macrostructure of FeCo nanoclusters formed using equal rates method

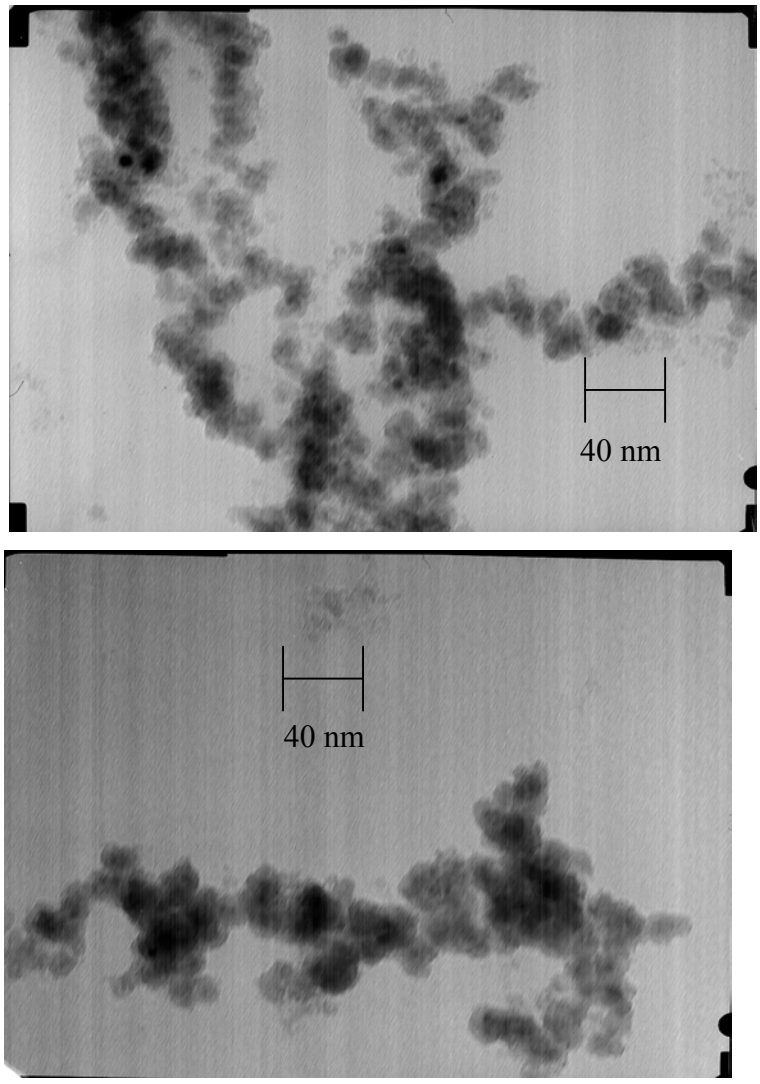

Figure 5.23: TEM micrographs showing the irregular structure of FeCo nanoclusters produced by the decomposition of metal carbonyl precursors with equal rates

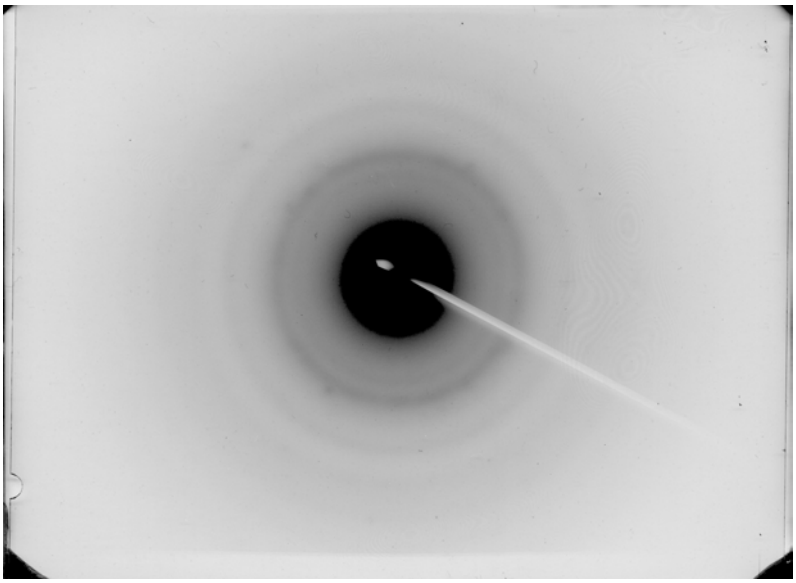

Figure 5.24: Electron diffraction pattern of FeCo nanoalloys synthesized from equal rates method showing a bcc structure

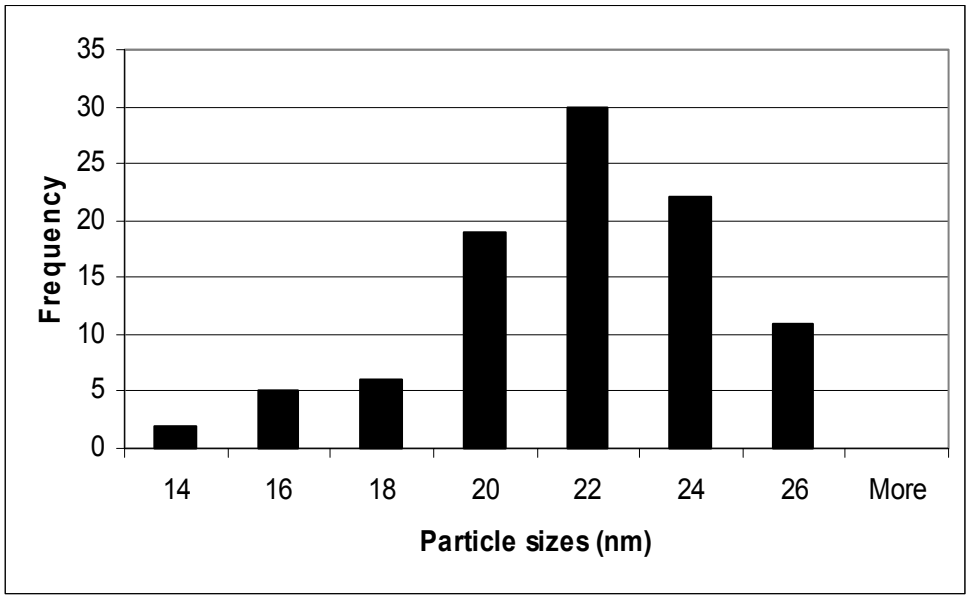

Figure 5.25: Histogram of particle sizes produced with equal rates method

5.5 Mixed carbonyl systems with 3:1 ratio of $Co_4(CO)_{12}$ and $Fe(CO)_5$

In order to examine a fuller composition range, another precursor ratio in the $Fe(CO)_5$-$Co_4(CO)_{12}$ binary system was chosen and a final trial was attempted with $7.5 \cdot 10^{-3}$ M $Co_4(CO)_{12}$ and $2.5 \cdot 10^{-3}$ M $Fe(CO)_5$. Actual concentrations in the solution were $[Co_4(CO)12] = 8.40 \cdot 10^{-3}$ M and $[Fe(CO)_5] = 2.63 \cdot 10^{-3}$ M.

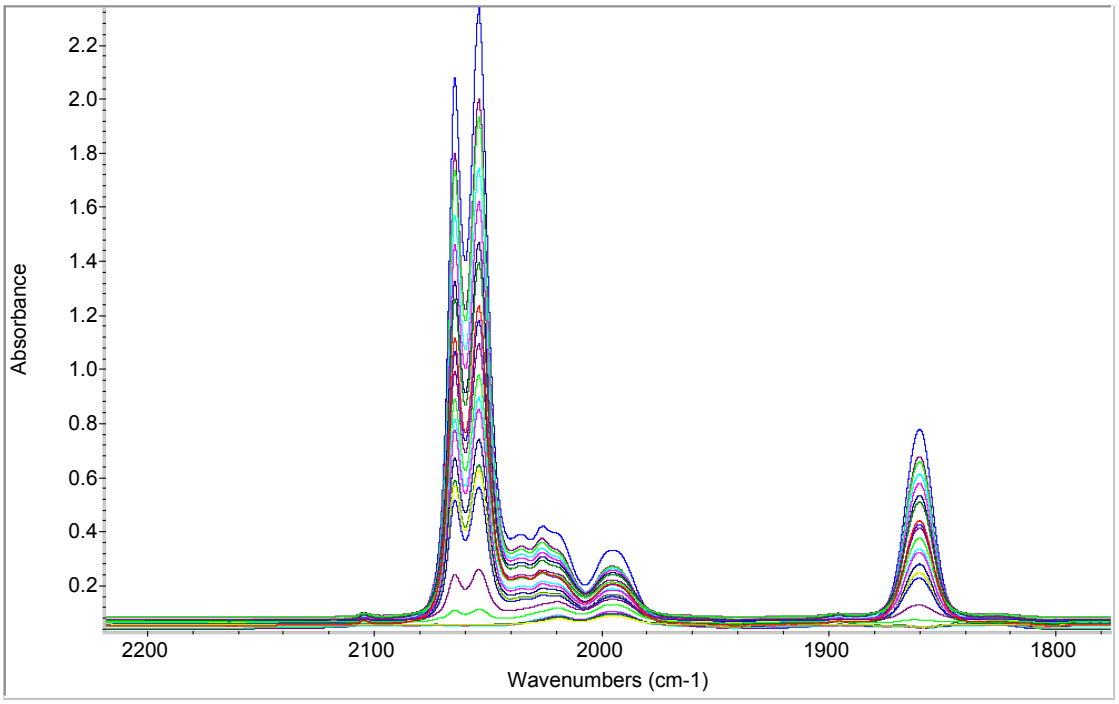

Figure 5.26: FT-IR spectra of co-decomposition of $Fe(CO)_5$ and $Co_4(CO)_{12}$

When the normalized initial rates of decomposition were calculated for these species, it is shown that the initial rate of decomposition of $Co_4(CO)_{12}$ is $2.20 \cdot 10^{-4}$, very similar to its decomposition rate in the other trials (Figure 5.28). The decomposition rate of this species is independent of the other species in the system. $Fe(CO)_5$, however, experiences a large increase in decomposition rate (increases to $3.39 \cdot 10^{-4}$ s^{-1}) (Figure 5.27). The decomposition reaction is clearly influenced by the presence of $Co_4(CO)_{12}$. It is predicted that with the difference in precursor decomposition rates, the cobalt species decompose more quickly, forming cobalt cores, and the iron species will form at a later time, forming shells on the cores.

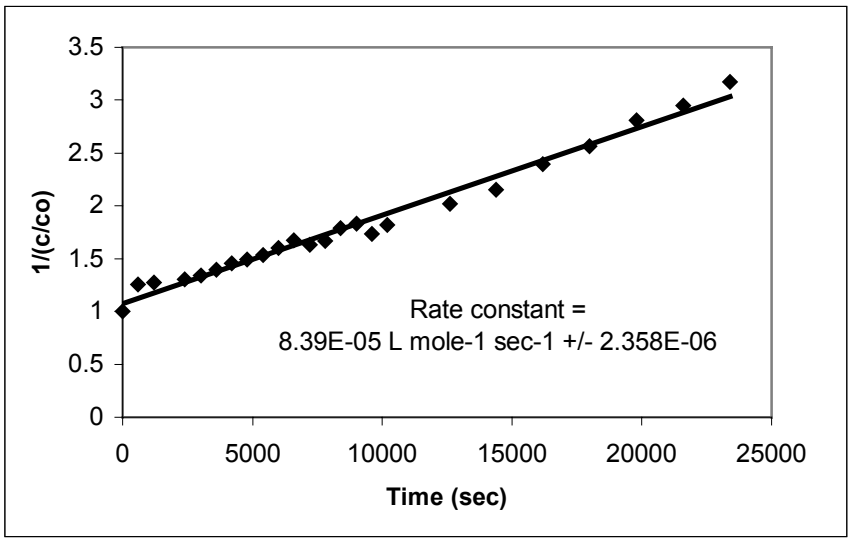

Figure 5.27: Second order decomposition kinetics of $Fe(CO)_5$ ($2.63 \cdot 10^{-3}$ M) with $Co_4(CO)_{12}$ ($8.40 \cdot 10^{-3}$ M)

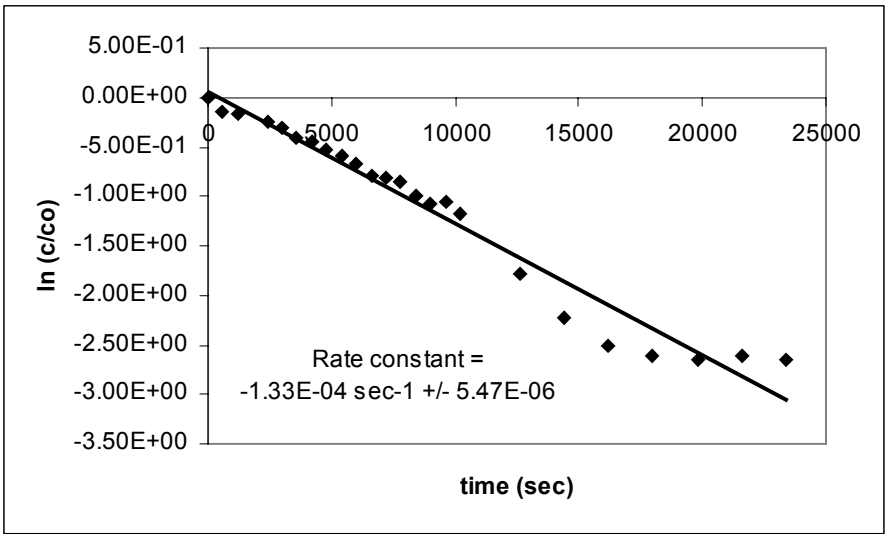

Figure 5.28: First order decomposition kinetics of $Co_4(CO)_{12}$ ($8.40 \cdot 10^{-3}$ M) with $Fe(CO)_5$ ($2.63 \cdot 10^{-3}$ M)

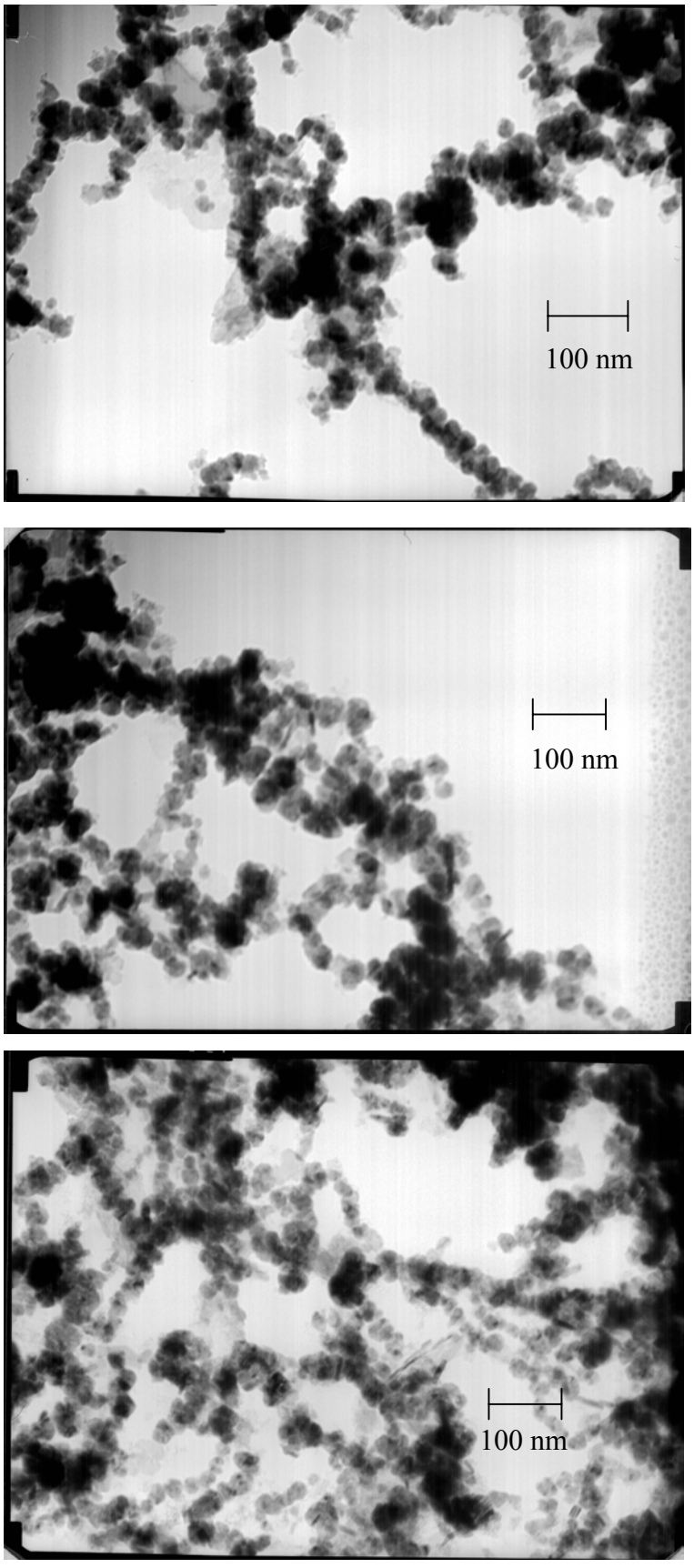

Figure 5.29: TEM micrographs showing the chain structure and spherical shapes of FeCo nanoclusters produced with a 3:1 ratio of $Co_4(CO)_8$ and $Fe(CO)_5$

TEM micrographs of the nanoclusters produced by this method indicate chain structures with clusters of diameter 45.4 ± 5.4 nm (Figures 5.28 and 5.29). They have visibly dark areas, indicating crystalline regions. Diffraction patterns of a collection of the clusters also indicate an hcp structure, commonly found in zero-valent cobalt. This could be expected if the system has such an overwhelming amount of cobalt (the reaction's initial cobalt/iron ratio was 92.7% Co and 7.3% Fe) and if the nanoalloys exhibit a core-shell structure with cobalt cores and iron shells. The core cobalt will be protected from oxidation by the iron shells during the diffraction, thus zero-valent cobalt should appear in the diffraction studies.

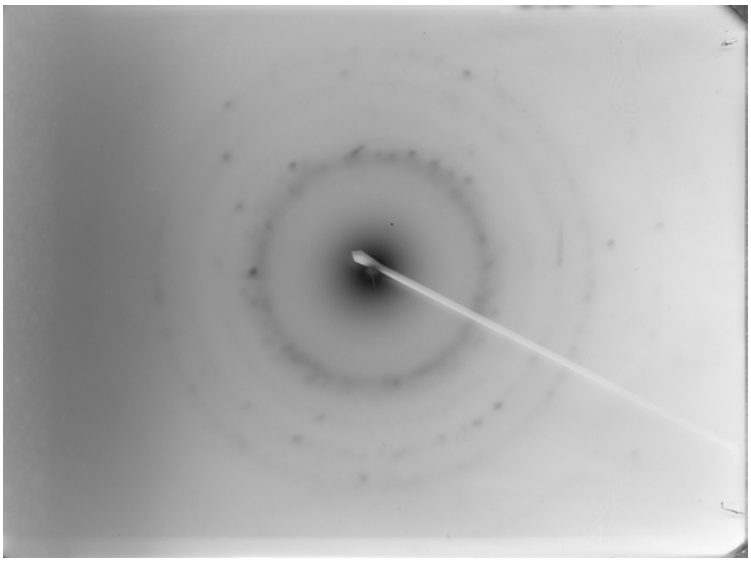

Figure 5.30: Diffraction pattern of FeCo nanoalloys from $Fe(CO)_5$ and $Co_4(CO)_{12}$ indicating an hcp structure

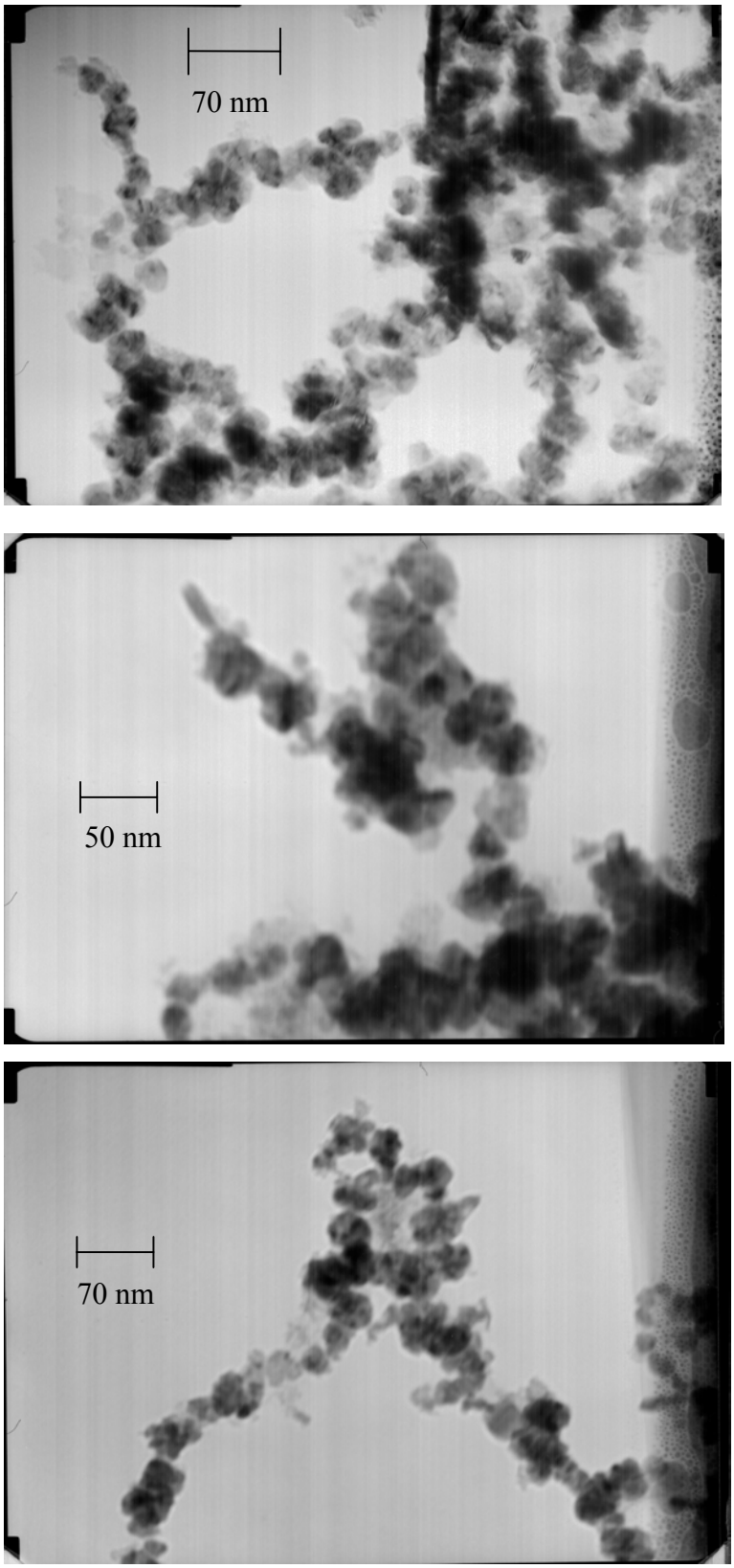

Figure 5.31: High resolution TEM micrographs showing the chain structure of FeCo nanoparticles created with a 3:1 $Co_4(CO)_{12}$ to $Fe(CO)_5$ ratio

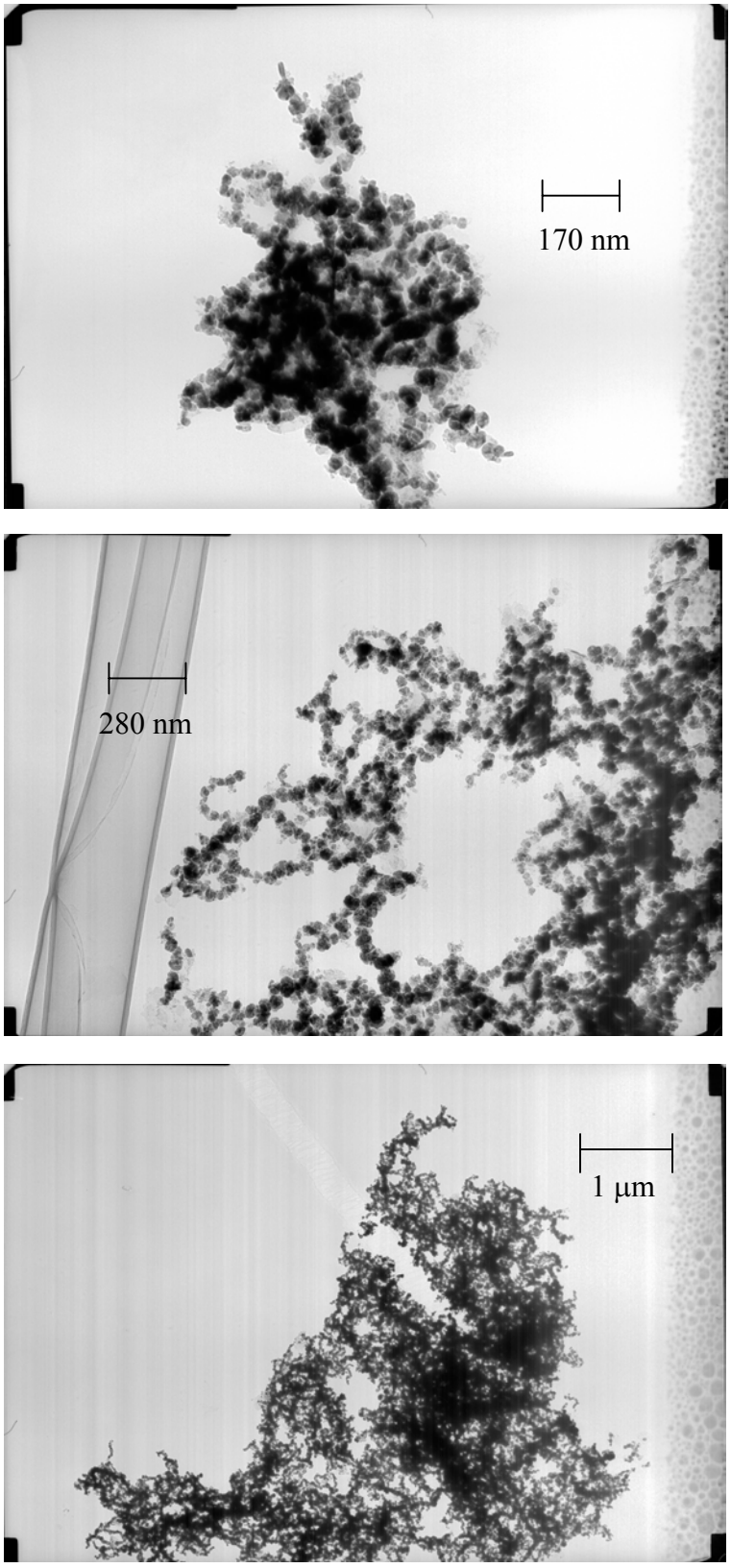

Figure 5.32: Low magnification TEM micrographs showing the chain structure of FeCo nanoparticles created with a 3:1 $Co_4(CO)_{12}$ to $Fe(CO)_5$ ratio

5.6 Kinetics as a function of mixed carbonyl composition

A compilation of the kinetic data from these trials strongly indicate the influence of the presence of $Co_4(CO)_{12}$ on the decomposition of $Fe(CO)_5$. From previous work, it was determined that the dilute concentration of the carbonyl precursors ensures that their decompositions occur independently and uninfluenced by the other precursors. However, in this case there is a clear indication that the $Fe(CO)_5$ decomposition into Fe metal and CO gas is being catalyzed by something in the system.

A possible explanation for the increase in decomposition rate of $Fe(CO)_5$ could be the relatively fast nucleation of Co clusters by the decomposition of the $Co_4(CO)_{12}$. Since the decomposition of $Co_4(CO)_{12}$ into Co and CO gas normally occurs much more quickly than the decomposition of $Fe(CO)_5$, the first homogeneously nucleated clusters will likely be cobalt. Once these seed clusters have formed, the energy required to homogeneously nucleate Fe clusters is no longer an impediment to the decomposition process and the formation of Fe metal. After cobalt clusters have homogeneously nucleated, the iron can collect on their surfaces heterogeneously. The heterogeneous nucleation energetic pathway requires much less energy than that of homogeneous nucleation, providing an explanation for the increase in decomposition rate of the transition of $Fe(CO)_5$ to Fe and CO gas.

Using the initial rate constants from the $Co_4(CO)_{12}$-$Fe(CO)_5$ decompositions and calculating the percent of cobalt (as compared to the total amount of iron and cobalt) in each system, one can plot the decomposition rate constants k_{dec} against composition (Figure 5.33).

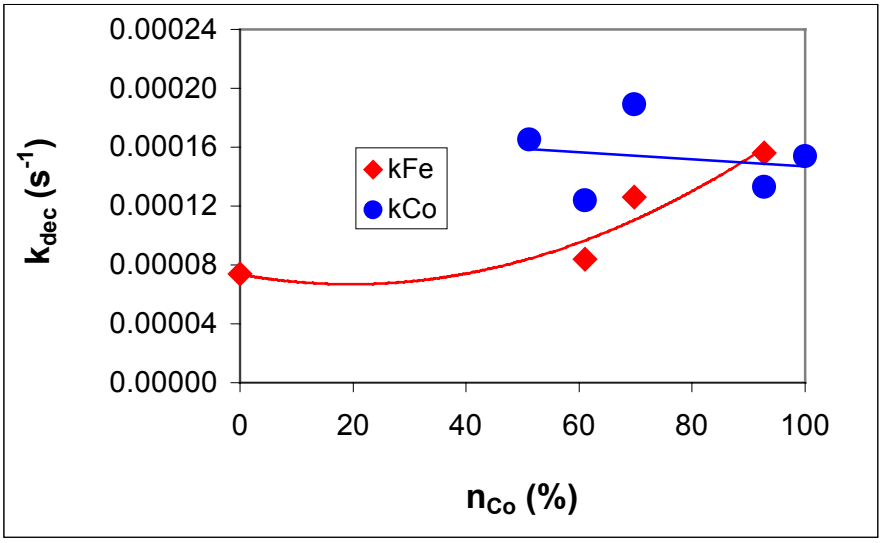

Figure 5.33: Decomposition rate constants of $Co_4(CO)_{12}$ and $Fe(CO)_5$ with respect to composition

Fitting the curves created with the kinetic information provides an overall picture of the $Fe(CO)_5$-$Co_4(CO)_{12}$ system. It is clear that the co-decomposition of these species influence each others' decomposition rate constants, but it is necessary to determine the impact on the actual decomposition rates.

Calculating and plotting the normalized initial rates of decomposition (c/co) versus composition, it is possible to observe the true impact of the presence of $Co_4(CO)_{12}$ on the decomposition of $Fe(CO)_5$ (Figure 5.34). It is obvious that the initial decomposition rate of $Co_4(CO)_{12}$ is relatively unchanged, regardless of the presence or amount of $Fe(CO)_5$ in the system. $Fe(CO)_5$, however, undergoes a drastic increase in initial decomposition rate, increasing to five times the original decomposition rate, catalyzed by the presence of $Co_4(CO)_{12}$.

Because the decomposition of $Fe(CO)_5$ occurs more quickly in these systems than individually due to the formation of cobalt seed clusters, it is assumed that the $Fe(CO)_5$-$Co_4(CO)_{12}$ systems create core-shell type mixed-metal structures with zero-valent cobalt cores. This assumption is supported by the presence of zero-valent cobalt in the diffraction studies of these systems.

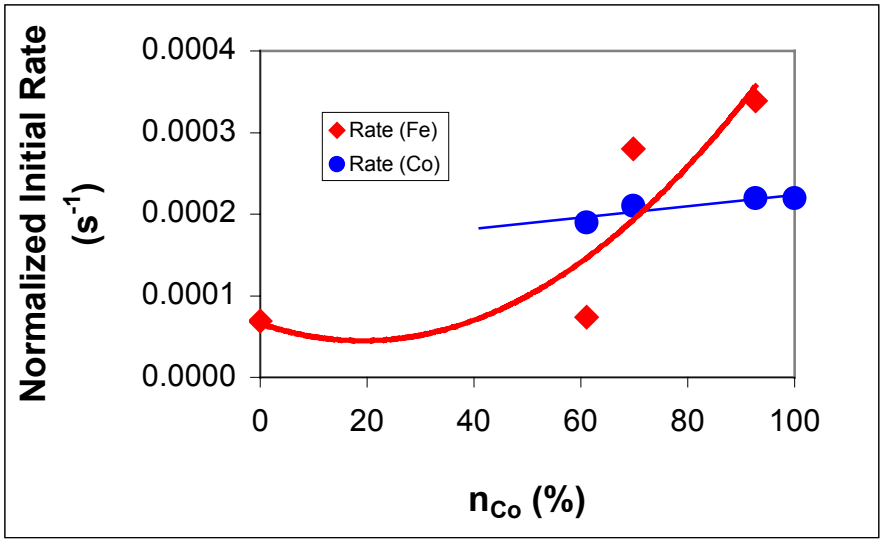

Figure 5.34: Normalized initial decomposition rates of $Fe(CO)_5$ and $Co_4(CO)_{12}$ with respect to composition

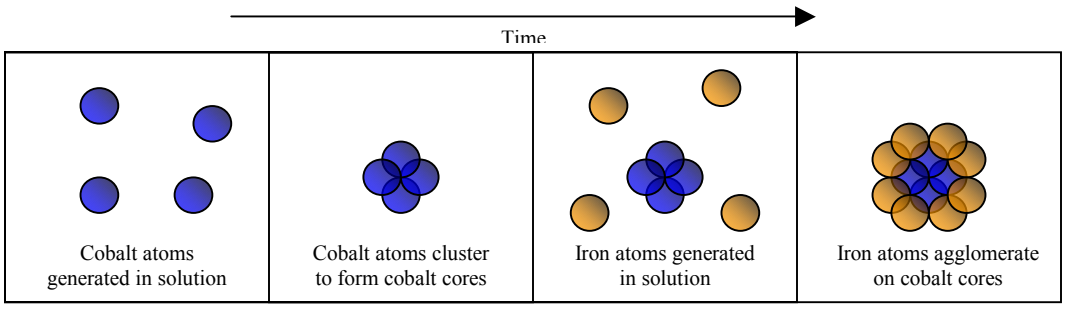

Figure 5.35: Schematic of formation of cobalt core, iron shell nanoalloys from the co-decomposition of $Fe(CO)_5$ and $Co_4(CO)_{12}$

5.7 Summary of $Fe(CO)_5$ and $Co_4(CO)_{12}$ based systems

Though its kinetics are similar to those of $Co_2(CO)_8$, the use of $Co_4(CO)_{12}$ provides a unique insight into the interaction between co-decomposing metal carbonyls. Unlike previous studies that have found that co-decomposing metal carbonyls do not interact, in this case it appears that one precursor is impacted by another precursor's presence. When the initial decomposition rates are very different, one species may form first and nucleate homogeneously, providing sites for the slower species to nucleate heterogeneously. This heterogeneous nucleation allows for an increase in decomposition rate for the slower species and influences the creation of core-shell structures.

CHAPTER 6

$Fe(CO)_5$ and $Co(CO)_2C_5H_5$ Based Systems

6.1 Overview

Another cobalt carbonyl that may be useful in the synthesis of FeCo nanoclusters is $Co(CO)_2C_5H_5$. It has been stressed throughout this work that the kinetics of decomposition of the metal carbonyl species are of utmost importance for the formation of mixed-metal nanoalloys. Several systems have been explored thus far in this study, however none provide the desired matching initial decomposition rates that the synthesis of true mixed-metal nanoalloys requires. $Co(CO)_2C_5H_5$ may be a good alternative cobalt precursor because of its decomposition kinetics. It is predicted that the presence of the C_5H_5 ligand in this species will hinder the loss of CO groups from the Co atom, slowing the decomposition reaction and thus the formation of Co metal. A slower-decomposing cobalt carbonyl species should have reaction kinetics more similar to that of the $Fe(CO)_5$ species, and thus should more easily create mixed-composition nanoalloys when they are co-decomposed.

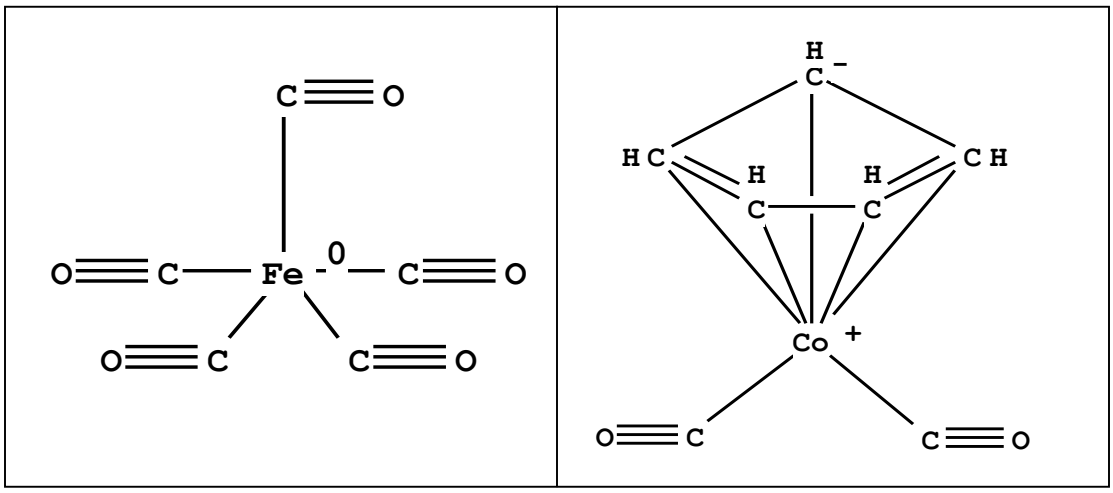

Figure 6.1: $Fe(CO)_5$ and $Co(CO)_2C_5H_5$, the metal carbonyls used in this section of the study

6.2 Kinetic analysis of the decomposition of $Co(CO)_2C_5H_5$

Relatively little is known about the decomposition of this compound and attempts to study its decomposition have been fairly unsuccessful.[43] The decomposition kinetics has been difficult to study previously because of the production of insoluble residue that interferes with FT-IR analysis; however, these previous decompositions were performed in pure solvent. When conducted in a stabilizing system (such as a polymer/solvent combination), the size and growth of residue could possibly be controlled and limited. The characteristic carbonyl peak that indicates the decomposition of this species and the release of $CO_{(g)}$ is at 2022 cm^{-1}.[43]

Because of the lack of kinetic information available about the decomposition of $Co(CO)_2C_5H_5$, it was necessary to determine its extinction coefficient in this system. Using a polystyrene/toluene solvent system, various masses of $Co(CO)_2C_5H_5$ were added to small amounts of polystyrene/toluene solution and analyzed using FT-IR. The height of the characteristic carbonyl peaks for these samples were measured and the information was manipulated as previously described to calculate the system-specific extinction coefficient, $\varepsilon = 8958$ L mol^{-1} cm^{-1}.

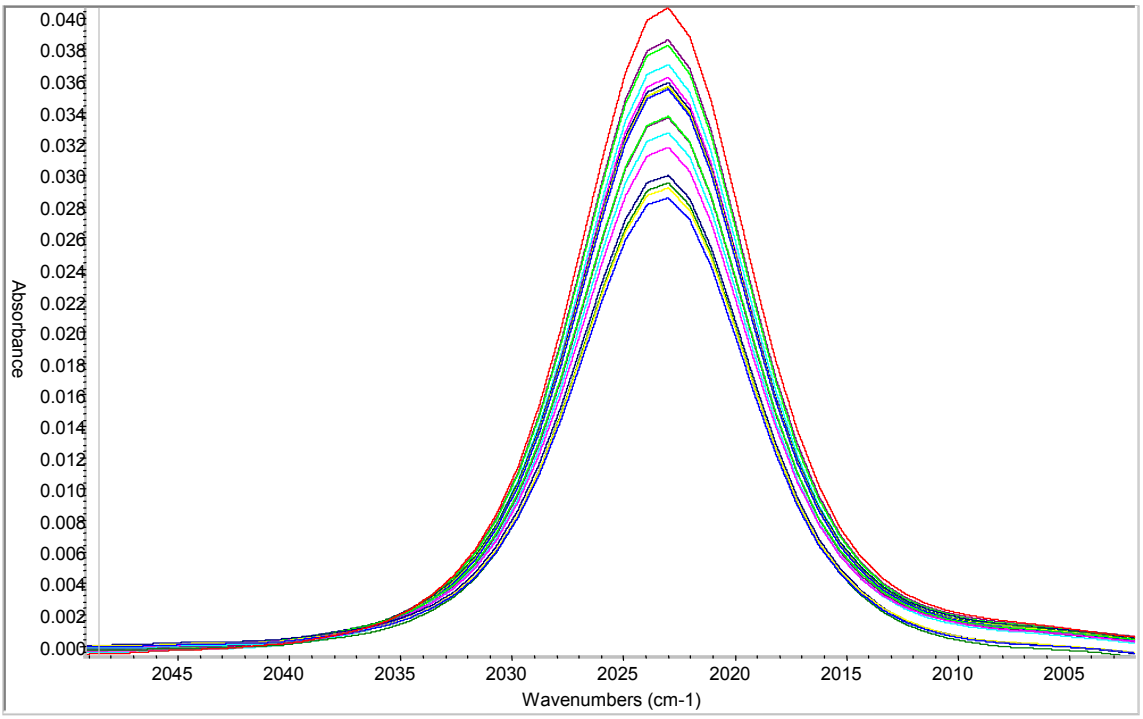

Figure 6.2: FT-IR spectra of $Co(CO)_2C_5H_5$ showing the characteristic carbonyl band

After the extinction coefficient of this species was determined, $Co(CO)_2C_5H_5$ was added to 100 ml of polystyrene and toluene, producing a solution concentration of $7.0 \cdot 10^{-3}$ M. This solution was decomposed as previously described and kinetic data was obtained, Figure 6.3.

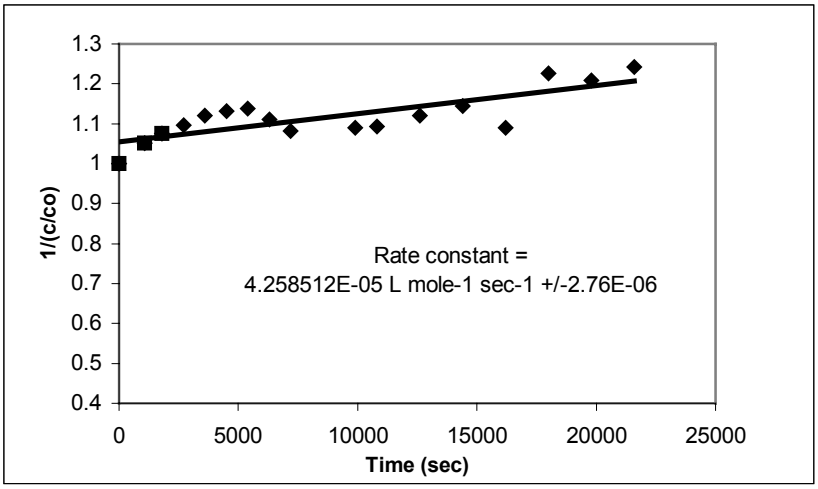

Figure 6.3: Second order initial kinetics of the decomposition of $Co(CO)_2C_5H_5$

Examining the initial decomposition rate of this species, it was determined that it is a second order process with a rate constant in the same order of magnitude as $Fe(CO)_5$. This is a very promising development, as this seems to be a species that may have very similar co-decomposition kinetics as $Fe(CO)_5$, making manipulations of their concentrations to control kinetics unnecessary.

Table 6.1: Individual rate constants and reaction orders of $Fe(CO)_5$ and $Co(CO)_2C_5H_5$

	$Co(CO)_2C_5H_5$	$Fe(CO)_5$
Initial rate constant	$4.26 \cdot 10^{-5}$ L^{-1} mol^{-1} s^{-1}	$7.28 \cdot 10^{-5}$ L^{-1} mol^{-1} s^{-1}
Reaction order	2	2

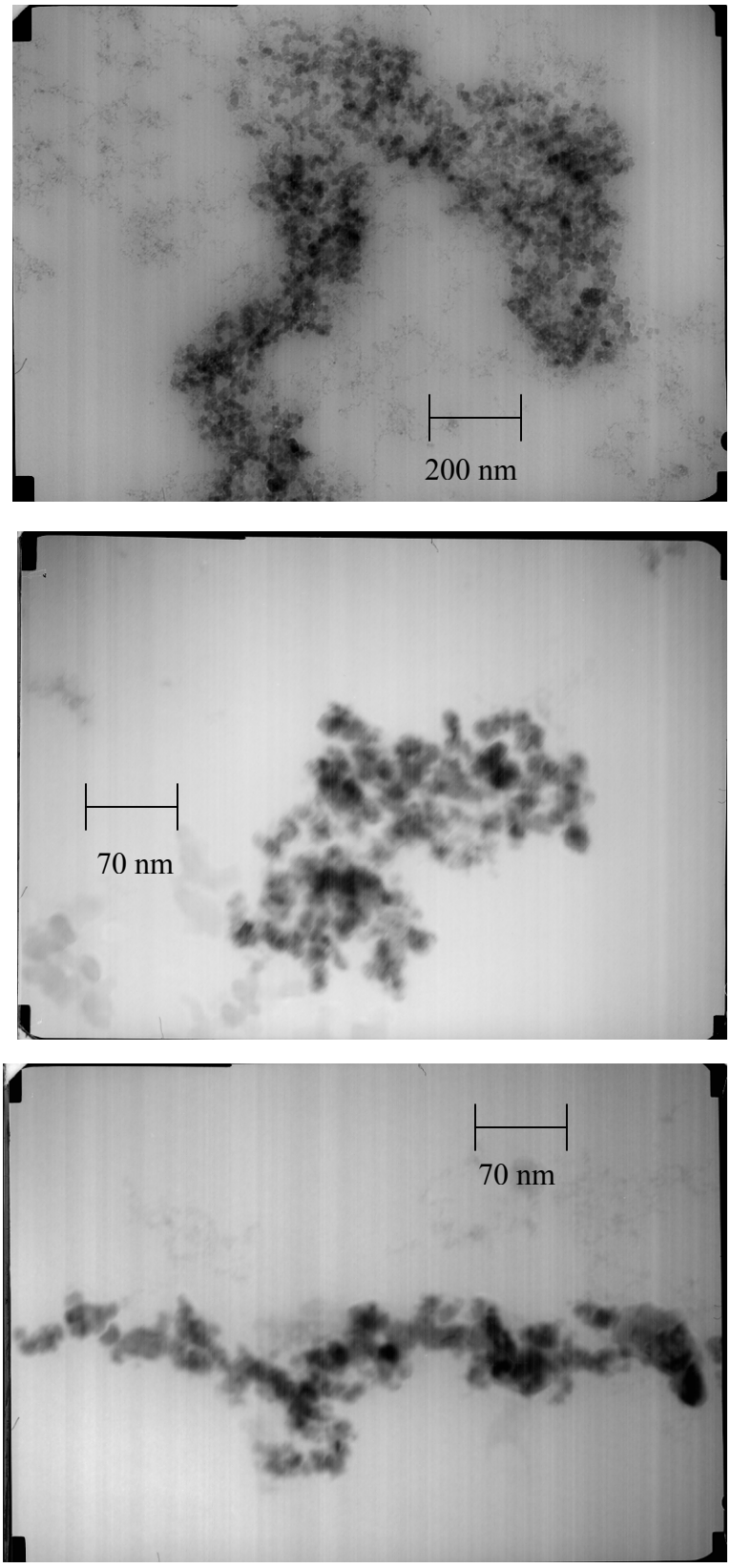

Figure 6.4: TEM micrographs of Co nanoparticles synthesized from the decomposition of $Co(CO)_2C_5H_5$

TEM micrographs (Figure 6.4) of nanoclusters produced from the decomposition of this species indicate clusters of irregular shape, with average cluster size 39.1 ± 5.1 nm. Electron diffraction (Figure 6.6) of these clusters indicates a bcc structure, which is not expected for bulk cobalt. This indicates the formation of a unique cobalt structure, which could be a characteristic of working at the nanoscale.

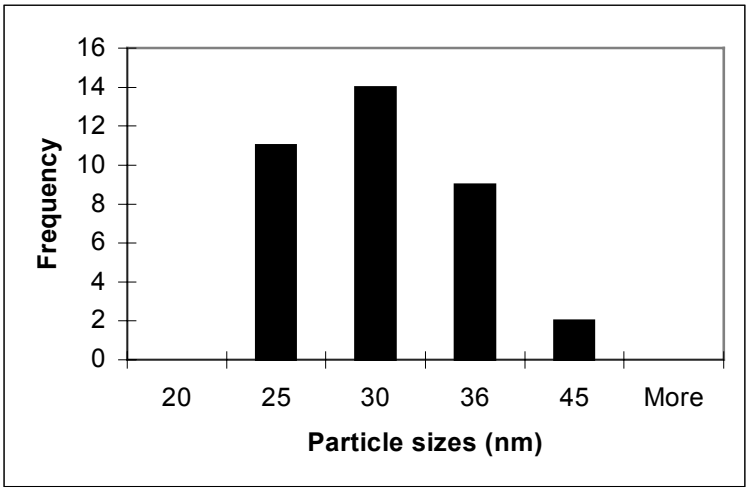

Figure 6.5: Histogram of nanocluster sizes produced by the decomposition of $Co(CO)_2C_5H_5$

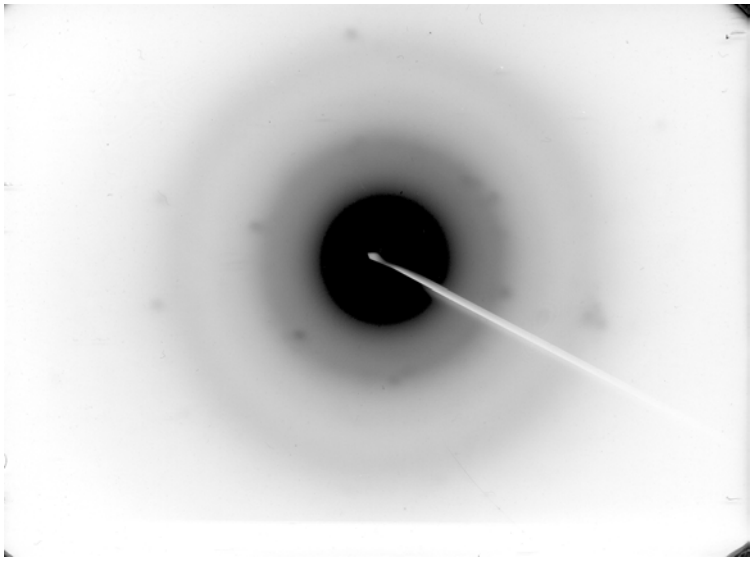

Figure 6.6: Electron diffraction pattern of Co nanoclusters created by the decomposition of $Co(CO)_2C_5H_5$

6.3 Kinetic analysis and nanoalloys from mixed system with equal concentrations

Because the decomposition rates and reaction orders of $Fe(CO)_5$ and $Co(CO)_2C_5H_5$ are so similar, the construction of an equation relating their concentrations is unnecessary. A trial was conducted to create nanoalloys by mixing equal amounts of $Fe(CO)_5$ and $Co(CO)_2C_5H_5$ and decomposing them simultaneously in a polystyrene and toluene solution. Actual solution concentrations were $[Fe(CO)_5]= 4.7 \cdot 10^{-3}$ M and $[Co(CO)_2C_5H_5]= 3.8 \cdot 10^{-3}$ M.

When studying the co-decomposition kinetics of these species it seems that their initial decomposition rate constants both increase as compared to their independent decompositions, the $Fe(CO)_5$ rate constant increases dramatically and the $Co(CO)_2C_5H_5$ rate constant increases slightly. This indicates that there is mutual influence of the precursors on each other's decompositions.

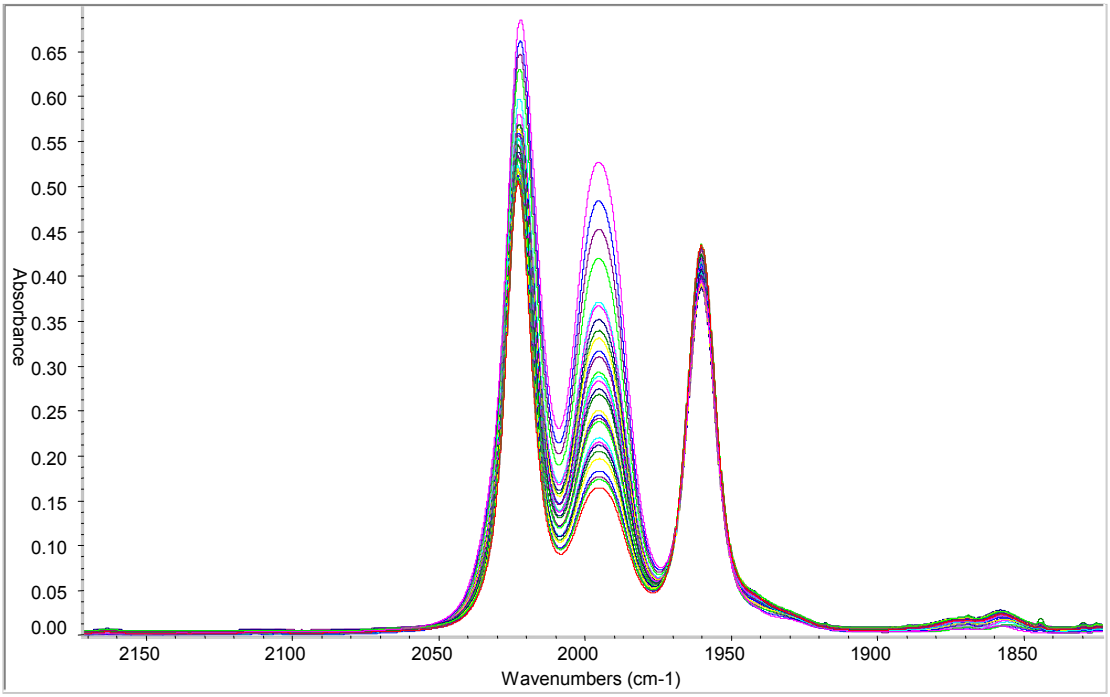

Figure 6.7: FT-IR spectra of $4.7 \cdot 10^{-3}$ M $Fe(CO)_5$ and $3.8 \cdot 10^{-3}$ M $Co(CO)_2C_5H_5$

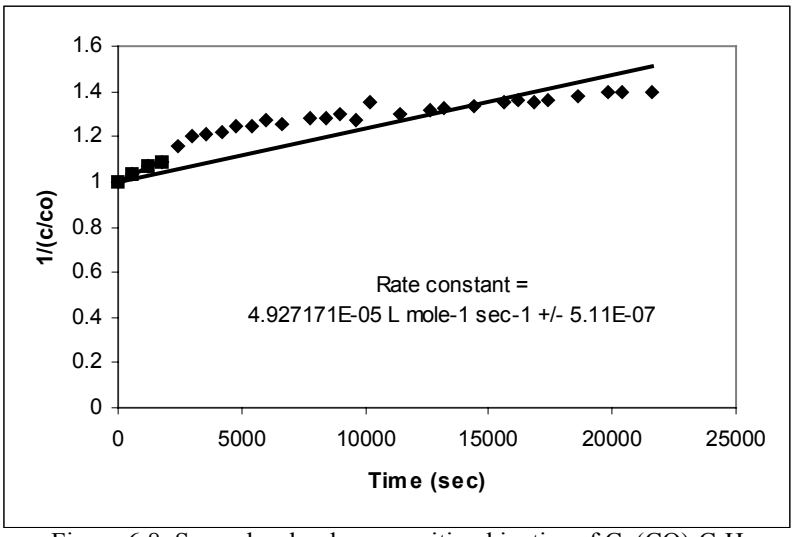

Figure 6.8: Second order decomposition kinetics of $Co(CO)_2C_5H_5$ co-decomposed with $Fe(CO)_5$

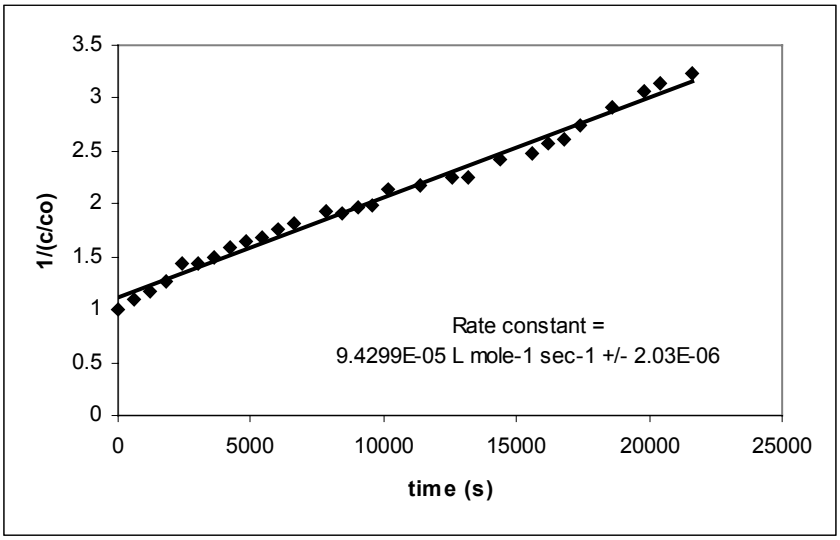

Figure 6.9: Second order decomposition kinetics of $Fe(CO)_5$ co-decomposed with $Co(CO)_2C_5H_5$

Table 6.2: Comparison of individual and co-decomposition rate constants

	$Fe(CO)_5$	$Co(CO)_2C_5H_5$
Individual decomposition rate constant	$7.3 \cdot 10^{-5}$ L^{-1} $mol^{-1}s^{-1}$	$4.26 \cdot 10^{-5}$ L^{-1} mol^{-1} s^{-1}
Co-decomposition rate constant	$1.43 \cdot 10^{-4}$ L^{-1} mol^{-1} s^{-1}	$4.93 \cdot 10^{-5}$ L^{-1} mol^{-1} s^{-1}

TEM micrographs (Figures 6.10-6.12) indicate that this precursor combination produces regularly shaped spherical particles in chain structures. The average particle size is 25.8 ± 4.2 nm.

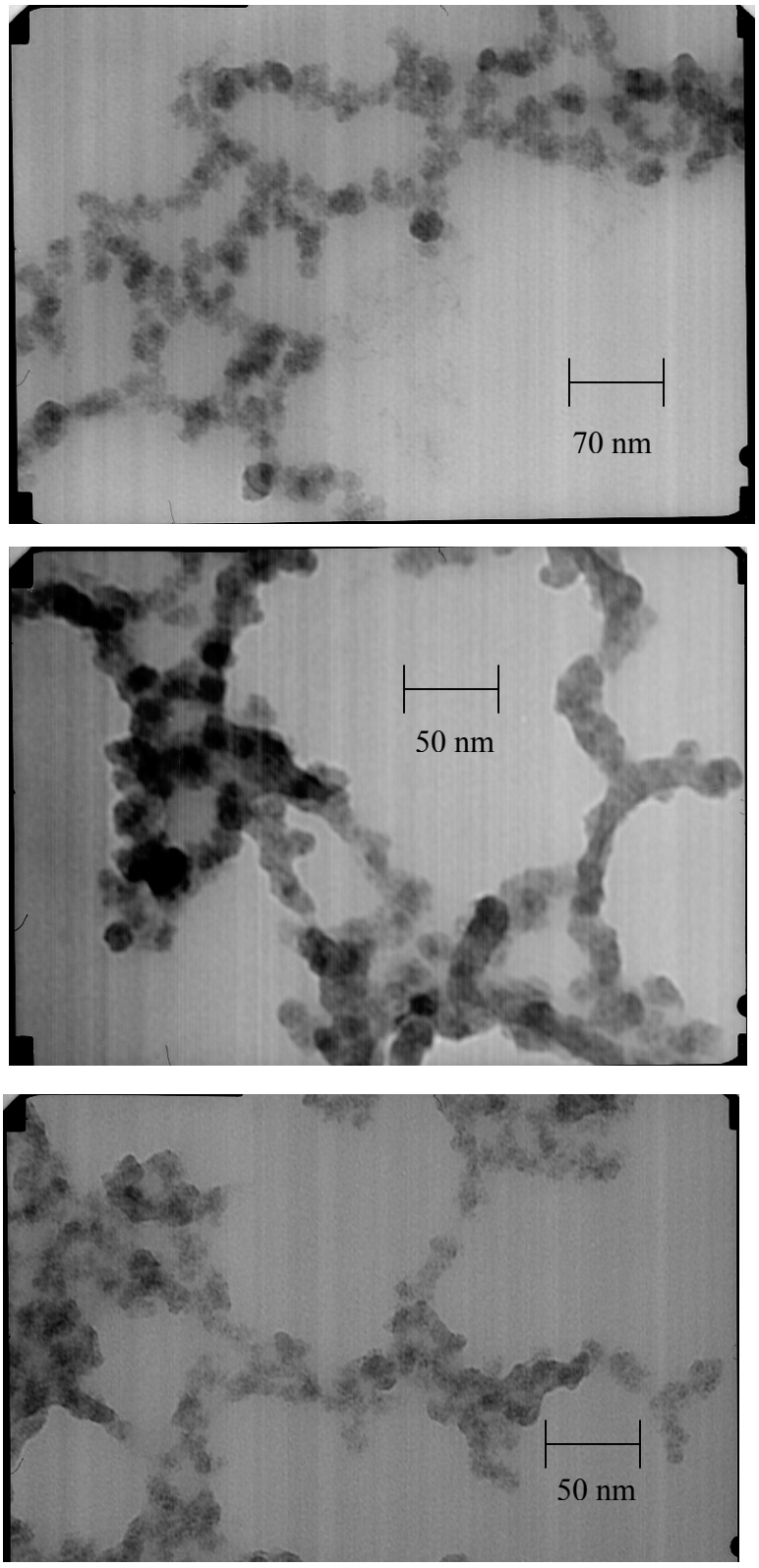

Figure 6.10: High magnification TEM micrographs showing the nanostructure of FeCo nanoclusters synthesized from $4.7 \cdot 10^{-3}$ M $Fe(CO)_5$ and $3.8 \cdot 10^{-3}$ M $Co(CO)_2C_5H_5$

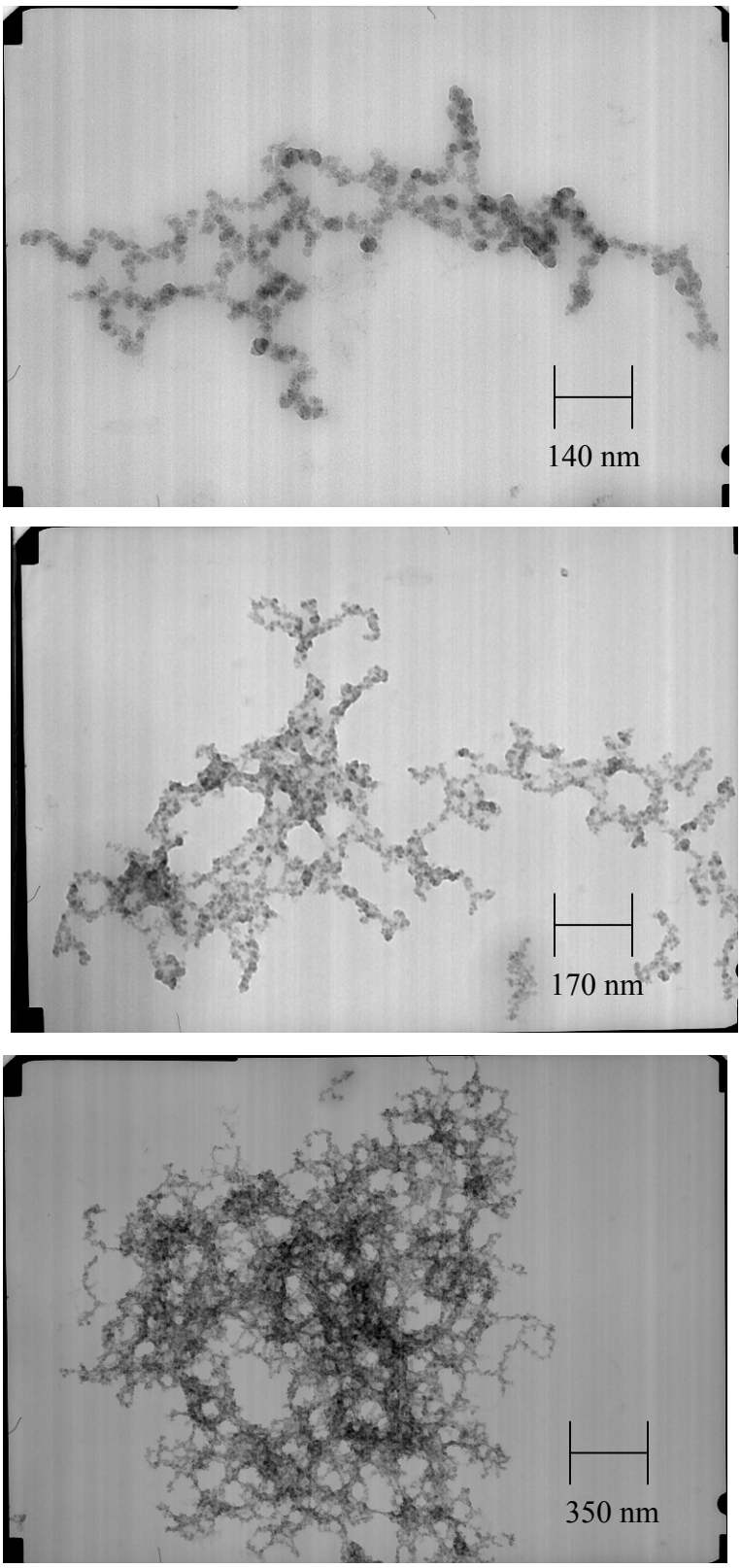

Figure 6.11: TEM micrographs showing the macroscale assembly of FeCo nanoclusters produced via the decomposition of $4.7 \cdot 10^{-3}$ M $Fe(CO)_5$ and $3.8 \cdot 10^{-3}$ M $Co(CO)_2C_5H_5$

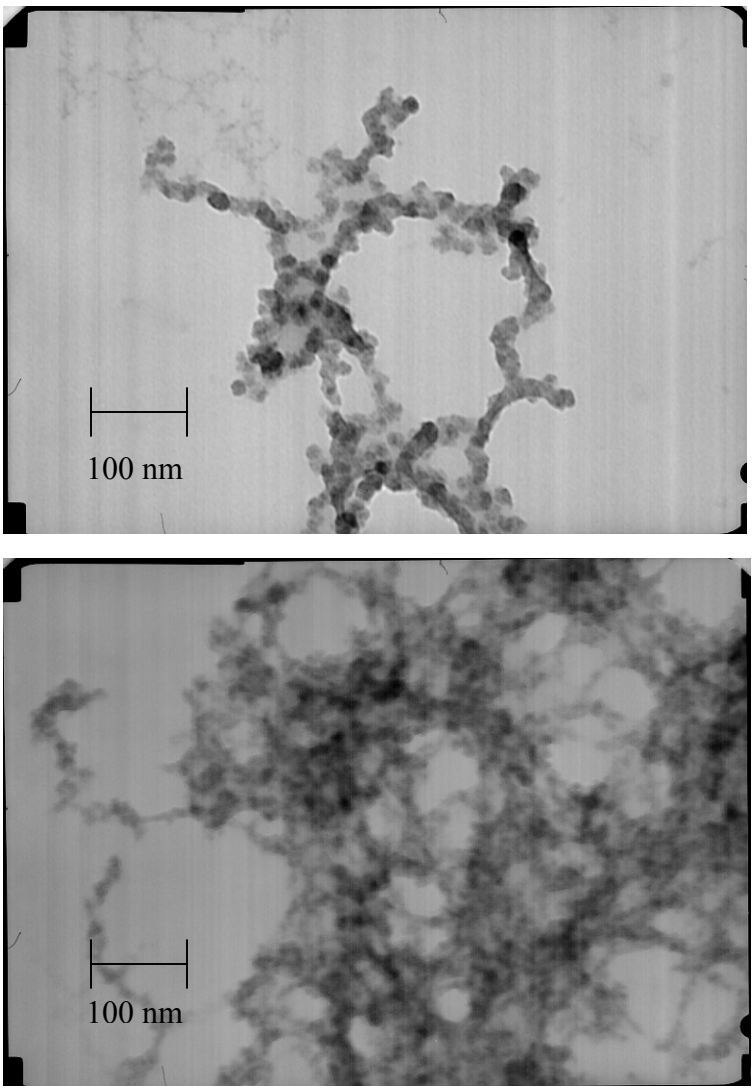

Figure 6.12: TEM micrographs showing the assembly of FeCo nanoclusters produced via the decomposition of $4.7 \cdot 10^{-3}$ M $Fe(CO)_5$ and $3.8 \cdot 10^{-3}$ M $Co(CO)_2C_5H_5$

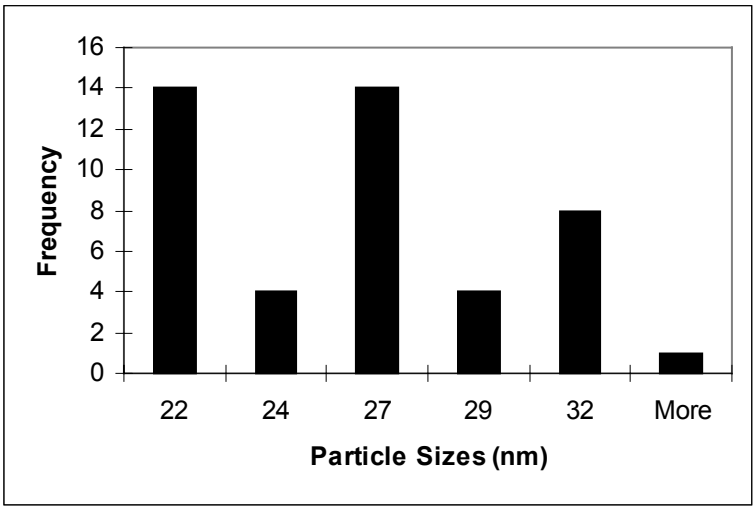

Figure 6.13: Histogram of particle sizes of FeCo synthesized with $Fe(CO)_5$ and $Co(CO)_2C_5H_5$

Electron diffraction performed on these species indicates a bcc structure, which is expected for this iron/cobalt ratio in the bulk phase diagram.

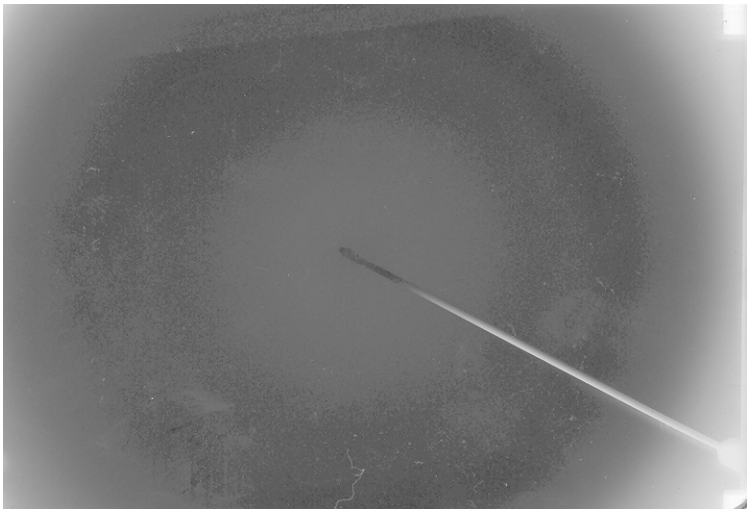

Figure 6.14: Electron diffraction pattern indicating a bcc structure in FeCo created with $Fe(CO)_5$ and $Co(CO)_2C_5H_5$

In addition, an attempt was made to examine the mutual influence of these species' decompositions with a different precursor ratio. The carbonyl precursors were added to a 100 ml polystyrene and toluene solution to produce concentrations of $[Co(CO)_2C_5H_5] = 1.75 \cdot 10^{-3}$ M and $[Fe(CO)_5] = 1.72 \cdot 10^{-3}$ M.

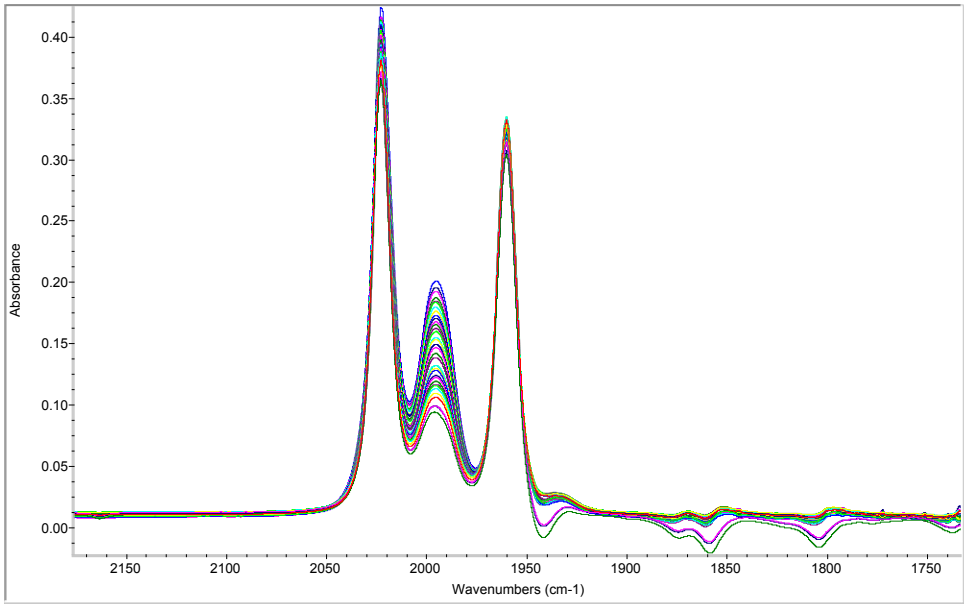

Figure 6.15: FT-IR spectra of $1.75 \cdot 10^{-3}$ M $Co(CO)_2C_5H_5$ and $1.72 \cdot 10^{-3}$ M $Fe(CO)_5$

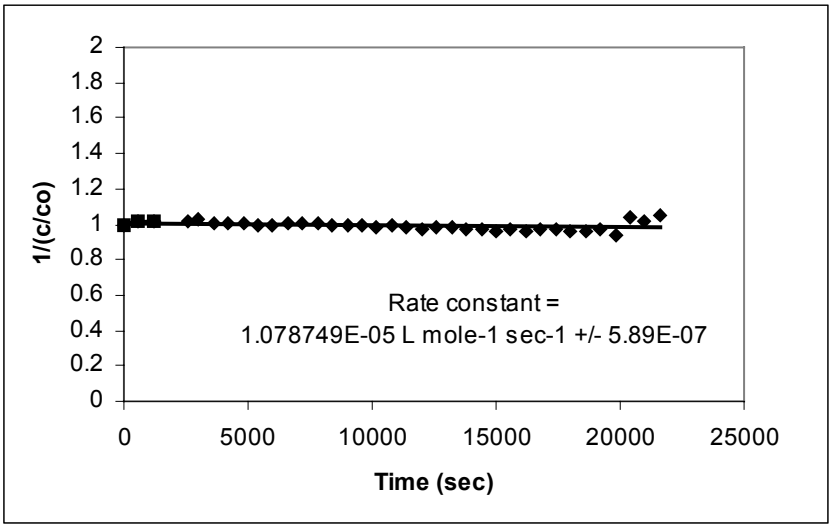

Figure 6.16: Second order decomposition kinetics of $Co(CO)_2C_5H_5$ with $Fe(CO)_5$

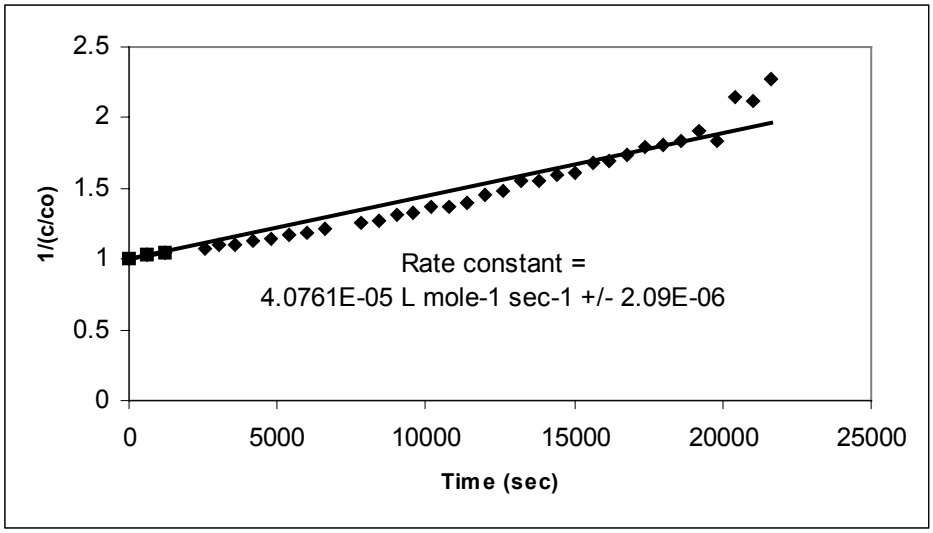

Figure 6.17: Second order decomposition kinetics of $Fe(CO)_5$ with $Co(CO)_2C_5H_5$

At this precursor ratio, the initial decomposition rate constant of $Fe(CO)_5$ is $4.8 \cdot 10^{-5} s^{-1}$ and the decomposition is a second order process. The decomposition of $Co(CO)_2C_5H_5$ is a second order process with an initial rate constant of $1.08 \cdot 10^{-5}$ s^{-1}.

TEM micrographs of the nanoclusters produced indicate clusters of average size 22.5 ± 3.4 nm with fairly regular spherical shape. The clusters organize into complex chain structures and appear to be relatively amorphous. There are fewer crystalline regions in these clusters than FeCo nanoalloys that were produced using other precursors.

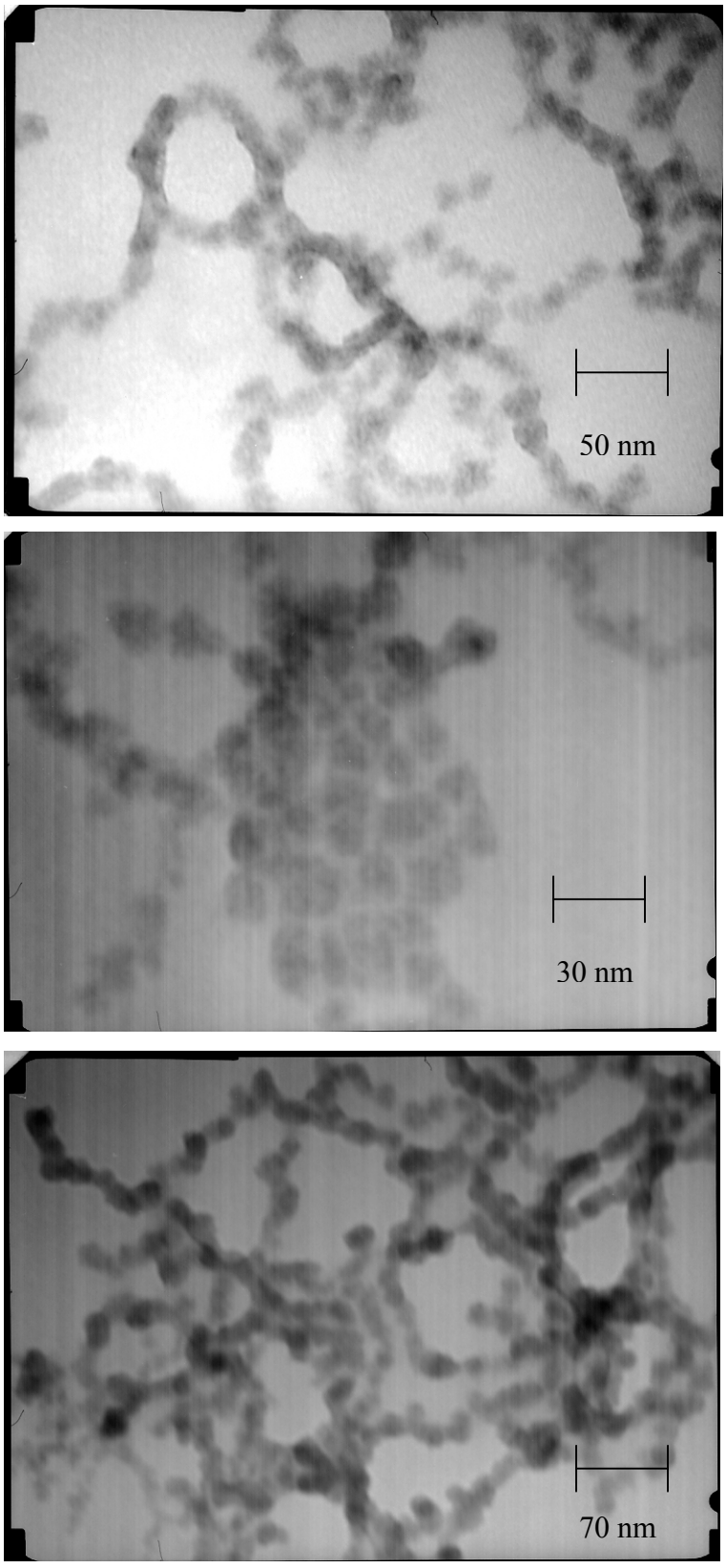

Figure 6.18: TEM micrographs showing nanostructure of FeCo nanoclusters created using $1.75 \cdot 10^{-3}$ M $Co(CO)_2C_5H_5$ and $1.72 \cdot 10^{-3}$ M $Fe(CO)_5$

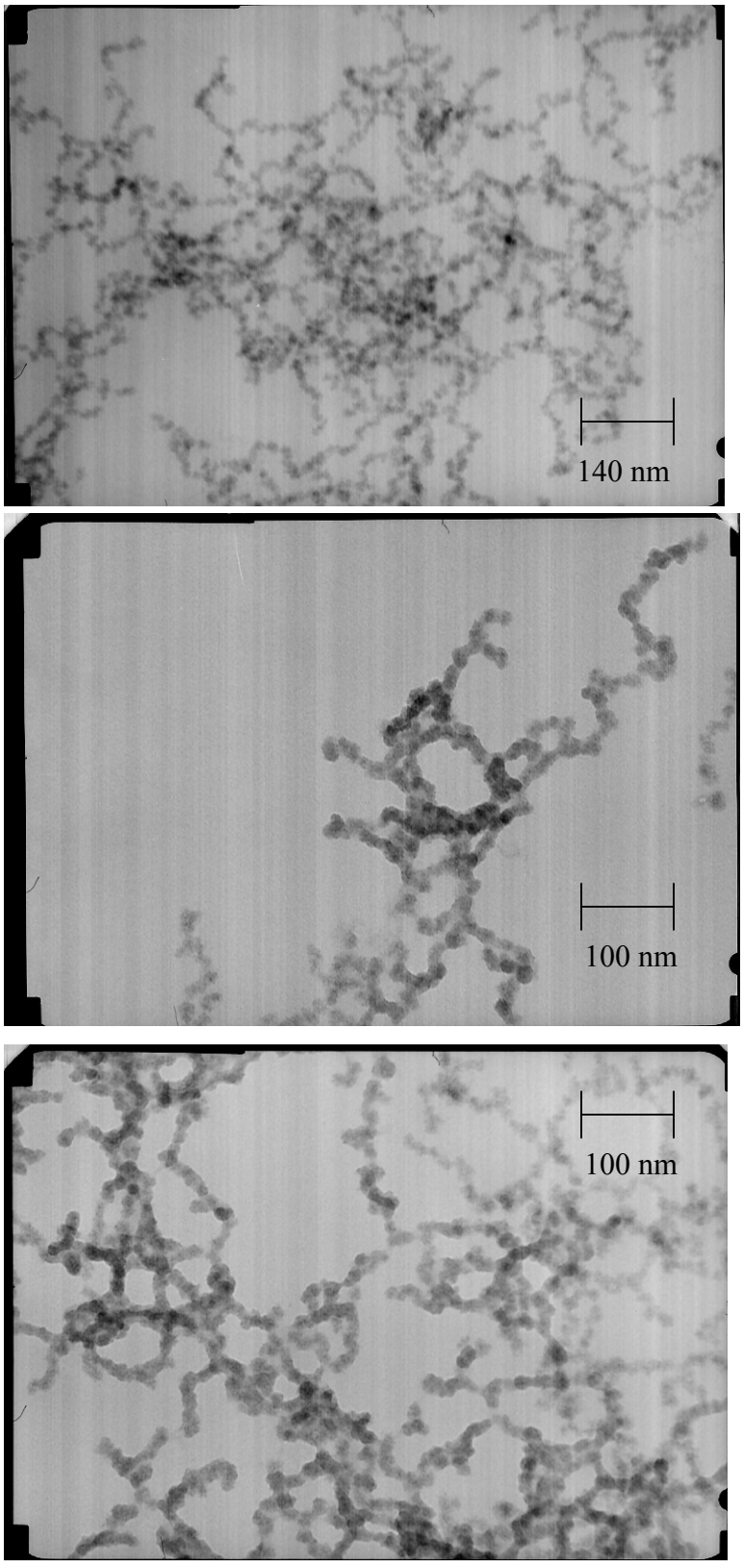

Figure 6.19: TEM micrographs showing the macrostructure of assemblies of FeCo nanoclusters created using $1.75 \cdot 10^{-3}$ M $Co(CO)_2C_5H_5$ and $1.72 \cdot 10^{-3}$ M $Fe(CO)_5$

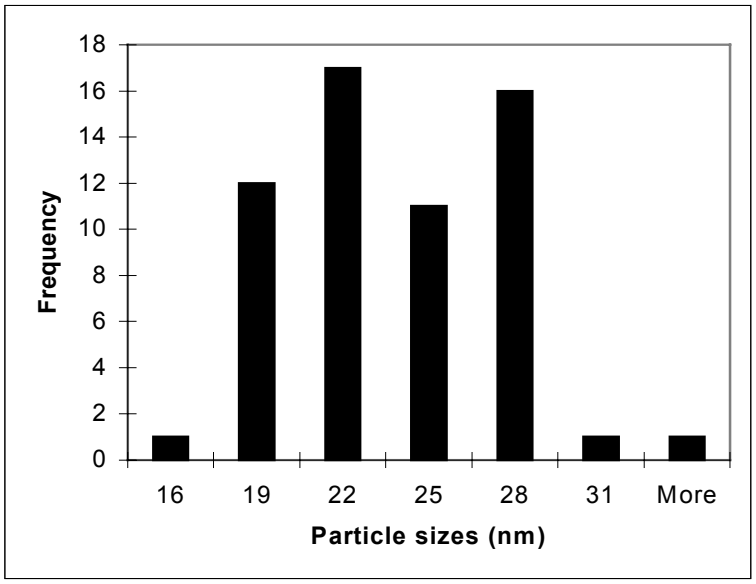

Figure 6.20: Histogram of particle sizes of nanoclusters created using $1.75 \cdot 10^{-3}$ M $Co(CO)_2C_5H_5$ and $1.72 \cdot 10^{-3}$ M $Fe(CO)_5$

Electron diffraction of these species indicates a bcc structure.

Figure 6.21: Electron diffraction pattern indicating a bcc structure

6.4 Kinetics as a function of mixed carbonyl composition

Using the initial rate constants from the $Co(CO)_2C_5H_5$-$Fe(CO)_5$ decompositions and calculating the initial percent of cobalt (as compared to the total amount of iron and cobalt) in each system, one can plot the decomposition rate constants k_{dec} against composition (Figure 6.22).

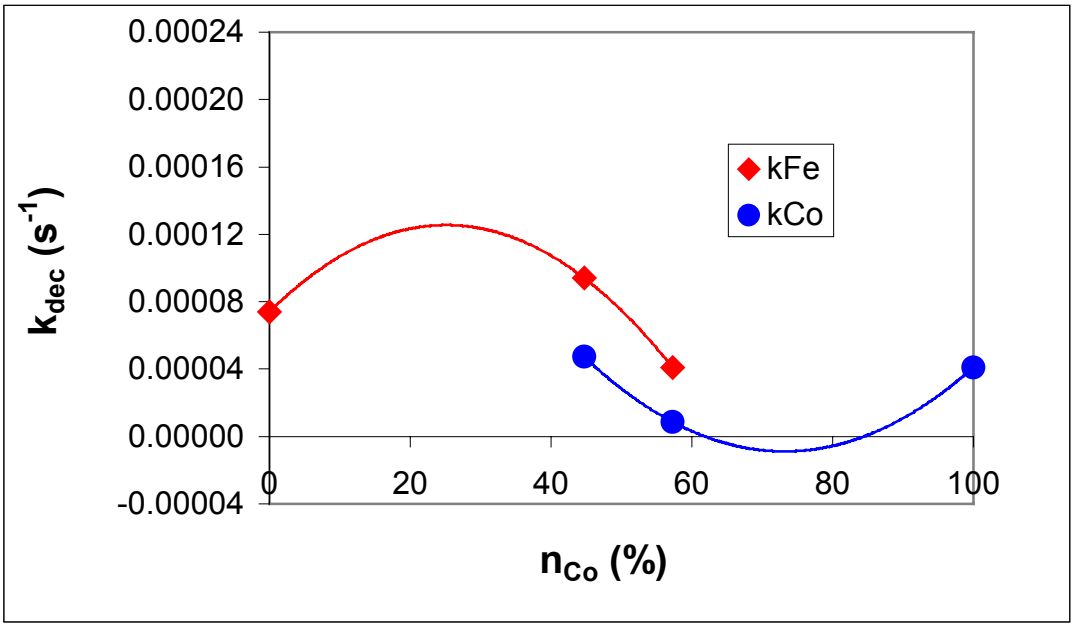

Figure 6.22: Decomposition rate constants of $Fe(CO)_5$ and $Co(CO)_2C_5H_5$ with respect to composition

When the decomposition rate constants are plotted against % cobalt in the systems it appears that there is a slight mutual influence of the precursors on their decomposition kinetics when they are co-decomposed. Calculating the normalized initial decomposition rates (c/c_o) for each trial and plotting those rates against composition in the systems, it is clear that the initial decomposition rates are influenced by the presence of another carbonyl precursor. When the data is polynomial-fitted, there appears to be a point where

the initial decomposition rates of these species will match closely, and the trial that involved 57% Co exhibits good matching of initial decomposition rates. Thus, combining these precursors and co-decomposing them has a positive influence on the attempt to match their initial decomposition rates and presents the possibility of creating well-mixed nanoalloys.

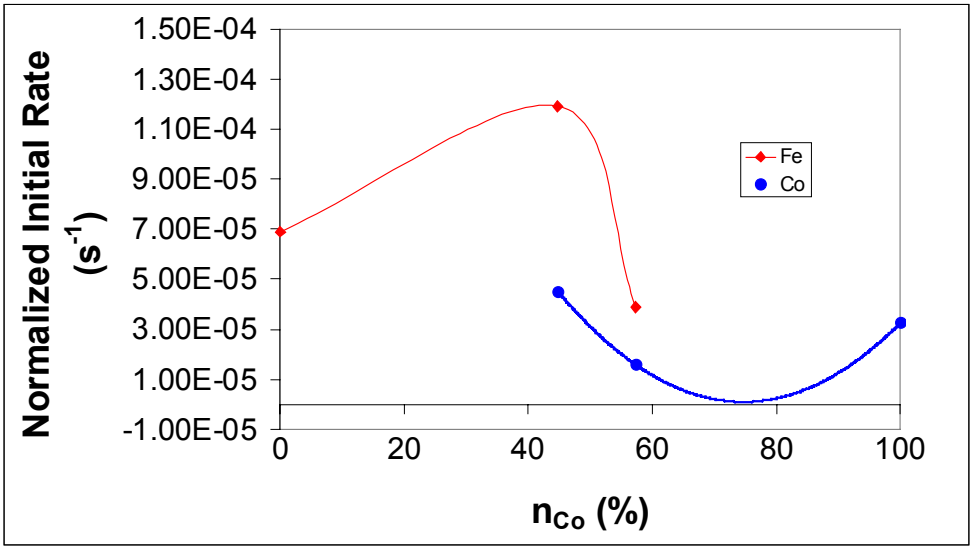

Figure 6.23: Normalized initial decomposition rates of $Fe(CO)_5$ and $Co(CO)_2C_5H_5$ with respect to composition

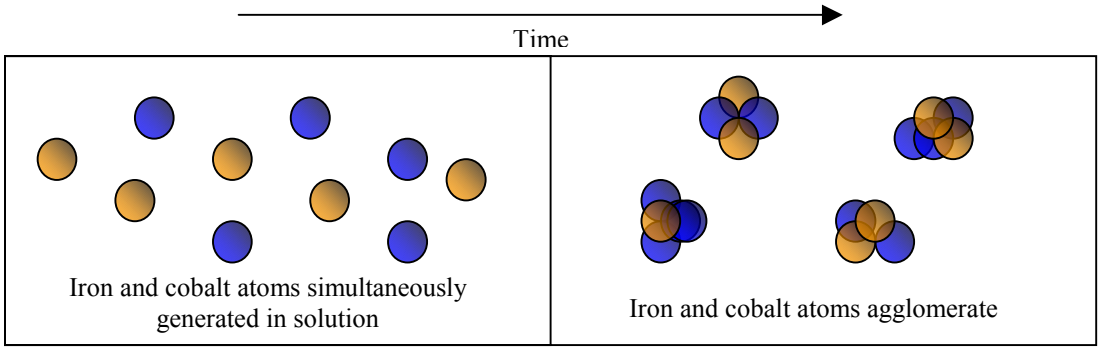

Figure 6.24: Schematic of formation of mixed FeCo nanoalloys from the co-decomposition of $Fe(CO)_5$ and $Co(CO)_2C_5H_5$

6.5 Summary of Fe(CO)5 and $Co(CO)_2C_5H_5$ based systems

$Co(CO)_2C_5H_5$ has proven to be an excellent kinetic match for $Fe(CO)_5$ in their co-decomposition to produce mixed composition nanoalloys. They have the same decomposition reaction order, which allows for easier manipulation of their initial decomposition rates in order to simultaneously generate iron and cobalt atoms in solution. FeCo nanoalloys produced with these precursors appear to have a homogeneous composition and bcc crystal structure.

CHAPTER 7

CONCLUSIONS

This work has detailed the design of synthesis procedures for the formation of controlled composition FeCo nanoalloys. In order to produce controlled composition nanoalloys, the kinetics of the metal carbonyl precursors needed to be carefully studied.

$Fe(CO)_5$ and $Co_2(CO)_8$ based systems

The decomposition kinetics of $Fe(CO)_5$ and $Co_2(CO)_8$ are relatively dissimilar, with different rate constants and reaction orders. Individually, the decomposition of $Fe(CO)_5$ is a second order process and decomposes much more slowly than $Co_2(CO)_8$, a first order decomposition process. In order to synthesize mixed-composition nanoalloys, it was necessary to construct a relationship between the concentrations of these precursors and their decomposition kinetics. This relationship was used to choose precursor concentrations that when co-decomposed induce equal initial decomposition rates. The co-decomposition of chosen concentrations using this ratio resulted in the increase in the rate of decomposition of the $Fe(CO)_5$ species, but the decomposition rate of $Co_2(CO)_8$ also increased and the rates became even more different than their individual decomposition rates. Thus, because of their different nucleation behavior, this method will not produce uniform composition clusters. The clusters produced have average size of about 10.5 nm with dark spots in their centers, indicating a heterogeneous structure. These nanoclusters appear to be bcc crystal structure, which is the expected crystal

structure for the binary bulk FeCo system with the iron/cobalt ratio present initially in the precursors for this system. TGA of a film of these clusters indicates a single type of cluster surface, which can be attributed to a core-shell structure.

In addition to kinetic control, attempts were made to control the structure of FeCo nanoclusters based on the thermodynamic bulk binary phase diagram. Initial concentrations of precursors were chosen such that specific ratios of iron and cobalt atoms were present in the system that correspond to significant compositions on the phase diagram. The decomposition of precursor ratios resulting in 2% Fe and 98% Co in the system resulted in the formation of bcc structured nanoclusters. This is not the predicted structure for this composition in the bulk, but at the nanoscale it is possible to defy the bulk phase diagram and create nanoalloys with thermodynamically unfavorable structures. The decomposition of precursor ratios resulting in 10% Fe and 90% Co also resulted in the production of bcc structured nanoclusters, as opposed to the α+β mixed phase predicted by the bulk phase diagram. Using chosen ratios of precursors allows for the creation of nanoalloys of compositions not normally available in the bulk.

The effect of polymer composition on the resulting nanocluster structure was evaluated with the use of polymethylmethacrylate. The decomposition kinetics of $Fe(CO)_5$ in a PMMA/chlorobenzene solution was evaluated and determined to be a second order process with a rate constant similar to that of $Fe(CO)_5$ in polysytrene and toluene. Two co-decompositions were performed with $Fe(CO)_5$ and $Co_2(CO)_8$, including one decomposition with equal molar amounts of the precursors and one decomposition using the previously constructed "equal rates" relationship to relate kinetics and concentrations and induce equal initial decomposition rates. When co-decomposed, the

rates of decomposition of $Fe(CO)_5$ and $Co_2(CO)_8$ stay relatively similar to their individually decomposed precursors, indicating that there is not effective matching of the initial decomposition rates in these species. Evaluation of the products of these decompositions indicate an average particle diameter of about 29.8 nm and bcc structure for the co-decomposition of equal amounts of the precursors and an average particle diameter of 15 ± 3.5 nm and bcc structure for the co-decomposition of precursors in the ratio of concentrations that induce equal initial decomposition rates.

The synthesis of FeCo oxides in PVF_2 resulted in the production of spherical nanoclusters connected in chains with average particle diameter around 154 nm. Electron diffraction of these species indicate the presence of an hcp structure, which is not the predicted structure for the ratio of iron and cobalt present in the system (2:1 Co to Fe ratio). It is assumed that this synthesis process has created a nanostructure not normally thermodynamically favorable at this metal-metal concentration ratio using the bulk phase diagram.

$Fe(CO)_5$ and $Co_4(CO)_{12}$ based systems

Because the decomposition rates of $Fe(CO)_5$ and $Co_2(CO)_8$ are so dissimilar, it was necessary to attempt to find a cobalt precursor with similar kinetics as $Fe(CO)_5$ in order to create mixed nanoalloys. $Co_4(CO)_{12}$ was considered a possibility because of its larger molecular structure. A larger, more complex structure should have slower decomposition than a simpler molecular structure. However, it was determined through decomposition kinetics analysis that the rate of decomposition of $Co_4(CO)_{12}$ is very similar to that of $Co_2(CO)_8$ and it is a first order decomposition reaction. It is noted that the decomposition of $Co_2(CO)_8$ produces $Co_4(CO)_{12}$ as an intermediate, and it is then

assumed that the decomposition of $Co_4(CO)_{12}$ is the rate limiting step in the decomposition of $Co_2(CO)_8$. When the normalized initial rates of decomposition were calculated for co-decompositions of various ratios of $Fe(CO)_5$ and $Co_4(CO)_{12}$, it was determined that the presence of $Co_4(CO)_{12}$ has a powerful effect on the decomposition of $Fe(CO)_5$. The decomposition rate of the $Fe(CO)_5$ seems to increase dramatically with the addition of $Co_4(CO)_{12}$ in the system. It is assumed that the formation of clusters in the co-decomposition of these species is by a heterogeneous nucleation process, where $Co_4(CO)_{12}$ is decomposing fairly quickly and forming seed Co clusters homogeneously. After these seed clusters have formed, Fe forms on these clusters via heterogeneous nucleation. The energetic pathway for heterogeneous nucleation requires far less energy than for homogeneous nucleation, explaining the apparent increase in the decomposition rate of $Fe(CO)_5$ for these situations. Experimental results support this hypothesis, with larger amounts of zero-valent cobalt (in the core of the clusters) present in those nanoalloys produced with large ratios of $Co_4(CO)_{12}$.

$Fe(CO)_5$ and $Co(CO)_2C_5H_5$ Based Systems

$Co(CO)_2C_5H_5$ was chosen as a possible cobalt precursor in combination with $Fe(CO)_5$ because of its complex structure. The presence of the C_5H_5 ligand is predicted to hinder the release of CO ligands from the cobalt complex, creating a slower decomposition than simpler cobalt carbonyls. The decomposition of this species is determined to be a second order process (which matches that of $Fe(CO)_5$) and has a decomposition rate constant comparable to that of $Fe(CO)_5$. The combination of equal amounts of $Fe(CO)_5$ and $Co(CO)_2C_5H_5$ should produce well-mixed nanoalloys. When

co-decomposed, there seems to be a mutual influence of the species on their decomposition rate constants and normalized rates. Analyzing this influence, it is possible to determine a precursor concentration ratio where the initial decomposition rates of these species should closely match and the resulting nanoalloys would be most thoroughly mixed.

Summary

Several methods have been constructed to create controlled composition nanoalloys with varying success. These methods have elucidated the co-decomposition kinetics of $Fe(CO)_5$ with $Co_2(CO)_8$, $Co_4(CO)_8$, and $Co(CO)_2C_5H_5$ and determined $Co(CO)_2C_5H_5$ to be the ideal choice for co-decomposition with $Fe(CO)_5$ to produce well-mixed nanoalloys.

CHAPTER 8

RECOMMENDATIONS

The kinetics of the co-decompositions of $Fe(CO)_5$ with $Co_2(CO)_8$, $Co_4(CO)_{12}$, and $Co(CO)_2C_5H_5$ have been thoroughly investigated. In addition to $Fe(CO)_5$, there are other iron carbonyl precursors commercially available (for example $Fe_2(CO)_9$, $Fe_3(CO)_{12}$) that may be viable options for creating FeCo nanoalloys when co-decomposed with a cobalt carbonyl precursor. The kinetics of these species have been investigated as intermediates in the decomposition of $Fe(CO)_5$,[10,11] but they should be investigated in combination with the currently investigated cobalt precursors in order to determine if two of these species have kinetics that are even more similar than those of $Fe(CO)_5$ and $Co(CO)_2C_5H_5$.

In addition to the single metal precursors, it is also possible to synthesize mixed-metal precursors. $H[FeCo_3(CO)_{12}]$ can be synthesized and subsequently decomposed in a polymer/solvent solution to produce nanoclusters.[44] It would be interesting to see what impact having both metals in the precursor and only one type of precursor molecule interacting with the polymer would have on the resulting morphology and structure of the resulting nanoclusters.

As discussed in this work, the choice of stabilizing polymer has an effect on the shape of the resulting nanoclusters produced by these metal carbonyl decompositions. For example, polystyrene, the polymer used most often in this study, produces chain structures due to incomplete cluster coverage. Different polymers and molecular weights could be used with these systems to manipulate cluster size and shape.

In addition to the construction of novel synthesis methods to control the morphology and size characteristics of FeCo nanoalloys, their magnetic properties should be evaluated. The magnetic nature of these materials and previous studies indicate that these nanoalloys likely possess single magnetic domains, with each nanocluster demonstrating a strong magnetic field in a single direction. The magnetic strength of these clusters should be evaluated and used to construct a relationship between iron and cobalt concentrations in the nanoalloys and magnetic strength. Thus, one could tune the magnetic properties of nanoalloy clusters by manipulating their synthesis conditions and controlling the resulting clusters' compositions.

REFERENCES

[1]Edelstein, A. S.; Harris, V. G.; Rolison, D.; Kurihara, L.; Smith, David J.; Perepezko, J.; da Silva Bassani, M. H. "Inversion of surface composition and evolution of nanostructure in Cu/Co nanocrystals." *Applied Physics Letters* (1999), **74**(21), 3161-3163.

[2]Lee, Jai-Sung; Kang, Yun-Sung; Kwon, Sang-Kyun; Cha, Bum-Ha; Qin, Xioaying. "A new processing route for net-shaped nanoparticulate materials." *Advanced Powder Technology* (2004), **15**(6), 639-655.

[3]Chen, Hongjie; Li, Zhiwei; Wu, Zhishen; Zhang, Zhijun. "A novel route to prepare and characterize Sn-Bi nanoparticles." *Journal of Alloys and Compounds* (2005), **394**(1-2), 282-285.

[4]Jesser, W. A.; Shneck, R. Z.; Gile, W. W. "Solid-liquid equilibria in nanoparticles of Pb-Bi alloys." *Physical Review B: Condensed Matter and Materials Physics* (2004), **69**(14), 144121/1-144121/13.

[5]Vallee, R.; Wautelet, M.; Dauchot, J. P.; Hecq, M. "Size and segregation effects on the phase diagrams of nanoparticles of binary systems." *Nanotechnology* (2001), **12**(1), 68-74.

[6]Shirinyan, A. S.; Wautelet, M. "Phase separation in nanoparticles." *Nanotechnology* (2004), **15**(12), 1720-1731.

[7]Wautelet, M.; Dauchot, J. P.; Hecq, M. "Phase diagrams of small particles of binary systems: a theoretical approach." *Nanotechnology* (2000), **11**(1), 6-9.

[8]Liang, L. H.; Liu, D.; Jiang, Q. "Size-dependent continuous binary solution phase diagram." *Nanotechnology* (2003), **14(**4), 438-442.

[9]Shirinyan, A. S.; Gusak, A. M. "Phase diagrams of decomposing nanoalloys." *Philosophical Magazine* (2004), **84**(6), 579-593.

[10]Zubris, Melissa; King, R. Bruce; Garmestani, Hamid; Tannenbaum, Rina. (2005) "FeCo nanoalloy formation by decomposition of their carbonyl precursors" *Journal of Materials Chemistry*, **15**(12), 1277-1285.

[11]Zubris, Melissa. "Synthesis and Microstructure of FeCo Nanoalloys" (2002), Masters Thesis, Georgia Institute of Technology.

[12]Sun, S., Murray, C. B. (1999). "Synthesis of monodisperse cobalt nanocrystals and their assembly into magnetic superlattices", *Journal of Magnetism and Magnetic Materials*, **85**, 8, 4325-4330.

[13]Solymar, L., Walsh, D. (1995). Lectures on the Electrical Properties of Materials. New York: Oxford University Press.

[14]Held, G. A., Grinstein, G., Doyle, H., Sun, S., Murray, C. B. (2001). "Competing interactions in dispersions of superparamagnetic nanoparticles", *Physical Review B*, **64** 012408.

[15]Hariharan, S.. (2001). "Mapping of switching and anisotropy fields in magnetic nanoparticles", *Mater. Phys. Mech.*, **4**, 1-4.

[16]Sun, S., Anders, S., Hamann, H. F., et. al. (2002). "Polymer Mediated Self-Assembly of Magnetic Nanoparticles", *J. Am. Chem. Soc.*, **124***(12)*, 2884.

[17]Shim, I-W., Choi, S., Noh, W-T., Kwon, J., Cho, J. Y., Chae, D.-Y., Kim, K.-S. (2001). "Preparation of Iron Nanoparticles in Cellulose Acetate Polymer and Their Reaction Chemistry in the Polymer", *Bull. Korean Chem. Soc.*, **22 (7)**, 772-774.

[18]Wilcoxson, J. P., Provencio, P. P., (1999). "Use of surfactant micelles to control the structural phase of nanosize iron clusters", *J. Phys. Chem.*, **103**, 9809-9812.

[19]Choi, C. J., Dong, X. L., Kim, B. K. (2001). "Characterization of Fe and Co nanoparticles synthesized by chemical vapor deposition", *Scripta Materialia*, **44**, 2225-2229.

[20]Kiely, C. J., Fink, J., Brist, M., Bethell, D., Schiffrin, D. J., (1998). "Spontaneous ordering of bimodal ensembles of nanoscopic gold clusters", *Nature*, **396**, 444-446.

[21]Han, S. W., Kim, Y., Kim, K. (1998). "Dodecanethiol-Derivatized Au/Ag Bimetallic Nanoparticles: TEM, UV/VI, XPS, and FTIR Analysis", *Journal of Colloid and Interface Science*, **208**, 272-278.

[22]Lee, G. H., Huh, S. H., Jeong, J. W., Ri, H.-C. (2002). "Excellent magnetic properties of fullerene encapsulated ferromagnetic nanoclusters" *Journal of Magnetism and Magnetic Materials*, 246, 404-411.

[23]Lee, G. H., Huh, S. H., Park, J. W., Ri, H.-C., Jeong, J. W. (2002). "Arrays of Ferromagnetic Iron and Cobalt Nanoclusters" *Journal of Physical Chemistry B*, **106** (9), 2123-2126.

[24]Park, J.-I., Cheon, J. (2001). "Synthesis of 'solid-solution' and 'core-shell' type cobalt-platinum magnetic nanoparticles via transmetalation reactions" *J. Am. Chem. Soc.*, **123**, 5743-5746.

[25]Kiely, C. J.; Fink, J.; Zheng, J.G.; Brust, M.; Bethell, D.; Schiffrin, D. J. (2000) "Ordered Colloidal Nanoalloys" *Adv. Mater.,* **12**, 640-643.

[26]Black, C. T., Murray, C. B., Sandstrom, R. L., Sun, S. (2000). "Spin-Dependent Tunneling in Self-Assembled Cobalt-Nanocrystal Superlattices" *Science,* **290**, 1131-1134.

[27]Suslick, K. S., Fang, M., Hyeon, T. (1996). "Sonochemical Synthesis of Iron Colloids" *J. Am. Chem. Soc.,* **118**, 11960-11961.

[28]Shouheng, S. Murray, C. B. Weller, D. Folks, L., Moser, A. (2000) "Monodisperse FePt nanoparticles and ferromagnetic FePt nanocrystal superlattices" *Science* **287**, 1989-1992.

[29]Murray, C. B., Sun, S., Gaschler, W., Doyle, H., Betley, T. A., Kagan, C. R. (2001) "Colloidal synthesis of nanocrystals and nanocrystal superlattices" *IBM J. Res. & Dev.,* **45 (**1) 47-55.

[30]Campbell, D., Pethrick, R.A., White, J.R. (2000). *Polymer characterization : physical techniques*. Cheltenham, U.K.: Stanley Thornes.

[31]Szymanski, H.A. (1964). IR: Theory and Practice of Infrared Spectroscopy. New York: Plenum Press.

[32]http://www.pslc.ws/macrog/index.htm (Accessed October 11, 2005).

[33]Brandrup, J., Immergut, E. H. (1999). Polymer Handbook. New York: Wiley Press.

[34]Braterman, P.S. (1975) Metal Carbonyl Spectra New York: Academic Press.

[35]http://www.met.kth.se/dct/pd/element/Co-Fe.html (Accessed October 11, 2005).

[36]Tannenbaum, R. (1994). "Thermal decomposition of cobalt carbonyl complexes in viscous media", *Inorganica Chimica Acta*, **227**, 233-240.

[37]Tannenbaum, R. (1990). "Magnetic Metal-Polymer Composites: Thermal and Oxidative Decomposition of $Fe(CO)_5$ and $Co_2(CO)_8$ in a Poly(vinylidene fluoride) Matrix", *Journal of Polymer Science: Part B: Polymer Physics*, **28**, 2421-2433.

[38]Tannenbaum, R.; Zubris, M.; Goldberg, E. P.; Reich, S.; Dan, N. (2005) "Polymer-Directed Nanocluster Synthesis: Control of Particle Size and Morphology"; *Macromolecules*; **38**(10), 4254-4259.

[39]Tannenbaum, Rina. (1997) "Polymer Matrix Influence on the Kinetics of Some Fundamental Inorganic Colloidal Reactions" *Langmuir*, **13**(19), 5056-5060.

[40]Tannenbaum, Rina; Flenniken, Cindy L.; Goldberg, Eugene P. (1990) "Magnetic metal-polymer composites: thermal and oxidative decomposition of iron pentacarbonyl and cobalt carbonyl [$Co_2(CO)_8$] in a poly(vinylidene fluoride) matrix" *Journal of Polymer Science, Part B: Polymer Physics* , **28**(12), 2421-33.

[41]Tannenbaum, R., Reich, S., Flenniken, C., Goldberg, E. (2002) "Shape control of Iron Oxide Nanoclusters in Polymeric Media" *Advanced Materials,* **14** (19) 1402-1405.

[42]Tadd, Erica; Zeno, Astra; Zubris, Melissa; Dan, Nily; Tannenbaum, Rina. (2003) "Adsorption and Polymer Film Formation on Metal Nanoclusters" *Macromolecules* , **36**(17), 6497-6502.

[43]Miksa, Davide; Brill, Thomas B. (2002) "Spectroscopy of Hydrothermal Reactions. 21. Decomposition Reactions and Kinetics of $Ni(CO)_4$, $Co(CO)_4^-$ and (η5-C_5H_5)$Co(CO)_2$ in High Temperature Water" *Industrial & Engineering Chemistry Research*, **41**(21), 5151-5157.

[44]Chini, Paolo; Colli, Luigi; Peraldo, Mario. (1960) "Preparation and properties of the hydrocarbonyl $HFeCo_3(CO)_{12}$ and of compounds prepared from the anion [FeCo3(CO)12]-" *Gazzetta Chimica Italiana*, **90**, 1005-20.

VITA

MELISSA ANN ZUBRIS WILLIAMS

ZUBRIS WILLIAMS was born in North Tonawanda, New York. She attended North Tonawanda Senior High School and received a B.S. in Materials Science and Engineering from Northwestern University, Evanston, Illinois in 2000. She earned a M.S. in Materials Science and Engineering from Georgia Tech in 2002 before continuing to pursue her doctorate.